2007

Synthesis and characterization of interfaces between naturally derived and synthetic nanostructures for biomedical applications

Souheil Zekri
University of South Florida

Synthesis and Characterization of Interfaces Between Naturally Derived and Synthetic Nanostructures for Biomedical Applications

by

Souheil Zekri

A dissertation submitted in partial fulfillment
of the requirements for the degree of
Doctor of Philosophy
Department of Mechanical Engineering
College of Engineering
University of South Florida

Major Professor: Ashok Kumar, Ph.D.
Rajiv Dubey, Ph.D.
Muhammad M. Rahman, Ph.D.
Thomas J. Koob, Ph.D.

Date of Approval:
May 25, 2007

Keywords: biosensor, porous silicon, orthopaedics, tissue engineering, collagen, carbon nanotube

DEDICATION

This dissertation is dedicated to my parent, brother, sister, wife and kids.

ACKNOWLEDGEMENTS

I would like to extend my gratitude and thanks to my research advisor, Dr. Ashok Kumar for his continuous support and guidance, which has helped and guided me thoughout my doctoral work. I would also like to thank my committee members: Dr. Rajiv Dubey (USF) and Dr. Muhammad M. Rahman (USF). Your input and guidance during my research has been invaluable and greatly appreciated. My special thanks go to Dr. Thomas J. Koob for his immense support and guidance throughout a large portion of my research. He has helped me understand the value of interdisciplinary research. Special acknowledge go to Douglas Pringle and Daniel Hernandez for their contributions to the collagen based nanocomposites project.

I am grateful to the GK-12 Fellowship for providing with the financial and professional support. My special thanks to Dr. Geoffrey Okogbaa, Dr. Tapas Das, Dr. Griselle Centeno and Dr. Martin-Vega for their assistance and guidance in the fellowship. I would like to recognize Dr. Kumar's financial assistance through NSF GK-12 (Grant # 0139348), NSF CAREER (Grant # 9983535) and NSF NIRT grants (Grant # 0404137)

I would like to acknowledge the great people at the ME department: Sue Britten and Shirley Trevor for their administrative help. I would also like to thank my co-workers and friends from the Advanced Materials lab for all their support.

Finally, I would like to thank my friends and family, especially my wife Tara and kids Abdul-Hakim and Abdul-Malik for supporting me throughout this endeavor.

TABLE OF CONTENTS

LIST OF TABLES

LIST OF FIGURES

SYNTHESIS AND CHARACTERIZATION OF INTERFACES BETWEEN NATURALLY DERIVED AND SYNTHETIC NANOSTRUCTURES FOR BIOMEDICAL APPLICATIONS

Souheil Zekri

ABSTRACT

The use of nanotechnology to develop methods for fabrication and characterization of organized hybrid nanostructures that include integrated polymeric, biological and inorganic compounds has increased exponentially during the last decade. Such bio-nano-composite materials could be used in solving current biomedical problems spanning from nanomedicine to tissue engineering and biosensing.

In this dissertation, a systematic study has been carried out on the synthesis, characterization, of two interfaces between naturally derived and synthetic nanostructures. Carbon nanotubes and porous silicon represent the synthetic nanostructures that were developed for the purpose of interfacing with the naturally derived bovine type I collagen and respiratory syncytial virus DNA respectively. Firstly, the synthesis of collagen-carbon nanotubes by two different techniques: fibrillogenesis through slow wet fiber drawing (gelation process) and electrospinning has been highlighted. Characterization of the novel nanocomposite was conducted using electron

microscopy, transmission electron microscopy, Fourier transform infrared spectroscopy, nanoindentation, and Raman spectroscopy. The collagen-carbon nanotube gelation process was found to have superior nanoscale surface mechanical properties that were more conducive to higher osteoblast specific protein expression such as osteocalcin. Applications of the developed nanofibers are detailed in the fields of orthopaedics and tissue engineering. Secondly, an overview of porous silicon synthesized by hydrofluoric acid is presented. A parametric study was performed to determine the optimal pore size was carried out. The use of porous silicon as a biosensor to detect RSV virus by DNA hybridization was then provided and the importance of the interface chemistry was highlighted.

CHAPTER 1: INTRODUCTION

The use of nanotechnology to produce organized nanostructured materials is yielding nanoscale devices with improved and often unique physico-chemical properties which are important for fundamental research and useful in a multitude of applications. Many innovative applications are proving to be of vital importance in the fight against diseases from viral and bacterial source, newly discovered genetic disorders, and many debilitating injuries. Nanotechnology is associated with any controlled process that yields nanometer-scale materials and devices for multiple interdisciplinary applications. Novel methods for fabrication and characterization of organized hybrid nanostructures that include integrated polymeric, biological and inorganic nanocomposites have increased exponentially during the last decade. Bio-nano-composite materials composed of organic matrices such as collagen and synthetic based fillers such as carbon nanotubes could be used in solving current biomedical problems spanning from nanomedicine to tissue engineering and biosensing.

The scientific community has been emphasizing the importance of multidisciplinary research in the field of orthopaedics due to the increase in human life expectancy – at least in the industrialized world- Advances in applications of biomaterials in the field of orthopaedics have seen steadily increasing breakthroughs throughout the 20th century.

Even though the two world wars were the main catalysts for the rapid advancement in orthopaedic surgical procedures and number of applicable biomaterials, increase in longevity of the human population counts as the primary vehicle for the recently observed developments[1]. Tendon, ligament, and joint capsular injuries represent 45% of the 32 million musculoskeletal injuries each year in the United States[2]. Furthermore, since 1990, the total number of hip replacements has been steadily increasing. Joint diseases, rheumatoid arthritis and osteoarthritis, osteoporosis, spinal disorders, low back pain, and severe trauma are among 150 musculoskeletal conditions affecting millions of people globally[3]. As a result, orthopaedic research has increasingly focused on the development of new approaches to improve the methods of correcting musculoskeletal problems. One emerging area of research that is showing promise in the field of orthopaedics is nanotechnology. The use of nanotechnology in orthopaedics focuses on the interaction between the implantable device and the soft or hard skeletal tissues at the molecular level.

Collagen is one of the most studied proteins due to its importance and abundance in mammalian organisms. Vertebrates have at least 20 collagen types with 42 distinct polypeptide chains and more than 20 additional proteins that have collagen-like domains. Collagen-rich extracellular matrices are not only critically important for the biomedical properties of tissues, but are also intimately involved in cell adhesion and migration during growth, differentiation, morphogenesis and wound healing[4]. Most collagens consist of three polypeptide chains, termed α chains, that are characterized by repeating glycine-X-Y sequences. Position X often is occupied by proline and position Y by 4

hydroxyproline (O). The three α chains (which can be identical or different, depending on the collagen type) form a right-handed triple helix, resembling a stiff cable. Glycine is required at every third position to allow the close packing of α chains within the triple helix. Hydroxyproline is required for triple helix stability, but the molecular mechanisms involved in stabilization are subtle and not completely understood[5].

Nanotechnology is a very attractive option in the design of orthopaedic implants. One reason is the potential solution for a recurring problem that troubles orthopaedic surgeons, which is implant loosening due to partial or no osteointegration around the device. It is believed that good initial protein (cell function specific) adhesion to the implanted biomaterial is essential to subsequent bone integration. Proteins such as vitronectin and fibronectin bind on nanoscale surfaces with highly specific properties[6, 7] (i.e. chemistry, charge, wettability, topography). It is also believed that surface roughness is of significant influence for protein interactions[8, 9], and nanophase materials present the promise of optimizing this early interaction. The use of nanophase materials at the organic-inorganic interface of implants, as opposed to the conventional microscale approach, offers a biomimetic approach which allows for tailored nanoscale surface modifications to optimize the interfacial mechanical properties. Research in polymer based nanocomposites has increased exponentially during recent years due to the ability to vary mechanical, electrical, optical and thermal characteristic with nanosize filler within the polymer matrix.[10] In particular, biopolymers nanocomposites are receiving increase attention due to their importance in tissue engineering, drug delivery, and orthopaedics because of the ability to tailor their mechanical and chemical characteristics

for improved osteogenic potential[11, 12]. Single wall carbon nanotube (SWCNT) are 1 to 2 nanometers in diameter and have a Young's modulus reaching as high as 1200 GPa. With an ultimate strength reaching 37 GPa, elongation reaching as high as 6%, and an aspect ratio (length/diameter) larger than 1000, SWCNT are considered to be excellent reinforcing material for polymeric composites[13,14]. Recent years have seen improvements to synthesis and dispersion techniques, which are leading to SWCNT with diminishing defects per unit area. To date, SWCNT loading levels of 1 to 5% in various synthetic polymer matrices have provided improved electrical[15] and mechanical[16, 17] properties; however, it is estimated that aligned SWCNT along the axial direction could improve properties at loadings as low as 0.1%[18]. The self assembly properties of type I collagen offer an attractive medium for the alignment of carbon nanotubes (CNT). The ability to tailor mechanical properties such as ultimate strength, Young's modulus and surface hardness is a definite advantage that carbon nanotubes bring to the nanocomposite as nanofillers. Furthermore, increase in the electrical conductivity of the nanocomposite may play a primary role in increasing cell proliferation when cyclic electrical stimulation is used, especially during the first days after surgery. Despite the evidence of CNT lung cytotoxicity[19, 20], in its unpurified form, there have also been a number of published studies into CNT-based biomaterials, which support the biocompatibility of CNT and CNT-based materials in presence of osteoblast cells[21, 22, 23].

Advances in biology have taken a quantum leap forward after the discovery of DNA in the middle of the twentieth century. DNA is the key molecule in many cellular processes like replication, homologous recombination and transcription. Besides holding

genomic information, DNA exhibits very interesting biophysical and physicochemical properties, which are essential for proper functioning of the biomolecular processes involved. Biochips, particularly those based on DNA are powerful devices that integrate the specificity and selectivity of biological molecules with electronic control and parallel processing of information. This combination will potentially increase the speed and reliability of biological analysis. Microelectronic technology is especially suited for this purpose since it enables low-temperature processing and thus allows fabrication of electronics devices on a wide variety of substances like glass, plastic, stainless steel and silica wafer. Ultra-high micro and meso-cavities on a silicon wafer chip using an electrochemical etching technique and a dry silicon-etching process can be used to fabricate the DNA biochip. Fundamental phenomena like molecular elasticity, binding to protein; super-coiling and electronic conductivity also depends on the numerous possible DNA conformations and can be investigated nowadays on a single molecule level.

Fluorescently labeled oligonucleotide probes are nowadays in much regular use for nucleic acid sequencing[24], sequencing by hybridization[25] (SBH), fluorescence in situ hybridization[26] (FISH), fluorescence resonance energy transfer[27] (FRET), molecular beacons[28], Taqman probes[29], and chip-based DNA arrays[30]. This has made fluorescent probes an important tool for clinical diagnostics and made possible real-time monitoring of oligonucleotide hybridization. Furthermore, fluorescent-based diagnostics avoids the problem of storage, stability, and disposal of radioactive labels[31-32]. DNA nucleotide sequence can be labeled with fluorescence at $5'$ and monitored.

Experiments with single DNA were reported with scanning tunneling microscopy[26,33], fluorescence microscopy[34], fluorescence correlation spectroscopy[26], optical tweezers[27], bead techniques in magnetic fields[35], optical micro fibers[36], electron holography[37] and atomic force microscopy[38,39,40]. All these methods provide direct or indirect information on molecular structure and function.

Knowledge of structural and physical properties in cell and their components is required to obtain a comprehensive understanding of cellular processes and their dynamics. The need for a nondestructive method was satisfied with the development of the Atomic Force Microscope (AFM). The last 15 years have witnessed the extraordinary growth of structural studies in biology, and the impact is being felt in almost all areas of biological research. Several groups have used AFM for the analysis of DNA, protein, and DNA–protein interactions[41]. AFM has been demonstrated to be a powerful and sensitive method for detecting surface-confined DNA molecules at molecular levels[42, 43].

Until recently, electron microscopy was used as the main tool for imaging DNA. However, this technique can be harsh on biological samples, making successful analysis extremely difficult. AFM allowed the analysis of biological molecules to be performed faster, easier and more accurately yielding successful characterization of biological specimens. Various methods can be employed to bind DNA to different hosts. An array of substances, including catalytic antibodies, DNA, RNA, antigens, live bacterial, fungal, plant and animal cells, and whole protozoa, have been encapsulated in silica, organo siloxane and hybrid sol-gel materials. Sol-gel immobilization leads to the formation of

advanced materials that retain highly specific and efficient functionality of the guest biomolecules within the stable host sol-gel matrix[44]. The protective action of the sol-gel cage prevents leaching and enhances their stability significantly. The advantages of these 'living ceramics' might give them applications as optical and electrochemical sensors, diagnostic devices, catalysts, and even bio-artificial organs. With rapid advances in sol-gel precursors, nano engineered polymers, encapsulation protocols and fabrication methods, this technology promises to revolutionize bio- immobilization. Biosensors using immobilized receptors are finding ever-increasing application in a wide variety of fields such as clinical diagnostics, environmental monitoring, food and drinking water safety, and illicit drug monitoring[45]. One of the most challenging aspects in development of these sensors is immobilization and integration of biological molecules in the sensor platform. Numerous techniques, including physical covalent attachment, entrapment in polymer and inorganic matrices, have been explored over the past decade. Sol-gel process are promising host matrices for encapsulation of biomolecules such as enzymes, antibodies, and cells[46]. Porous silicon[47] was discovered in 1956 by Uhlir[48] while performing electro polishing experiments on Silicon wafers using an HF-containing electrolyte. He found that increasing the current over a certain threshold, a partial dissolution of the silicon wafer started to occur. PS formation is then obtained by electrochemical dissolution of silicon wafers in aqueous or ethanoic HF solutions.

Micro and mesocavities are of interest for a wide range of fundamental and applied studies, including investigations of cavity quantum electrodynamics[49], optical elements for telecommunications[50], single-photon sources[51], and chemical or biological sensors[52].

Micro-fabrication techniques allow reproducible fabrication of resonators with lithographically controlled dimensions. Biological sensors fabricated on the nanoscale offer new ways to explore complex biological systems because they are responsive, selective and inexpensive. Two primary advantages make nanoscale PS based DNA biochips a very attractive option: (i) enormous surface area ranges from 90 to 783 m^2/cm^3, which provide numerous sites for potential species to attach[53]. Its room temperature luminescence spans the visible spectrum, which makes it an effective transducer. In case of PS the most commonly used method for binding DNA involves coating of sol-gel material containing DNA on an oxidized silicon surface. The function of tetra-ethyl-ortho-silicate (TEOS) is to provide a stable coupling between two non-bonding surfaces: an inorganic surface to a biomolecule. The most interesting feature of PS is its room temperature visible luminescence. PS mesocavity resonators possess the unique characteristics of line narrowing and luminescence enhancement[54]. The emission peak position is completely tunable by modifying the coating over the surface of porous silicon[55]. The direct epifluorescent Filter Technique (DEFT) is a rapid method for enumerating bacteria. Used widely in the dairy industry for milk and milk products, it has also been applied to beverages, foods, clinical specimens and in environmental research.

A mesocavity DNA biosensor was chosen to diagnose RSV virus because by nature, DNA is highly selective as ssDNA strand pairs only bind to its complementary strand. When two non-complementary strands of DNA are exposed together no binding will occur[56]. In chapter 5, detailed studies of mesocavities on silicon wafer are detailed for immobilization of RSV F gene specific ssDNA with sol-gel coating over silicon surface to develop the probe for the recognition of cDNA by the attached ssDNA. This

dissertation presents a novel optical and mechanical approach to detect DNA hybridization by properly coating over the surface of PS mesocavities with highly selective receptor molecules ssDNA using TEOS to quickly determine the presence of complementary (cDNA). This novel approach is part of the global theme of developing interfaces for biomedical applications –in this case biosensing application- using fabricated nanostructures. Many characterization techniques have been used to determine the viability of the DNA biochip including a Digital Instruments Atomic Force Microscope (AFM) with nanoscope dimension 3000 software, a Hitachi S800 Scanning Electron Microscope (SEM), a Vanox research grade optical microscope, and an SPEX 500M temperature stabilization Photoluminescence (PL) spectrometer.

1.1 Objectives

The objective of this research is to demonstrate the feasibility of producing interfaces between naturally derived and synthetic nanostructures for applications in biomedical fields such as orthopaedics, tissue engineering, and biosensors. The following synthesis and chemico- physical characterization of two such interfaces are presented in this dissertation in the following way:

1. Synthesis of the first interface that consists of type I collagen (fetal bovine source) and single wall carbon nanotubes developed by a gel drying process for orthopaedic bio-insert applications
   - Collagen extraction in a water soluble form.
   - Dilution and suspension of collagen in acetic acid
   - Development of a dispersion technique of SWCNT within the collagen matrix

- Chemico-physical characterization of the nanocomposite
    - ✓ Scanning Electron Microscopy (SEM)
    - ✓ High Resolution Transmission Electron Microscopy (HRTEM)
    - ✓ Raman Spectroscopy
    - ✓ Fourier Transform Infra Red (FTIR)
    - ✓ Differential Scanning Calorimetry (DSC)
    - ✓ Thermal Gravimetry Analysis (TGA)
- Study of the effect of SWCNT concentration on the bulk and surface characteristics of the nanocomposite
    - ✓ Micro tensile testing
    - ✓ Nanoindentation
- In vitro study of the effect of SWCNT on the cytotoxicity and general biocompatibility of the nanocomposite using a cell line derived from human osteoblasts transfected with SV40 T antigen

2. Synthesis of the second interface that consists of type I collagen (fetal bovine source) and single wall carbon nanotubes developed by an electrospinning process for tissue engineering applications
    - Collagen extraction in a water soluble form.
    - Dilution and suspension of collagen in acetic acid
    - Development and optimization of the electrospinning parameters to obtain nanocomposite fibers with desirable diameter range and mechanical strength
    - Chemico-physical characterization of the nanocomposite
        - ✓ Scanning Electron Microscopy (SEM)

- ✓ High Resolution Transmission Electron Microscopy (HRTEM)
- ✓ Raman Spectroscopy
- ✓ Fourier Transform Infra Red (FTIR)

3. Synthesis of the third interface that consists of porous silicon and a Respiratory Syncytial Virus (RSV) single strand DNA for biosensing applications
   - ➢ Fabrication an optimization of n-type porous silicon
   - ➢ Chemico-physical characterization of the nanocomposite
     - ✓ Scanning Electron Microscopy (SEM)
     - ✓ Atomic Force Microscopy (AFM)
     - ✓ Photoluminescence (PL)

1.2 Significance of the Study

Nanotechnology has become one of the main "buss" words of this century for many reasons. Many significant achievements are being made by multidisciplinary scientists and engineers using nanotechnology in different biomedical fields. The developments of methods for fabrication and characterization of organized hybrid nanostructures that include integrated polymeric, biological and inorganic compounds has proven very valuable in positively impacting areas such as orthopaedics, tissue engineering, drug delivery, and biosensors. Figure 1 shows how science and the rapidly emerging new technologies are moving from the more traditional macro based research towards micro and nanotechnology that exists today and that will dominate future industries.

Designing bio-nano-composite materials as interfacial devices using a combination of naturally occurring and synthetic compounds is at the forefront of research in

biomedicine due to the potential that these materials have. One such advantage is the simplicity and the availability of biocompatible inserts that would virtually eliminate the need for tissue and organ transplant from human source. Another advantage materializes in the development of cheaply manufactured biosensing devices that minimize the diagnosis time from several days to a few minutes.

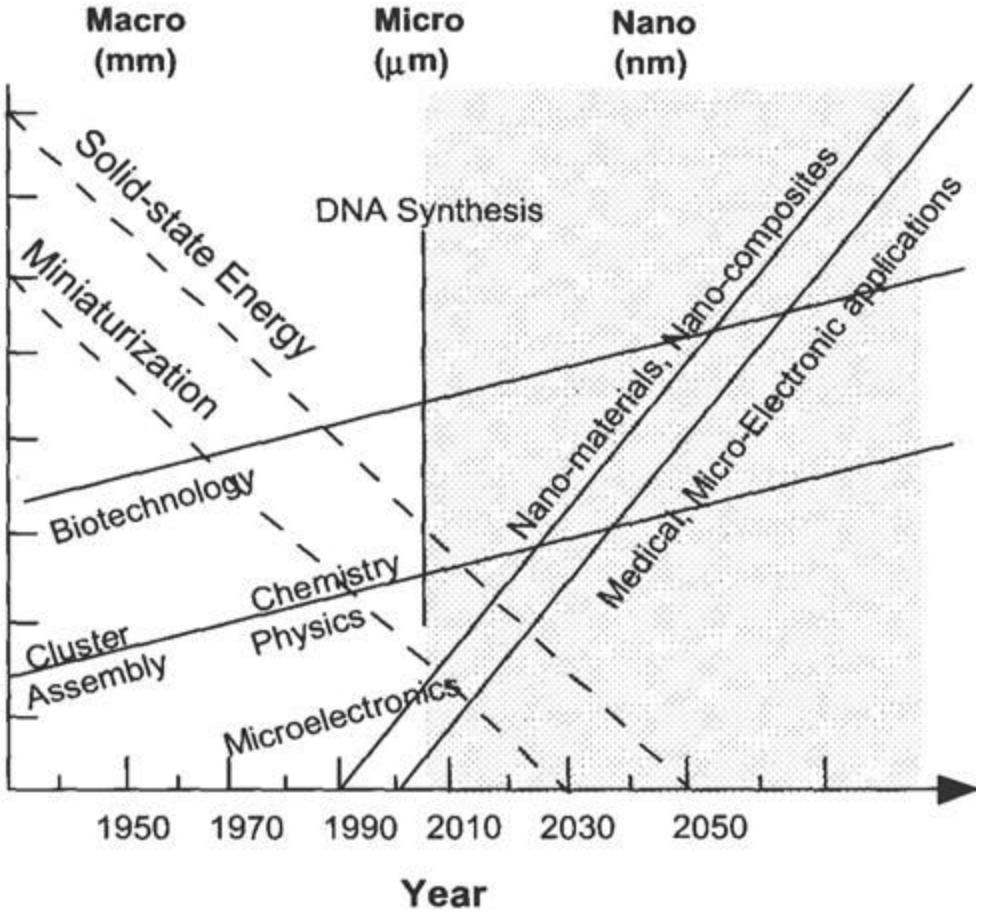

Figure 1: Evolution of science and technology and the future[57].

CHAPTER 2: BACKGROUND AND LITERATURE REVIEW

An overview of the historical background of the developed bio interfaces and the performance of synthetic nanostructures such as carbon nanotubes and porous silicon is provided in this chapter. The importance of using these two materials in such biomedical applications such as orthopaedic, tissue engineering, and biosensing is also detailed.

2.1 Overview of Nanostructures

Nanostructures constitute a class of materials in which at least one-dimension measures within the range of 1 to 100 nm. As the size reaches a critical threshold (typically 1-10 nm) Quantum effects start to appear due to size confinement in nanostructures. These effects give rise to novel and, in some cases, very interesting physico-chemical properties that are completely different from the materials traditional bulk properties. Quantum effects occur when the characteristic size of the object is comparable with the critical lengths of the corresponding physical process, such as the mean free path of electrons. Two-dimensional (2D) quantum wells, one-dimensional (1D) quantum wires, and zero-dimensional (0D) quantum dots are the typical structural forms.

A variety of nanostructures have been fabricated, including tubes, cages, cylindrical wires and rods, co-axial and bi-axial cables, ribbons or belts, sheets, and diskettes[58]. These nanostructures have fascinating properties, and applications that are shifting

certain paradigms in materials science. The ability to generate such minuscule structures is essential to much of newly developed fields such as nanotechnology. There are a large number of opportunities that might be realized by making new types of nanostructures, or simply by down-sizing existing microstructures into the 1-100 nm regime. One very successful example is found in microelectronics. Since the mid 1950's, great improvements were brought to this field, where "smaller" has meant greater performance ever since the invention of integrated circuits. The exponential increase in the number of components per chip lead to faster operation, lower cost, and less power consumption. This model, however is reaching its limit as researchers reach the quantum barriers were novel fabrication techniques and theoretical models have to be developed. Miniaturization may also represent the trend in a range of other technologies. In information storage, for example, there are many active efforts to develop magnetic and optical storage components with critical dimensions as small as tens of nanometers. This could lead to miniature biomedical devices that could be implanted in the body, gather and store large information for future analysis. It is also clear that a wealth of interesting and new phenomena are associated with nanometer-sized structures, with one of the best established examples including the discovery of carbon nanotubes and their superior mechanical properties when compared with the more traditional bulk carbon based material. Another interesting effect of carbon nanotubes is its ability to behave as a conductor, semi-conductor or as an insulator depending on its chiral directions. Two-dimensional (2D) nanostructures have been extensively studied by the semiconductor community because they can be conveniently prepared using chemical vapor and physical vapor deposition techniques which yield thin films with superior surface

properties due to the increase in reactive atoms as compared with the traditional bulk structures.

Recently, one-dimensional (1D) nanostructures such as wires, rods, belts tubes are showing promising results. Such material emerged from nanotechnology procedures developed in recent years and are used in unique biomedical applications such as scaffolds in tissue engineering. Solving complex problems by using nanoscale devices that operate as sensors for diagnostics, and functional mechanical structures for musculoskeletal tissue growth and replacement is an important goal undertaken by current research. Two and three dimensional structures are routinely developed using microelectronic based fabrication techniques such as etching. One such interesting structure is developed by etching silicon and creating pores of tunable dimensions depending on the parameters dictated by the process. Porous silicon is becoming an increasingly important and versatile material in today's fabrication technology. The quantum aspects of porous silicon have been investigated as a prospective optoelectronic material for biosensing applications.

This chapter provides a comprehensive review of the nanostructured materials used as interfaces for biomedical applications such as biosensing, orthopaedics, and tissue engineering. Synthesis, characterization and potential applications of developed nanostructures including meso-porous silicon, carbon nanotube, and collagen fibrils will detailed in following chapters.

2.2 Collagen

By weight, collagen is one of the most abundant proteins accounting for about 30% of all proteins in mammals[59]. Much of the development in collagen related research has occurred in the second half of the twentieth century thanks to the rapid advancements made in the materials characterization techniques. Both microscopic and spectroscopic techniques are usually used to determine the molecular and crystal structure of collagen. The molecular unit constituting collagen is a rigid rod shaped protein of approximately 300 nm in length and 1.5 nm in diameter[60]. In nanotechnology terms, collagen could be branded as a nanorod or nanowire. Many research teams across the globe are developing synthetic structures using biomimetic approaches to copy both the shape and the functional structures of this protein.

The word collagen finds its root in Greek and is divided into *kola* meaning glue and *genēs* meaning born. It is found in multiple genetically distinct polypeptides or chains of amino acids linked together by peptide bonds. The polypeptide chains make up at least 20 distinct collagen types that have multiple functions in different tissues of mammalian organisms. Collagen types are classified based on their supramolecular structure into classes identified by roman numerals. Table 1 shows list the most abundant types with their relative distribution in the organism.

Table 1: The most abundant types of collagen[61].

Type	Chain Composition	Distribution
I	$[\alpha1(I)]_2$ α 2(I)	Skin, bone, tendon, blood vessels, cornea
II	$[\alpha1]_3$[53]	Cartilage, intervertebral disk
III	$[\alpha1]_3$ [53]	Blood vessels, fetal skin

The primary molecular unit in collagen is tropocollagen. In most tropocollagen forms, a triple helix formed by two α1 chains and one α2. In 1994 Helen Berman and Barbara Brodsky confirmed the helical structure using X-ray crystal structure studies[62]. The three polypeptide chains, termed α chains as shown in table 1. The composition of collagen is nearly one-third by the amino acid Glycine (Gly), another 15 to 30 % Proline[63], and lastly by 4-hydroxyprolyl (Hyp). The three α chains (which can be identical or different, depending on the collagen type) form a right-handed triple helix, resembling a stiff cable. Glycine is required at every third position to allow the close packing of α chains within the triple helix. Hydroxyproline is required for triple helix stability, but the molecular mechanisms involved in stabilization are subtle and not completely understood[5].

Collagen is naturally synthesized by mammalian organisms by the initial transcription of a specific messenger-RNA (mRNA)[64]. This process is then followed by the splicing of the gene which yields a functional mRNA that contains about 3000 bases. The mRNA is then transported to the cytoplasm and translated in membrane-bound polysomes to the rough endoplasmic reticulum (RER) where the polypeptides are synthesized. During this

process, important co-translational events occur including the prolyl and lysyl hydroxylases enzymatic reactions which yield the hydroxylation of proline and lysine. Additional enzymatic reactions associated with orienting pro-α chains in the correct chain registration and triple helix formation also occur. The molecules are the brought to the Golgi apparatus, still within the cell, through the microsomal lumen. The molecules are then packed into secretory vesicles and translocated to the surface of the cell, where they are secreted outside the cell membrane by exocytosis[65]. Once the collagen molecules are in the extra cellular matrix (ECM), further enzymatic reactions take place and the units start aligning in a crystalline formation which yields crosslinked fibrils. The crosslinking is initiated by the enzyme lysyl oxidase, which produces a delamination of certain lysine and hydroxylysine residues located at the end of the helical regions. Bi-functional cross-links undergo further intra and intermolecular reactions to form a variety of mature, tri-functional cross-links. In cross-link diversity lie the major differences between skeletal and non-skeletal connective tissues[66]. The subject of synthetic isolation of tropocollagen molecules and the introduction of novel biocompatible crosslinking agents will be detailed further in chapter 3.

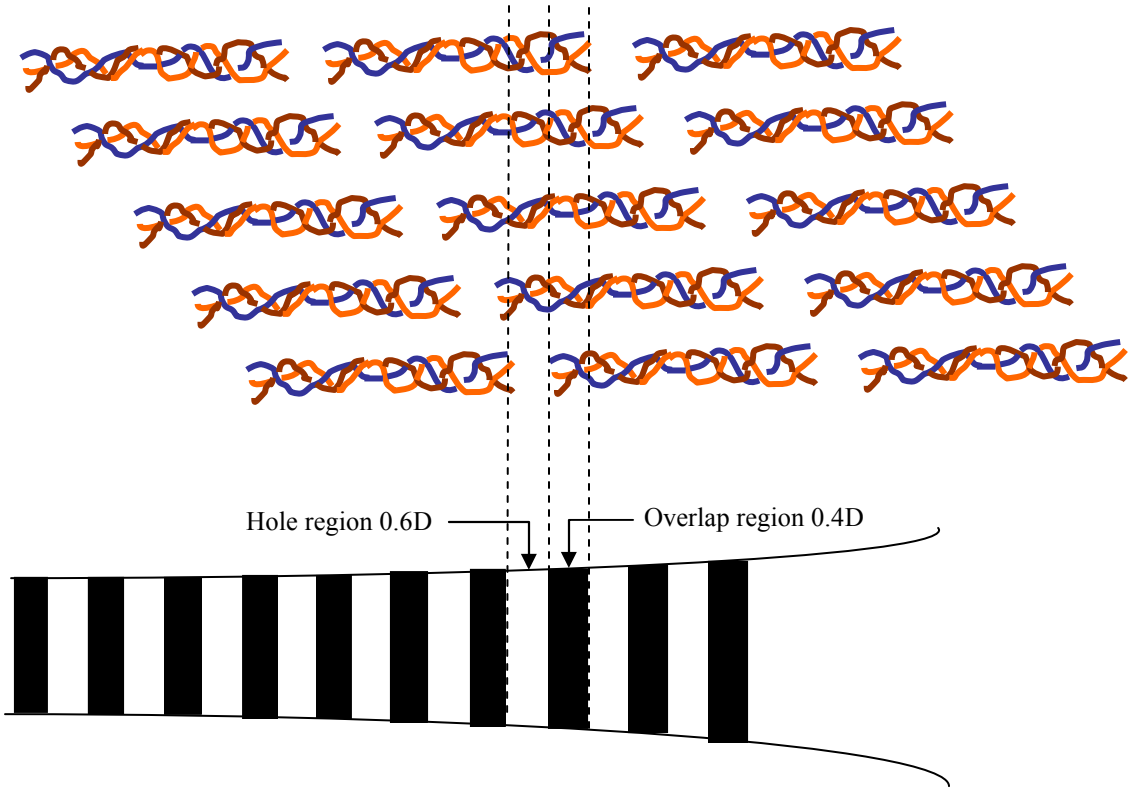

Figure 2: Illustration of the characteristic packing of fibril like collagen molecules.

An illustration of the triple helix with the characteristic banded appearance is shown in figure 2. The gap between triple helices is actually a hydrogen bond formed between residues of different chains. Type I, II, III, V, and XI collagens form distinctive banded fibrils, which is a crystalline structure composed of the repeating amino acid chains. The highly organized crystalline structure of these fibrils provides structural support for the different tissues where collagen is a main component (i.e. skeleton, skin, fibrous capsules of organs, blood vessels, nerves, intestines, and fibrous capsules of organs)[64]. The organization of the fibrils into bundles and lamellae, and the supramolecular arrangements of these fibrils give rise to highly specific biomechanical characteristics and other biological properties[63].

The importance of collagen as a biomaterial is evident when we consider its chemical and biophysical properties. Solubility in water, biomechanical strength, mediation of intercellular interactions, controllable stability, biodegradability and low immunogenicity are only few of the collagen's favorable properties, which are attractive in biomimetic applications and interfacial solutions between organic and inorganic materials. One biomechanical property found in certain types of fibrillar collagen is the high tensile strength and minimal extensibility that depends on the amount of insoluble collagen present and the interaction with glycoproteins and proteoglycans. In other words, the fibrillar nature of the collagen coupled with the crosslinking chemistry defines the nonlinear spring-dashpot like mechanical behavior that collagenous tissues exhibit. Therefore, collagen has the capability of transmitting tensile (tendon) and compressive (cartilage) forces of great magnitudes[67]. The arrangement of collagen fibrils differ depending on the biomechanical demands of the tissue. Tendons and ligaments for instances mainly require tensile strength. For this reason collagen fibrils are found stacked in parallel bundles in the aforementioned tissues. Collagen in skin, on the other hand, forms in sheets of fibrils layered at many angles which provide an anisotropic elastic characteristic. It is important to note that most laminated composites developed by engineers follow this biomimetic approach to achieve the anisotropy needed for different manufacturing applications. Collagen formation in the cornea follows a planar sheet design stacked crossways in order to minimize light scattering. Finally collagen molecules in cartilage do not display any distinct arrangement. All these examples of collagen fibril construction are optimized for different biomechanical stresses in any of the one, two or three dimensions.

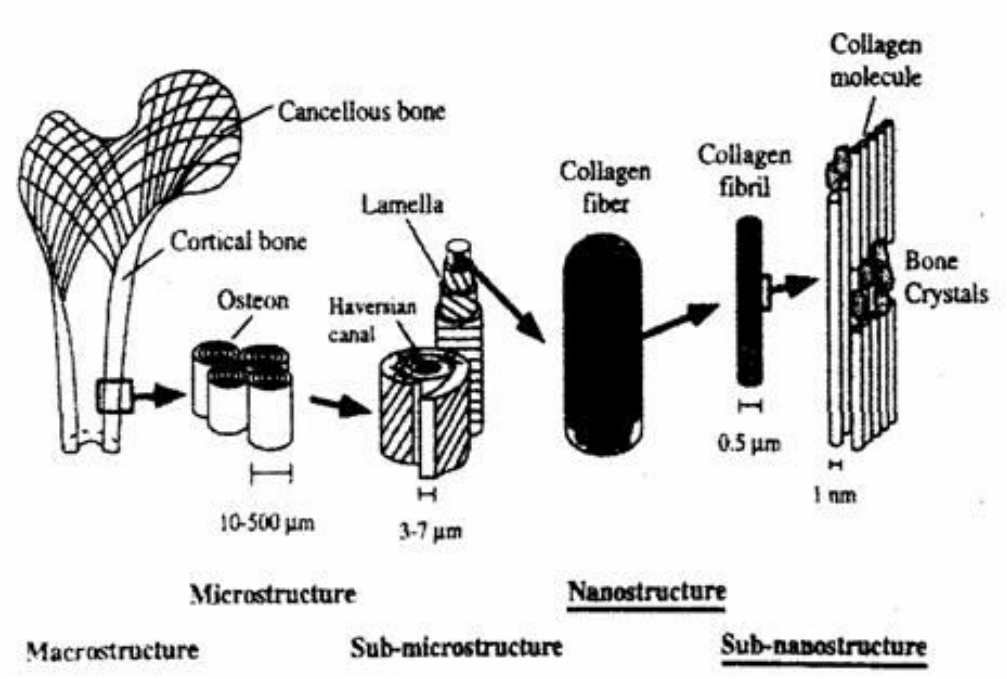

Figure 3: Macro, micro and nano organization of type I collagen in bone[68].

Figure 3 illustrates the organization of type I collagen from the nanoscale up to the macro scale in bone. The formation of specific arrays of collagen fibrils is not yet understood. However, it is possible to achieve certain fibril alignments by putting certain physical constraints on the collagenous structure during fibrillogenesis.

As mentioned above, the chemical and resulting biomechanical properties of collagen directly depend on the presence of covalent cross-links. This binding between tropocollagen molecules provides a tunable factor that controls the biomechanical stability of the fibers. There are two types of crosslinking schemes: intramolecular (within the molecule) and in intermolecular (between molecules).

In this dissertation, the author used Nordihydroguaiaretic acid NDGA as a biocompatible intermolecular crosslinking agent as detailed by Koob et al[69].

The biodegradability of collagen provides a solution for multiple biomedical problems including drug delivery and scaffolding for tissue engineering applications. The enzyme collagenase biodegrades collagen in-vitro, which produces cleavages under physiological conditions of pH and temperature[70]. This cleavage process is used as a biological mechanism that, concomitantly with collagen biosynthesis, control growth, morphogenesis, and repair, it also provides flexibility to the assembly process.

One of the major benefits of collagen as a biocompatible material is its low immunogenicity, or likelihood of triggering an immune response within the hosting organism. This characteristic is even more enhanced when collagen is in its purest non denatured form. In summary, collagen displays favorable biochemical and biomechanical properties, which result in this material being used extensively in many interfacial applications.

2.3 Carbon Nanotubes

Crystalline carbon has two well known forms, namely: Diamond and graphite. Diamond is formed by a three dimensional network of sp^3 carbon atom bonds. Graphite, on the other hand, displays an in-plane sp^2 bond structure that forms sheets of six-member benzene ring. A new class of carbon structures has been synthetically derived by Chemical Vapor Deposition (CVD) methods. In 1985, fullerene allotropes formed by

closed cage carbon molecules in a spherical shape were discovered by Kroto et al[71]. The best known example of these fullerene structures is the C_{60}, which displays a truncated icosahedral structure formed by twelve pentagonal rings and twenty benzene rings. Figure 4a shows a schematic representation of a C_{60} nanostructure. Five years after the discovery of fullerene structures, Krätschmer et al[72] discovered that soot produced by arcing graphite electrodes contained C_{60} nanostructure among other fullerene compounds. This lead to an explosion in fullerene related research due to the ability to inexpensively produce them in gram quantities in a laboratory setting. Using the same simple apparatus, carbon nanotubes (CNT) were discovered by Iijima[53] as elongated fullerenes in 1991. Since then research on growth, characterization and application development has exploded due to the unique electronic and extraordinary mechanical properties of CNTs. The CNT can be metallic, semiconducting or insulating depending on the directional vector of its graphitic disposition. This chiral vector is defined by two variables (n,m), where n and m are two integers. Figure 4a shows how carbon nanotubes could have different atomic distributions depending on the way it is formed from a graphite sheet.

This offers possibilities to create semiconductor–semiconductor and semiconductor–metal junctions useful in devices. At the present, carbon nanotubes have been produced primarily by arc discharge, laser ablation, and catalyzed chemical vapor deposition (CVD)[73]. Chemical vapor deposition techniques have been used widely in silicon based microelectronics manufacturing to grow a variety of thin films with a wide range of electro-mechanical properties.

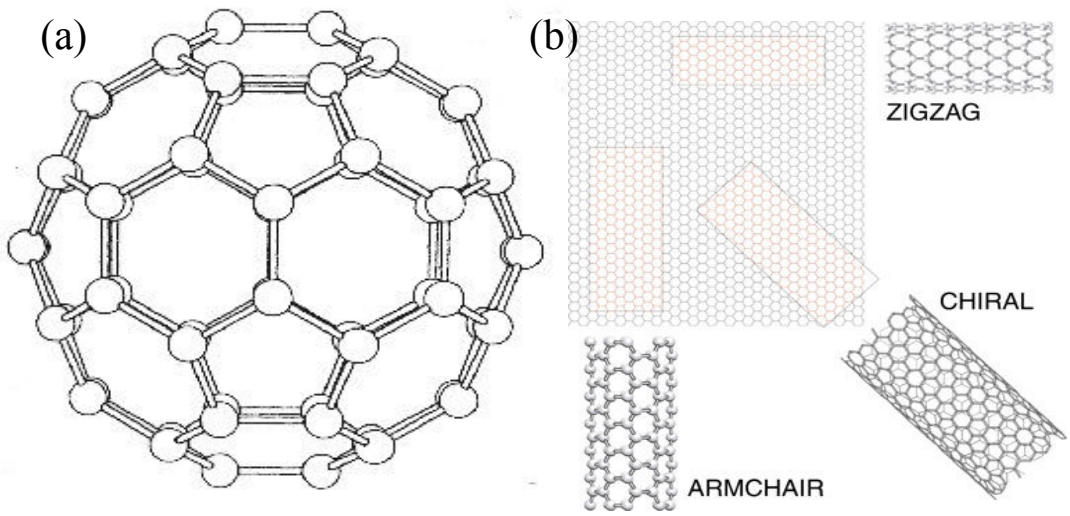

Figure 4: Schematic representation of a C_{60} fullerene structure (a) and three possible single wall nanotube structures from one graphite sheet (b)[71,74].

Typical CVD relies on thermal generation of active radicals from a precursor gas which leads to the deposition of the desired elemental or compound film on a substrate. Glow discharge is often used to grow films at a lower temperature by dissociating the precursor with the aid of highly energetic electrons. In either case, catalysts are almost never required. In the case of carbon nanotubes, a transition metal catalyst is necessary to grow these one-dimensional nanostructures from some form of hydrocarbon (CH_4, C_2H_2, C_2H_4 etc…). Another way of producing carbon nanotubes is accomplished by using another type of CVD reactor called thermal CVD. This system is simple and inexpensive to construct, and consists of a quartz tube enclosed in a furnace. Usually, quartz tubes of 1 or 2" diameter are used, which are capable of holding small substrates. The substrate material may be Si, mica, quartz, or alumina. The setup is equipped with auxiliary components that are needed to control the mass flow and pressure transducer within the

tube. The growth temperature is in the range of 700-900° C. To grow single wall carbon nanotubes, a theoretical study suggests that a high kinetic energy is needed, which translates into temperatures exceeding 900° C and low supply of carbon are necessary to form SWCNTs[75]. Carbon monoxide and methane are the main gases used to grow SWCNTs in a thermal CVD environment. MWCNTs are grown using CO, CH_4 as well as other higher hydrocarbons at lower temperatures 600-750°C. Figure 5a shows an ASTeX MPCVD system found in the advanced materials laboratory of the University of South Florida. This system is routinely used to grow MWCNT and carbon fibers. Figure 5b shows a one stage furnace CVD system that is also used in the laboratory to grow SWCNTs and MWCNTs.

(a) (b)

Figure 5: An ASTeX MPCVD system (a), and a one stage furnace CVD system (b) for carbon nanotube growth.

As mentioned earlier, CNT growth requires a transition metal catalyst. The type of catalyst, particle size, and the catalyst preparation techniques dictate the yield and quality of CNTs and this will be covered in more detail shortly. There has been several catalyst preparation techniques reported in literature. Cassell et al[76] reported a recipe based on a liquid-phase catalyst precursor solutions that was printed onto iridium-coated silicon

substrates. The catalyst precursor solutions were composed of inorganic salts and a removable triblock copolymer $(EO)_{20}(PO)_{70}(EO)_{20}$ (EO = ethylene oxide, PO = propylene oxide) structure. Following a long catalyst preparation, a CVD reaction is initiated to grow nanotube towers with millions of multiwalled tubes supporting each other by van der Waals force. If the catalyst solution forms a ring during annealing, then a hollow tower results. Several variations of solution based techniques have been reported in the literature. Although all these liquid-based catalysts have done remarkably well in growing carbon nanotubes, a common problem emerged due to the difficulty in confining the catalyst from solutions within small patterns. Another problem is the excessive time required to prepare the catalyst. A typical solution based technique for catalyst preparation involves several steps lasting hours. In contrast, physical processes such as sputtering and e-beam deposition, not only can deal with very small patterns but are also quick and simple in practice[77,78]. Delzeit et al reported catalyst preparation using ion beam sputtering wherein an under layer of Al (~ 10 nm) is deposited first, followed by 1 nm of Fe active catalyst layer[79]. Figure 6 shows a patterned sample of SWCNTs grown by thermal CVD on a 400 mesh TEM grid used to pattern the substrate. Methane feedstock at 900° C was used to produce these nanotubes. This procedure yields SWCNTs when using a high processing temperature such as 900° C grown by thermal CVD. The same catalyst formulation at 750° C with ethylene as the source gas yields MWCNT.

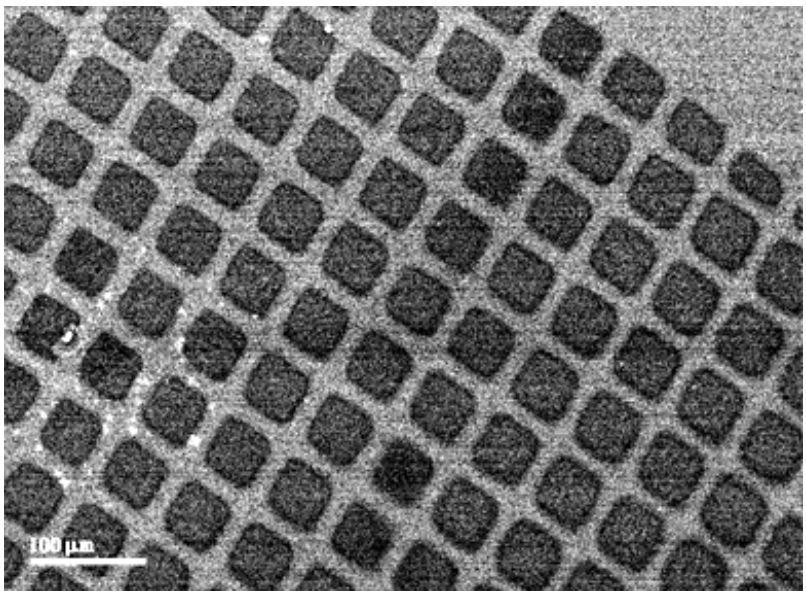

Figure 6: SWCNTs grown by thermal CVD on a 400 mesh TEM grid used to pattern the substrate[79].

A more recent approach in growing patterned arrays of carbon nanotubes involves the use of a nanochannel alumina template for catalyst patterning[80]. The process used in Papadopoulos et al involves the anodization of aluminum on a substrate such as Si or quartz which provides ordered, vertical pores. Anodizing conditions are varied to tailor the pore diameter, height and spacing between pores. This is followed by electrochemical deposition of a cobalt catalyst at the bottom of the pores. The catalyst is activated by reduction at 600° C for 4-5 hours. Figure 7A shows schematic diagram of a typical fabrication process flow of patterned carbon nanotube growth on aluminum oxide anodized nanotemplate**.** Figure 7B shows an example of a resulting ordered array of MWCNTs (mean diameter 47 nm) grown by CVD from 10% acetylene in nitrogen. The use of a template not only provides uniformity but also vertically oriented nanotubes.

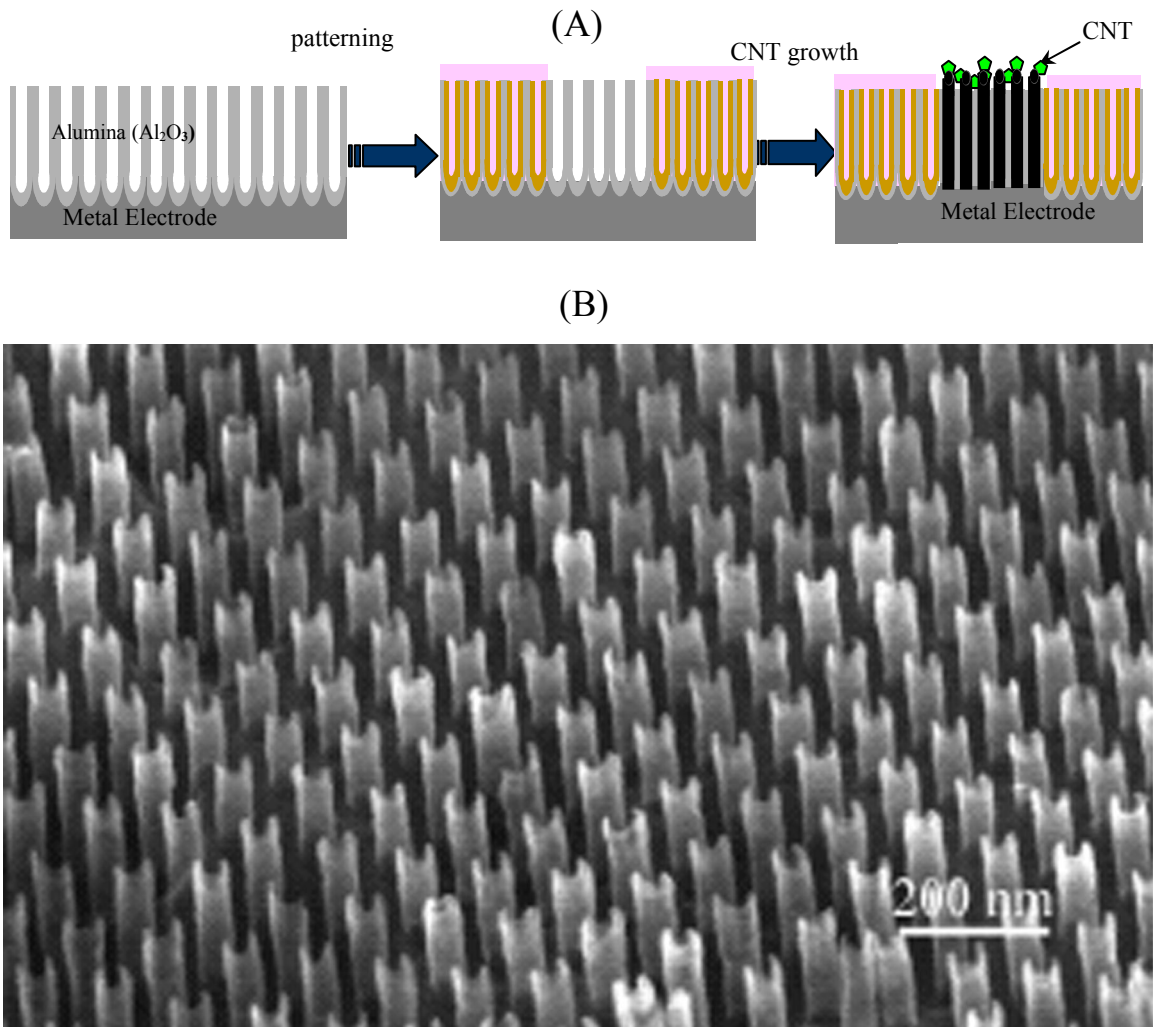

Figure 7: (A) schematic diagram of a typical fabrication process flow of patterned carbon nanotube growth on aluminum oxide anodized nanotemplate. (B) Ordered array of multi wall carbon nanotubes grown from an anodized aluminum template[80].

Anodization coupled with other microelectronics fabrication techniques such as thin film deposition, pattern etching, and physical vapor deposition leads to fairly precise development of arrays of carbon nanotubes for applications as bio and environmental sensors. One example schematic of such a design is shown in figure 8. The very large aspect ratio and dense structure of carbon nanotubes provides improved sensitivity when compared to micro structure based biosensors.

Nanotechnology has produced novel materials such as carbon nanotubes and fullerene nanospheres that feature amazing mechanical properties. Carbon fibers are another example of carbon based nanostructure that brought an important addition to the arsenal of engineering materials during the 20th century. These fibers possess an elastic modulus ranging between 200 and 300 GPa and an ultimate strength of about 3.5 GPa at a density of 1.8 g/cc[81]. The demand for carbon-based fibers as fillers in composites increased dramatically due to the weight saving versus the increase in mechanical strength. Historically, a general approach to improve the strength of fibers is to reduce the probability of radial defects by reducing the fiber diameter.

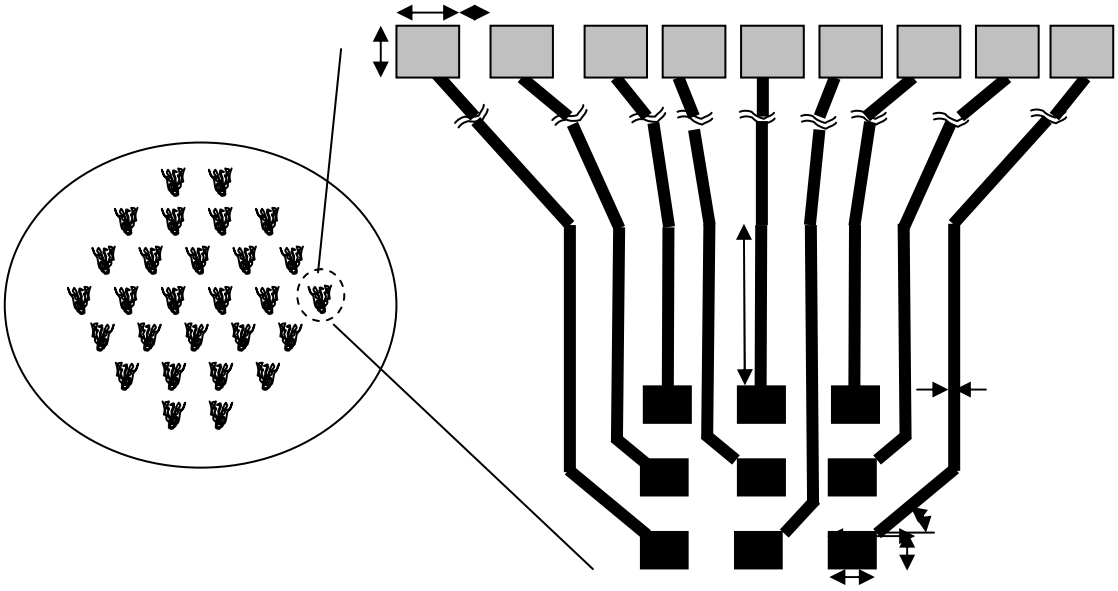

Figure 8: Carbon nanotube based pattern for biosensing applications.

The recent development in advance materials with the advent of carbon nanotubes helped scales down the diameter of carbon fibers down to the nanometer range (1 to several nanometers in diameter). Nanofillers such as carbon nanotubes, and more

specifically single wall and multi wall carbon nanotubes have been widely investigated as multifunctional materials due to their remarkable electrical, thermal and mechanical properties. Single wall carbon nanotube tubes are 1 to 2 nanometers in diameter and have a Young's modulus reaching as high as 1200 GPa. With an ultimate strength reaching 37 GPa, elongation reaching as high as 6%, and an aspect ratio (length/diameter) larger than 1000, SWCNT are considered to be excellent reinforcing material for polymeric composites.[13] The excellent elasto-mechanical properties of single and multi-wall nanotubes is due to the two dimensional arrangement of carbon atoms in a graphene sheet, which allows large out-of-plane distortions. The strength of carbon-carbon in-plane bonds, on the other hand, keeps the graphene sheet exceptionally strong against any in-plane distortion or fracture. These structural and materials characteristics of nanotubes point towards their possible use in making next generation of extremely lightweight but highly elastic and very strong composite materials.

Recent years have seen improvements to synthesis and dispersion techniques, which are leading to SWCNT with diminishing defects per unit area. The high tensile strength, Young's modulus and other mechanical properties hold promise for high strength composites for structural applications especially in biomedical applications that require load bearing structures to support injured or severed biological components that use to bear axial stresses such as tendons and ligaments. Furthermore, carbon nanotubes could help solve interfacial adhesion problems between synthetically designed material and biological matrices. This could be further evident in inserting soft tissues such as tendons in bone tunnels similar to the naturally occurring insertions between muscles and bones.

More specifically, the high aspect ratio and very small diameter of single wall carbon nanotubes could help osteoblast or bone forming cells attach around a synthetically designed tendon.

A large portion of carbon related research is focused on the use of carbon nanotubes as reinforcing nanostructures in composite materials. Theoretical modeling and experimental work has been done on CNT-polymer composites. Several experiments, for examples, have been conducted to determine the mechanical properties of multiwall carbon nanotube-polymer composites[82-84]. Wagner et al studied the fragmentation of MWCNTs experimentally within thin polymeric films composed of urethane/diacrylate oligomer EBECRYL 4858 under compressive and tensile strain. They found that the nanotube-polymer interfacial shear stress was of the order of 500MPa, which is much larger than that of conventional fibers with polymer matrix. The team then suggested the possibility of chemical bonds existing between the multiwall nanotubes and the polymer in the composite. However, the nature of the bonding is not clearly known.

Lourie et al[85] have studied the fragmentation of single-walled CNT within conventional epoxy resin under tensile stress. Their experiment displayed findings that were consistent in suggesting a good bonding between the nanotube and the polymer in the sample. Shanmugharaj et al[86], on the other hand, investigated the influence of silane functionalized carbon nanotubes on the rheometric and mechanical properties of natural rubber vulcanizates. They deduced from different characterization techniques such as Raman, FTIR, and XRD that rheometric properties like scorch time and optimum cure

time increase. Modulus and tensile strength also increase due to higher polymer-filler interaction between the carbon nanotube and natural rubber vulcanizates.

The growing process of carbon nanotubes yields an unpurified form that includes a mixture of SWCNTs, MWCNTs, amorphous carbon and catalyst metal particles. Purification is then necessary to eliminate the unwanted constituents the ratio of which varies from process to process and depends on growth conditions for a given process. Single wall carbon nanotubes are known to need the most purification because of their very small size. One of the highest quality methods of producing CNTs is the high-pressure carbon monoxide (HiPco) which was invented by the Smalley group[87]. This method also requires a purification method that involves the use of concentrated acids such as HCl and HNO_3 to remove iron and graphite residues. The resulting suspension is transferred into centrifuge tubes and spun to collect the residues. After pouring off the supernatant, the solid is re-suspended and spun several times in deionized water (DI). Next, the solid is treated with NaOH and centrifuged for again. This process yields nanotube bundles with tube ends capped by half fullerenes. The product is finally dried overnight in a vacuum oven. One major problem is that purification methods available in literature yield a fairly low percentage of carbon nanotubes since much of the initial amount is washed away along with impurities. Functionalization of nanotubes is an option taken by many researching groups to improve the sensitivity and selectivity of biosensors based on carbon nanotubes. Chemical groups such as carboxyl, amine, and others are covalently attached to the nanotube sidewalls in an attempted to modify the properties required for specific applications. Other than the improvement in sensitivity of

biosensor, chemical modification of the sidewalls may improve the adhesion characteristics of nanotubes in a host polymer matrix to make functional composites, although this is strictly dependent on the type of polymer used and the type of functionalization chemistry. This is due to the matrix-to-nanotube load transfer that is found to have a major effect on the extent of nanotubes-induced stiffening and strengthening particularly in the cases when the loads have a component in a direction normal to the nanotubes axis. Figure 9 shows a schematic of the steps taken to functionalize SWCNT with a carboxyl group for a biosensing application.

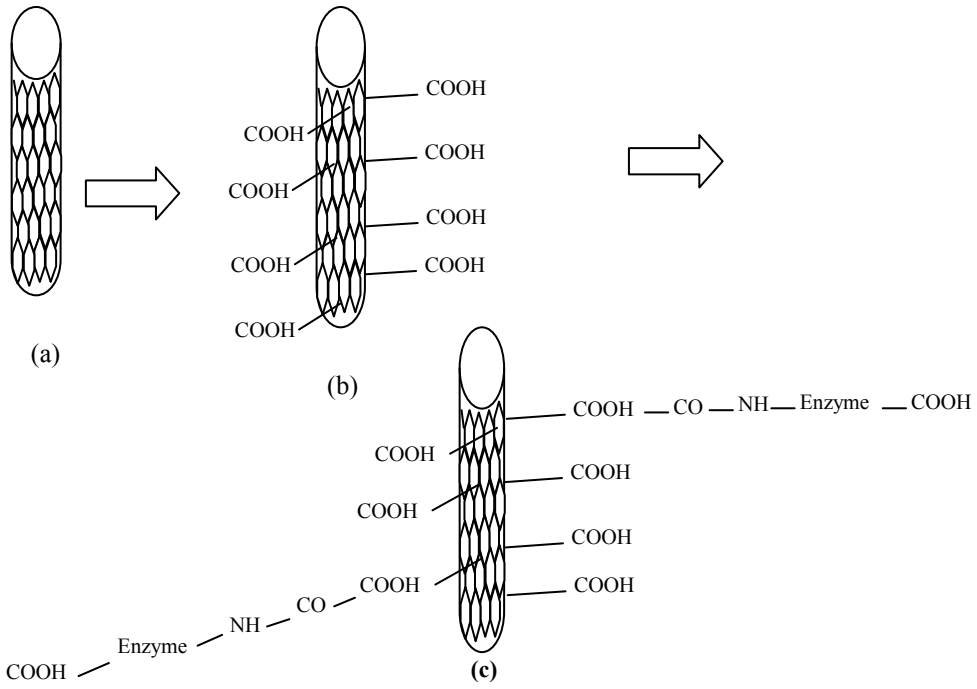

Figure 9: Schematic representing the functionalization procedure of carbon nanotube (MWCNT)/ carbon fiber (a) CNT, (b) functionalization of CNT with carboxyl group, (c) covalent attachment of enzyme to the carboxyl group to make it highly specific for target molecule.

Fourier transform spectroscopy is a measurement technique that produces spectra collected from measurements of the temporal coherence of a radiative source. Using time-domain measurements of the electromagnetic radiation or certain type of radiation,

it is possible to gain a qualitative understanding of the nature of the atomic bonds within a target material. Figure 10 shows sample spectra of pure SWCNT and functionalized SWCNT with a carboxyl group. A clear distinction between the two spectra could be observed due to the introduction of carbon C-O, O-O, and O-H covalent bonds to the benzene ring on the SWCNT surface, which changes the vibration frequencies reflected from two samples.

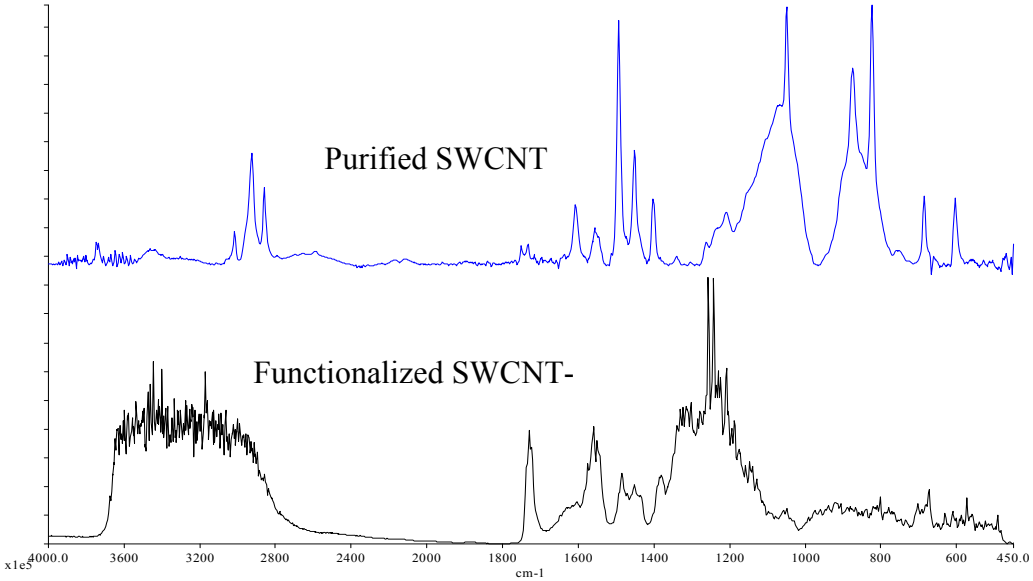

Figure 10: Fourier Transform Infra Red (FTIR) spectra of purified SWCNT and carboxyl functionalized SWCNT.

As mentioned earlier, Shanmugharaj et al[86] showed that modulus and tensile strength of MWCNTs increase due to higher polymer-filler interaction between the carbon nanotubes and vulcanized rubber thanks to surface functionalization carried out by acid treatment and followed by reaction with multifunctional silane, 3-aminopropyltriethoxysilane. Garg et al,[88] on the other hand, found that covalent chemical attachments, in certain instances, decrease the maximum buckling force by about 15% regardless of tubule helical structure or radius.

The combination of CNT functionalization and use as polymer matrix filler is yielding promising results in recent research. Schadler et al[89] focused more on the mechanical properties of specific CNT weight ratios. They investigated the tensile and compressive behavior of 5 wt. % MWNTs within epoxy matrix by measuring the Raman peak shift when the composites are under compression and or under tension. The tensile modulus of the composites, in this experiment, was found to enhance much less than the enhancement of the same composite under compression. This difference has been attributed to the sliding of inner shells of the MWNTs when a tensile stress was applied. In cases of SWNT polymer composites, the possible sliding of individual tubes in the SWCNT rope may also reduce the efficiency of load transfer. It is suggested that for the SWNT rope case, interlocking using polymer molecules might bond SWCNT rope more strongly. Andrews et al[82] have also studied the composites of 5 wt. % of SWNT embedded in petroleum pitch matrix and their measurements show an enhancement of the Young's modulus of the composite under tensile stress.

It is also important to mention that the range of SWCNT and MWCNT used in the majority of nanocomposite research falls within the range between a fraction of a percent and 5 to 10 percent. Measurements by Qian et al[90] of a 1 wt. % MWNT-polystyrene composite under tensile stress also show a 36% increase of Young's modulus compared with the pure polymer system. The possible sliding of inner shells in MWCT and of individual tubes in a SWNT rope is not discussed in the above two studies. There are currently no extensive characterization studies in literature available on SWCNT-polymer composites, especially nanocomposites with biopolymers.

To date, SWCNT loading levels of 1 to 5% in various synthetic polymer matrices have provided improved electrical and mechanical properties[15]; however, it is estimated that aligned SWCNT along the axial direction could improve properties at loadings as low as 0.1%.[18] The self assembly properties of type I collagen offer an attractive medium for the alignment of CNTs. The ability to tailor mechanical properties such as ultimate strength, Young's modulus and surface hardness is a definite advantage that carbon nanotubes bring to the nanocomposite as nanofillers. Furthermore, increase in the electrical conductivity of the nanocomposite may play a primary role in increasing cell proliferation when cyclic electrical stimulation is used, especially during the first days after surgery. Despite the evidence of CNT lung cytotoxicity[91], in its unpurified form, there have also been a number of published studies into CNT-based biomaterials, which support the biocompatibility of CNT and CNT-based materials in presence of osteoblast cells[21].

It is evident that carbon nanotube based biocomposites will eventually improve the design and properties of implants where optimum mechanical strength and durability are critical. Presently, nano-structured surfaces represent a very active field of research and development, which may ultimately lead to improved biocompatibility of nanomaterials. New materials, including nanotubes, nanospheres, and nanowire structures may improve mechanical properties and biocompatibility of implants and will allow new approaches in drug targeting.[92]

2.4 Porous Silicon

Porous silicon (PS) has been investigated for over 40 years. The first report came during the electro polishing of silicon in aqueous hydrofluoric acid when Uhlir discovered a new porous structure in1956[48]. Following this discovery, many researchers starting extensively investigating the different properties and processing techniques to produce PS for different applications. During the 1990's, researchers started to focus more on silicon, which was already a well-known semiconducting material. The enormous increase in interest was triggering by a paper written by Dr Leigh Canham (Defense Research and Evaluation Agency, UK) who observed a bright red photoluminescence from the surface of electrochemically etched Si wafer[93]. Silicon was originally considered as a suitable material for electronic applications (local insulation, gettering of impurities, sacrificial layers, etc.) but never in relation with optical applications. Thanks to the introduction of tunable energy band gap to silicon, by introducing a certain degree of porosity, different photoluminescence spectra could be obtain depending on the pore structures.

Recently, a lot of investigations have been carried out in modeling the growth and pore formation of PS layer on p-type Si wafer[49,94-98]. Pascual et al[98] proposed a theoretical model concerning initial pore nucleation, which takes place during the first minutes of the anodization (pore incubation stage). This nucleation step is later followed by dissolution of silicon mass through two competitive processes. Some part gets lost through electrochemical etching and the remaining part gets dissolved chemically. Kwon et al[99] checked the validity of some of the propositions in case of anodization in light on

n-type silicon. Kwon et al studied the pore formation process by scanning electron microscopy (SEM) in conjunction with the corresponding PL spectra from the porous surface. An initial pore incubation period was registered during the first 60 seconds followed by a nucleation process that dominated over pore propagation. Chemical dissolution of silicon ran in parallel with the electrochemical loss which led to a direct correlation between PS surface roughness increases and etching time. One of the important aspects of electrochemical etching of silicon is the ability to tune current density to obtain a target pore size that follows a specific crystallographic orientation.

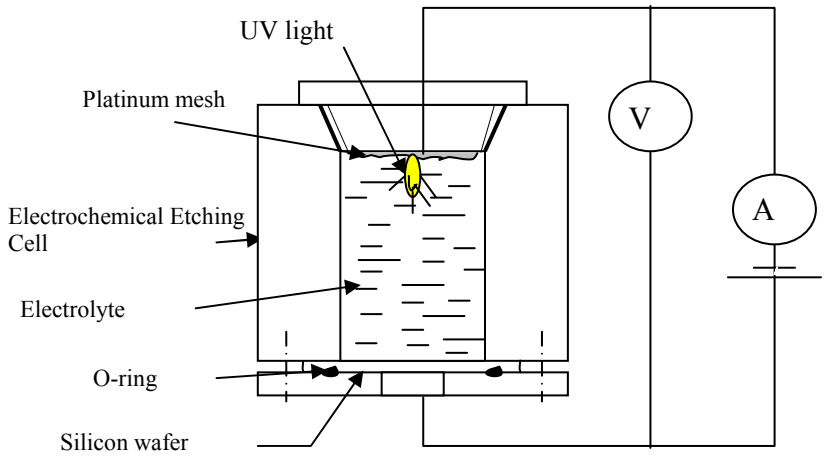

Figure 11: Schematic set for porous silicon preparation.

The simplicity of the apparatus needed to produce PS is one of the advantages that make the process very accessible. Figure 11 shows a schematic representation of the different components that exist in an electrochemical etching cell used for porous silicon preparation. In the representation shown above, the silicon wafer is the anode. This is done by sputtering a layer of gold or aluminum thin film on the back side of the silicon

wafer. The cathode is the platinum mesh that is setup at the top of the cell. There are many electrolytes used to etch silicon. Table 2 shows a group of silicon etchings agents with specific physical characteristics that these agents engender. Because these agents etch silicon differently, a specific mixture of high purity hydrofluoric acid (HF) and 40% aqueous solution diluted in ethanol (C_2H_5OH) has been optimized to produces the characteristic pore structures through silicon. In order to create lateral uniformity in the hollow cylindrical shape of the pores, dilution is necessary in an ethanoic environment because silicon displays a certain degree of hydrophobicity which needs to be overcome for the solution to infiltrate the cavities.

In addition, ethanol decreases the surface tension on the pore walls, which allow for extracting hydrogen bubbles that are formed as a byproduct of the HF etching. Furthermore, the electrochemical cell design and increase in the solution viscosity could improve the hydrogen bubble removal rate. Due to the use of highly corrosive acids in the etching process, the cell body has to be made of materials such as Teflon, which resists the effect of HF. One advantage of the cylindrical geometry shown in figure 11 is the relative uniformity in the etching rate across the silicon wafer. The main requirements for porosity to occur are linked with three important rules. The first has to do with the anodization bias. Forward biasing is applied to p-type and reverse biasing for n-type doped silicon. UV light has to be applied to n-type and current density below a certain critical value must be used.

Table 2: Summery of different physical characteristics resulting from commonly used wet Si etching agents[100].

Comparison of Example Silicon Wet Etchants				
	HNA ($HF+HNO_3$ +Acetic Acid)	Alkali-OH	EDP (ethylene diamine pyrocha-techol)	TMAH (tetramethyl-ammonium hydroxide)
Anisotropic	No	Yes	Yes	Yes
Availability	Common	Common	Moderate	Moderate
Si etch rate µm/min	1 to 3	1 to 2	1 to 30	About 1
Si roughness	Low	Low	Low	F(wt% of TMAH)
Nitride etch	Low	Low	Low	1 to 10 nm/min
Oxide etch	10 to 30 nm/min	1 to 10 nm/min	1 to 80 nm/min	About 1nm/min

All of these three conditions are important in the formation of PS which is a self regulating process. A current density beyond the critical value, for example would increase the hole formation to an extent where surface etching will take place much fast than pores and electro polishing would occur. Figure 12 shows a scanning electron microscopy image of the surface and cross section areas of p-type porous silicon. Many parameters are involved in determining the removal rates, the size and shape of the pores. The amount of n-type or p-type doping is one of the parameters influencing the profile of pores due to the resistivity factor of the wafers. As mentioned above, current density greatly impacts the size and thus porosity of silicon. HF concentration, ambient humidity, drying conditions, illumination and etching time are other important parameters involved in determining the primary characteristics of pore structures.

Several different mechanisms have been proposed regarding the dissolution chemistry of silicon.[101,102] Amongst the various models proposed for the silicon dissolution reactions, the mechanism presented by Lehmann and Gösele[103] is the most accepted in current literature. The mechanism is based on a surface bound oxidation scheme, with hole capture, and subsequent electron injection, which leads to the divalent Si oxidation state that is shown in the following equation:

$$Si + 6HF \rightarrow H_2SiF_6 + H_2 + 2H^+ + 2e^- \qquad \text{Equation 1}$$

According to the model, the Si hydride bonds passivate the Si surface unless a hole is available. Once PS is formed, the interpore region is depleted of holes as evidenced by the high resistivity of PS. Further dissolution occurs only at the pore tips, where enough holes are available. In this way the etching of PS proceeds in depth with an overall directionality which follows the anodic current paths inside the silicon. Pore direction and overall shape depends on the silicon directional crystallinity and doping agents used. Doping with phosphorus or arsenic provides an extra electron, which is loosely bound in the crystal lattice. The resulting, electron rich material is called n-type silicon. For p-type (hole rich lattice), boron is used to dope the silicon.

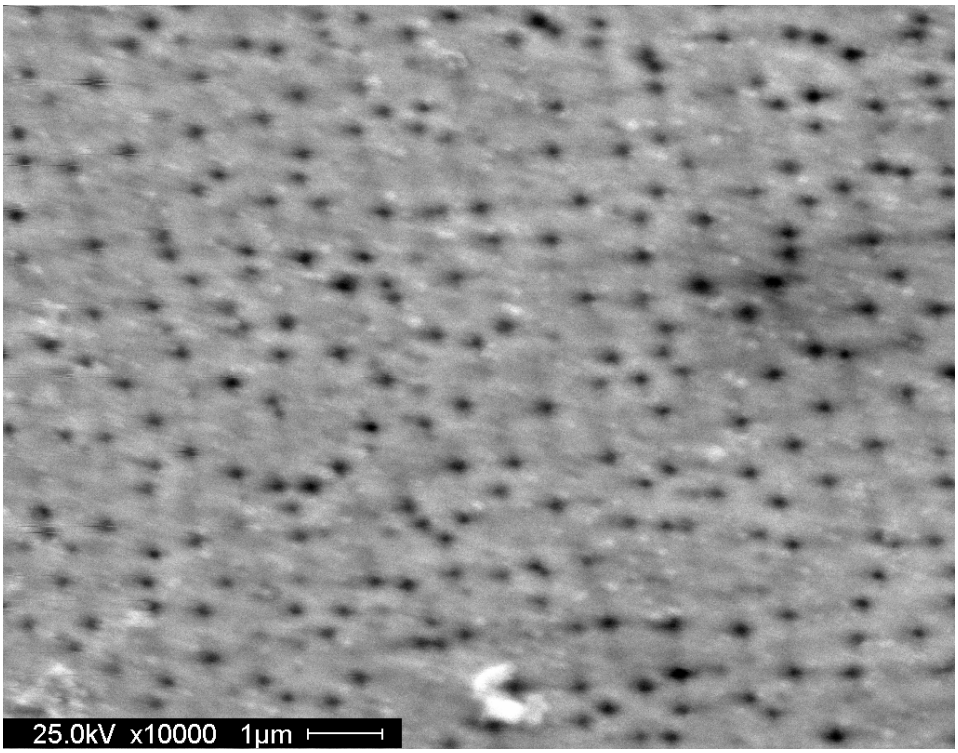

Figure 12: Surface SEM image of an n-type porous silicon structure.

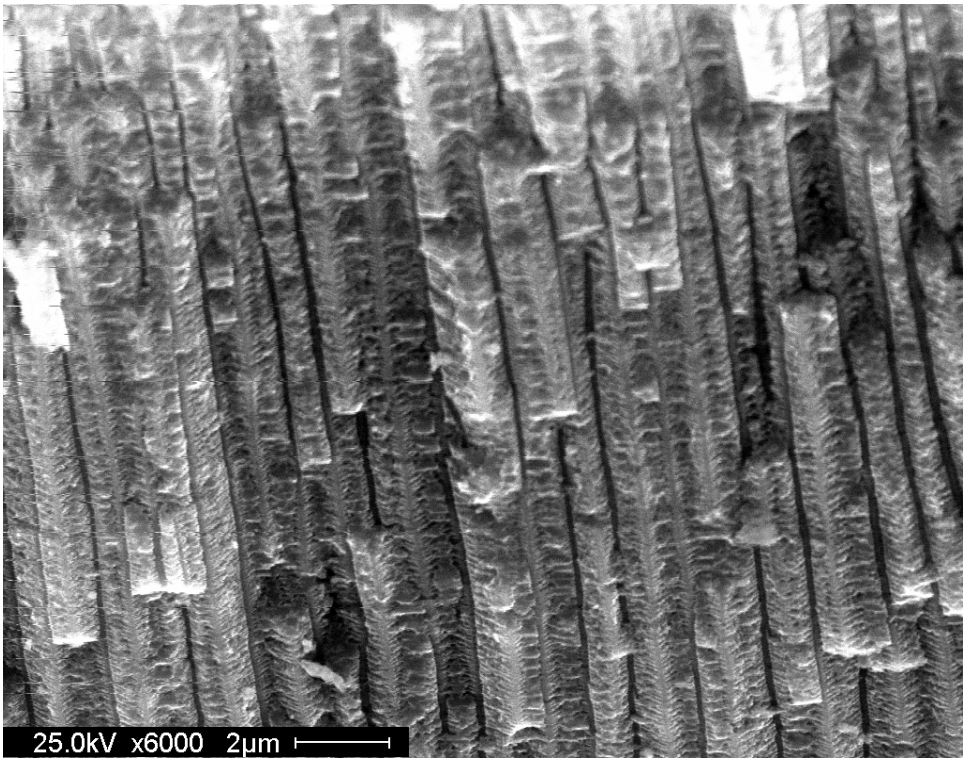

Figure 13: Cross section SEM image of an n-type porous silicon structure.

2.5 Applications of Nanostructures in the Biomedical Field

Development of nanoscale materials is at the forefront of research at the moment due to the diverse potential of applications in multiple fields. Both theoretical work and practical applications have been the fruit of such intensive focus on nanotechnology during the past 20 years. The biomedical field has gained tremendously from nanostructure development in a multitude of applications. From tissue engineering to biosensing, nanostructures are being integrated in very small devices that are providing faster and more reliable diagnostic tools and functional bio-inserts.

Cells represent the building unit of living organisms. Their typical size falls within the micrometer range. Cell organelles and proteins found on the membrane, however, are much smaller. Integrin is an example of a membrane protein that plays a major role in the attachment of a multitude of cells to the extracellular matrix (ECM) and to other cells. This protein is also vital in signal transduction from the ECM to the cell and has a size that is within the nanometer scale, which is comparable with the dimensions of smallest man-made nanostructures. Many nanostructures are currently being produced for biomedical applications such as: drug and gene delivery, bio detection of pathogens, fluorescent biological labels, detection of proteins, probing DNA structure, tissue engineering, separation and purification of biological molecules and cells, and bio inserts.

As mentioned above, the fact that nanostructures exist with size domain comparable to proteins makes nanomaterials suitable a multitude of biological applications. The significant increase in surface area to volume ratio found in nanomaterials is a definite

advantage they bring to the cutting edge bio-applications where they are being used. The result of such structure related properties is very prominent in the material's electrical, thermal conductivity, electron affinity, density states, magnetic and optical aspects. Even more interesting is the ability to fine tune the aforementioned physico-chemical properties by varying the synthesizing processes, thus controlling specific dimensions at the nanoscale. The fine tuning capabilities developed by nanotechnology open great possibility in devising biomimetic systems that integrate biological environments by providing an easily processed biocompatible interface that could replace damaged tissue. Great hopes and expectations are put on bioengineering related nanotechnology due to the importance of developing a tissue or bioinsert bank which could potentially solve the traditional tissue replacement system. There has been substantial progress made in development of synthetic methods for preparation of inorganic based nanostructures, and in studies of their properties[104-106]. Polymeric and composite materials are currently widely used in many biomedical technologies and commercial applications especially in regenerative medicine. High mechanical and thermal stability, rich structural and functional variety due to possibilities for controlled phase separation and wide functionalization by incorporation of functional chemical groups or nanocomponents, efficient processability and low cost of polymers result in high potential for future practical applications of organized polymeric nanostructures and nanocomposites[107]. A schematic example of how nanostructures could be functionalized to enhance the interfacial properties of a device destined for many different biomedical applications is shown in figure 14.

Although many synthetically based polymers are being used for biomedical applications, biologically based polymers or biopolymers such as collagen are showing great promise as coatings, scaffolds, and bioinserts thanks to the inherent biocompatibility. Collagen readily self assembles from a water soluble solution through a process called fibrillogenesis, which is the development of fine fibrils and collagen fibers that help support connective tissue, as shown in figure 2. Biophysical and biochemical properties of collagen such as solubility, crystallinity, mediation of intercellular interactions, controllable stability, biodegradability and low immunogenicity make this biomaterial an excellent choice for medical and dental applications, both as a host for subsequent growth of other biomaterials (e.g. tissue for grafting) and as a functional interfacial insert. Collagen is also an excellent dispersing agent that acts like a bio-surfactant. This property has been taken advantage of in the work presented in this dissertation through the development of collagen-carbon nanotube composites for orthopaedic and tissue engineering applications.

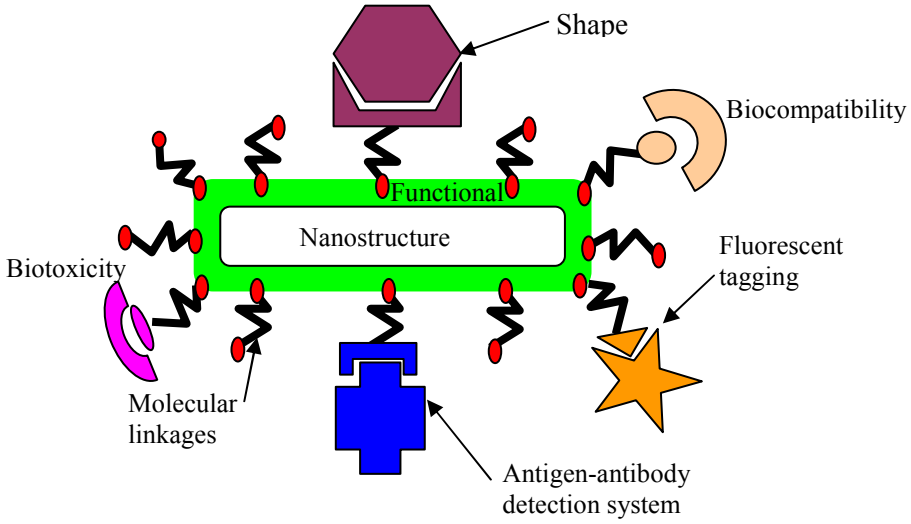

Figure 14: Typical configurations utilized in nano-bio materials applied to medical or biological problems[108].

Nanostructures usually form the core of novel nanoscale biomaterial. Whether considering a 0D, 1D, 2D, or a 3D structure, interfacing nanoscale devices with multiple molecular configurations is a reality. There are many decisions to be made when choosing the proper materials for a specific biomedical application. However, the majority of today's biomaterials are composed of inorganic and polymeric structures. Porous silicon is one inorganic material used as an electrical interface for many biosensing applications due to its excellent optoelectronic properties. DNA sensing constitutes one of the major areas where silicon is used. The following sub-chapters discuss the use of collagen, carbon nanotubes, and porous silicon as biomaterials for biomedical applications such as orthopaedics, tissue engineering, and biosensors.

2.5.1 Collagen-Carbon Nanotube Composites for Applications in the Biomedical Field

Nanotechnology is a very attractive option in the design of orthopaedic implants. One reason is the potential solution for a recurring problem that troubles orthopaedic surgeons, which is implant loosening due to partial or no osteointegration around the device. It is believed that good initial protein (cell function specific) adhesion to the implanted biomaterial is essential to subsequent bone integration. Proteins such as vitronectin and fibronectin bind on nanoscale surfaces with highly specific properties (i.e. chemistry, charge, wettability, topography)[6]. It is also believed that surface roughness is of significant influence for protein interactions[109], and nanophase materials present the promise of optimizing this early interaction. The use of nanophase materials at the organic-inorganic interface of implants, as opposed to the conventional microscale

approach, offers a biomimetic approach which allows for tailored nanoscale surface modifications to optimize the interfacial mechanical properties.

One of the novel interfaces developed and introduced in this dissertation involves two types of processing techniques to design novel nanophase biomaterials developed using type I bovine collagen and single wall carbon nanotubes. The first processing technique yields collagen/CNT fibers with diameters larger than 100 microns. The second technique, called electrospinning, yields collage/CNT nanocomposite nanoropes that are less than 300 nanometers in diameter. These nanoropes were used as surface coatings to act as effective interfaces between biological orthopaedic devices and bone. The advent of nanotechnology fabrication and processing techniques offers many possible solutions to the rising health care costs associated with orthopaedic surgery by shortening the hospital stay and decreasing the number of reoccurring surgeries due to lack of sufficient bone regeneration around the implant immediately after the device insertion. Furthermore, the surge in patents awarded annually for nanotechnology inventions have tripled since 1996, with 10-fold or greater increases in some areas during the past three years,[110] which shows and exponentially increasing interest in nanotechnology.

2.5.2 Electrospinning for Tissue Engineering Applications

Much has been done to characterize novel electrospun material and improve on the century old manufacturing technique. The recent interest exponential growth of nanotechnology related fields had propelled electrospinning at the forefront of research. From defense and security to environmental engineering and Biotechnology,

electrospinning is being used to develop novel nanofibers for a wide variety of applications. Biomedical and bioengineering represent the largest sectors of electrospinning research with 26 %[111] due to the possibilities for developing tissue engineering scaffolds. These two fields are at the forefront of novel applications where nanofibers are being developed for tissue engineering, wound dressing, and drug delivery purposes. The present section addresses recently developed applications of electrospun polymers in the biomedical field.

2.5.2.1 The Electrospinning Process

Electrospinning is a process which uses an applied electric field to draw fibers from a solution (normally a polymer melt) with diameters in ranging from the micro to the nanoscale. Electrospinning was first discovered in 1902 by Cooley and Morton; however its slow production rate limited its application in textiles and other dominant industries of the time. It wasn't until the recent explosion in nanotech, and specifically, nanofiber research that electrospinning was re-popularized. In the last decade alone, more than 500 papers have been published on electrospinning and its related applications.

Electrospinning employs a rather simple setup, requiring only a spinneret to draw a solution through, an applied electric field to generate the drawing forces, and a collector to collect and orient the fibers produced. Generally, multiple spinnerets are used and collector types vary from one setup to another in an effort to produce fibers in some desired pattern. For example, parallel electrode collectors are used to produce aligned fibers. Most electrospinning designs can be classified into this category, however,

specialty setups have been established to more closely control viscosity, temperature, pressure, and other parameters. The relative simplicity of the electrospinning setup allows for easy modification and design, and thus a host of setups have been investigated.

The fundamental basis for electro-spinning first began to surface when S. Gray first meticulously observed water's behavior under the influence of electrostatics. The theoretical work was continued by Larmor in the late 1800s, but it was Cooley and Morton who were first able to electrospin fibers in 1902[112]. The work was further pioneered by Formhals who patented at least ten different electro-spinning designs in the 1930s[112]. However, due to production speed, electrospinning never gained much interest in the industrial sector[113]. Dry spinning produced yarn more than six times faster than that which could be produced by electrospinning[114]. As a result, electrospinning engineering research faded into the background until recently. The theoretical work continued on, but more slowly. Taylor modeled the electrostatic jet in the 1960s and Baumgarten established a few design parameters in the early 1970s[115]. However, the recent explosion of electrospinning research can be attributed to the potential for electrospun fibers in the field of nanotechnology[116]. In the early 1990s, the potential for electrospun nanometer sized fibers in the fields of filtration, nano-catalysis, protective clothing, absorbent materials, and more were published and popularized [115]. As a result, in the last decade alone, more than 500 papers have been published on electrospinning techniques and their applications and more than a hundred synthetic and natural fibers have been electrospun[112,113].

Often, designs are formulated with certain parameters in mind. Recently, much work has been done on both solution and processing parameters in electrospinning. It has been suggested that the electrospun fibers are much more sensitive to variation in solution characteristics that process parameters, however, both need to be controlled to produce consistent fibers. Fiber characteristics such as diameter, tensile strength, elasticity, conductivity, and more can be tailored to specific needs by varying these parameters.

As mentioned above, solution parameters play an important role in determining the characteristics of the final fiber. Obviously, the material composition of the solution is key in determining the solution parameters, and therefore the final fiber's characteristics. Traditional fabrication methods vary from material to material and are also very limited. For example, most metallic fibers are drawn rather than spun, and this can only be accomplished when the metallic material or composite has suitable melting temperatures. Electrospinning, on the other hand, is extremely versatile in terms of materials and processing parameters. A host of materials and mixtures can be electrospun to produce fibers with a wide range of possible parameters and characteristics. The impact of these parameters can be verified through a host of characterization methods. Many aspects of nanostructures can be analyzed using electron microscopy tools such as scanning and tunneling microscopes. The surface morphology of electrospun fibers is an important aspect to characterize due to the large surface to volume ratio provided by such structures. Molecular structures and mechanical properties are two related characteristics, which are also important to describe for different functional biomedical applications.

Electrospinning allows the formation of nano-scaled fibers with a host of tunable parameters. This, in particular, is well suited for the design of many biomedical instruments and devices. Most obviously, smaller diameter fibers can improve filtration techniques which, in turn, can be used to improve dialysis and other selective screening methods. Additionally, the large surface area to volume ratios attained from fibers with nanometer sized diameters make them ideally suited for drug delivery and catalysts. This also makes them excellent sensors, providing a large sensing surface with very little mass. Lastly, electrospinning's versatility and ease of setup allows the production of fibers with unique compositions and patterns. Conductive materials can be electrospun to form conductive scaffolds for tissue engineering applications or textiles fibers can be electrospun to incorporate moisture, pulse, and other human vital sign sensors. Electrospinning's versatility and ease of setup combined with the small diameters and large surface area to volume ratios produced give it the potential to possibly revolutionize the field of bioengineering and medicine.

2.5.2.2 Electrospun Fibers for Tissue Engineering Scaffolds

One of the first definitions of tissue engineering was probably issued by Langer et al who stated it to be an interdisciplinary field that applies the principles of engineering and life sciences toward the development of biological substitutes that restore, maintain, or improve tissue function or a whole organ[117]. Generally, tissue engineering involves the fabrication of three dimensional scaffolds with the main aim of seeding cells that will subsequently grow and proliferate into specific tissues. One important aspect of producing scaffolds is the ability to generate tailored structures that closely mimic highly

complex natural extra cellular matrices by controlling fiber size within the three dimensional structure[73,118-126]. Electrospinning has emerged as a cheap and viable technique, which is capable of producing continuous polymeric fibers with diameters ranging from several microns to tens of nanometers. Although the equipment and setup of an electrospinning unit is relatively inexpensive, biodegradable polymers such as lactic-co-glycolic acid (PLGA) and other biological molecules (growth factors, cytokines) could have a too large of a price tag thus turning electrospinning into a non economical option for developing scaffolds. The problem is compounded by the general inefficiency of the most widely used approaches which tend to yield an unfocused electrospun jet[127] thus wasting much of the used biomaterials.

While the electrospinning process itself is over 70 years old, the concept of electrospun scaffolding for biomedical applications appears to have first emerged in 1978. "An Elastomeric Vascular Prosthesis" was reportedly produced from polyurethane elastomer utilizing "electrostatic spinning" by Annis et al[128]. The authors produced tubes onto a rotating mandrel. These tubes were used to replace lengths of the thoracic aorta in 42 mini-pigs. Even without prior cell seeding, these grafts apparently demonstrated full functionality over a period of many months *in vivo* even though the maximum burst pressure was only ~ 80 mm Hg[128]. Much has been accomplished since

Kwangsok Kim at Stonybrook Technologies and Applied Research (STAR) has developed a specialty composite which can be electro-spun to produce a biodegradable scaffold for medical applications. The setup employed is very similar to the multiple

spinneret setups used to electrospin scaffold designs, but the polymer melt is a composite of poly(d,l-lactide) (PLA), poly(lactide-co-glycolide, LA/GA=50/50) (PLGA), lactide, and poly(lactide-b-ethylene glycol-b-lactide) (a triblock polymer) dissolved in N,N-dimethyl formamide (DMF) to a 30%-50% concentration by wt.[129]. This blend has allowed STAR to develop scaffolds with a highly specific tunable degradation rate. This ability to adjust the degradation factor is very important in the success of scaffolds where mechanical competency of the tissue to be reconstructed is important.

In many synthetic polymers, the degradation mechanism is accomplished by the hydrolytic reactions at the ester bonds that occur slowly in the body[130]. Thus, lactide is incorporated in many scaffold designs as a degradation catalyst. The lactide reacts with the water to form lactic acid, which lowers the pH and increases the degradation rate [131]. In practice, there is a limit to the amount of lactide which can be used because very acidic solutions impair the scaffold's mechanical strength as well as cell viability. Much of the electrospun polymeric composites have degradation rates that are tuned grossly and then finely. The bulk part of the degradation rate is controlled by the percentage of the main polymer in the composite fiber, while fine tuning is indirectly accomplished by adjusting the percentage of the existing co-polymer.

Collagen, as a natural biopolymer is extremely useful as scaffold due to a number of biochemical and biophysical properties, some of which has been mentioned earlier in this document. Type one collagen has excellent biodegradation properties. Similar to synthetic polymers such as PLA and PLGA, collagen can be tuned to degrade both in

vivo and in vitro by collagenases, which are enzymes that are able to cleave the peptide bonds in the triple helical collagen molecule. The introduction of cleavage is achieved under specific physical conditions of pH and temperature. In naturally produced animal collagen, other factors accompany its degradation that are not present in the synthesized form. These processes include collagen biosynthesis, control growth, morphogenesis, and self repair[132]. In the case of transplanted synthetically derived collagen into tissues, its degradation rate leaves virtually no permanent foreign residue. This property can be tuned by using a crosslinking agent that binds the collagen fibrillar structure and controls its degradation. Many crosslinking agents could be used as mentioned in the collagen section of the chapter. Nordihydroguaiaretic acid (NDGA) is the only completely biocompatible agent that is available for crosslinking with no adverse biological effect.

2.5.2.3 Electrospun Fibers as Drug Release Structures

Controlled release and zero order kinetics are two terms which preoccupy research in the fields of catalysis and drug delivery[73,133]. Both processes rely on the controlled release of certain substances over time. Catalysts increase the rate of a reaction. By controlling the amount released over time, it is possible to control the rate at which a reaction progresses. Similarly, the idea behind drug delivery is the controlled released of medications over time without the need for constant intake or injection. Both fields, currently predominantly rely on the mechanism of diffusion to govern the release of substances, however, this has posed a problem to many researchers due to an initial burst released[133]. The simple solution is quite simply the degradation of composites constructed with the medicine or catalyst of interest[73]. In other words, producing structures with the

desired molecules embedded allows a controlled release of that molecule as that structure degrades. In order to discuss diffusion of drugs into the body using media such as electrospun fibers, one has to state the mathematical models driving the physical phenomenon involving the release of the target substances. One of the fundamental equations that describe diffusion is a partial differential equation which describes density fluctuations in a material undergoing diffusion. Equation 1 is the typical representation of the diffusion equation:

$$\frac{\partial \Phi}{\partial t} = \nabla(D(\phi,\vec{r})\nabla\phi(\vec{r},t)) \qquad \text{Equation 2}$$

where Φ is the density of the diffusing material, t is time, D is the collective diffusion coefficient, $\vec{r}$ is the spatial coordinate and the nabla symbol ∇ represents the vector differential operator del. If the diffusion coefficient depends on the density then the equation is nonlinear, otherwise it is linear. If D is constant, then the equation reduces to the following linear equation:

$$\frac{\partial \Phi}{\partial t} = D\nabla^2\phi(\vec{r},t) \qquad \text{Equation 3}$$

Equation 2 is also called the heat equation. In practical applications it is important to look at the diffusion flux and its proportionality to a concentration gradient.

For this correlation to be defined, it is necessary to re-write the diffusion equation in a form that includes a flux component. This equation is derived is a fairly straightforward manner which yields equation 3:

$$\frac{\partial \Phi}{\partial t} + \nabla \vec{j} = 0 \qquad \text{Equation 4}$$

This equation states that a change in density in any part of the system is due to inflow and outflow of material into and out of that part of the system. This is another way of stating that no material is created or destroyed. The vector $\vec{j}$ is the flux of the diffusing material. The diffusion equation is finally deduced as a function of the diffusion flux when combined with the Fick's first law, which assumes that the flux of the diffusing material in any part of the system is proportional to the local density gradient:

$$\vec{j} = -D(\phi)\nabla\phi(\vec{r},t)) \qquad \text{Equation 5}$$

Diffusional flux is proportional to the concentration gradient, which by its very nature is constantly changing. Thus, a release mechanism based on diffusion kinetics can not truly provide a constant flux unless the flux is 0 or equilibrium state. During the early stages when the drug or catalyst is first released, the flux of substance into the desired medium is larger than later on. This is categorized as a first order kinetics process and can be seen in figure 2. The diffusion, in this case decreases as time progresses thus

presenting a challenge for anyone hoping to achieve a constant reaction rate which would translate into an effective drug release system for only a short period of time. While mathematics and engineering can be utilized to minimize this problem, it will always be inherent to any design based on diffusion.

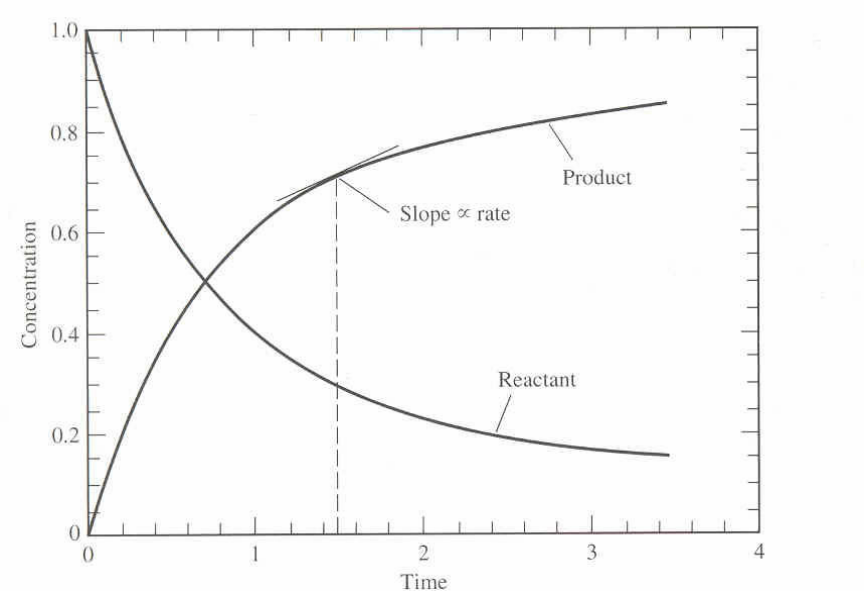

Figure 15: Illustration of a first order kinetics reaction[134].

There is great benefit to developing polymeric structures for drug delivery purposes as compared to conventional dosage drugs. The advantages of drug delivery are further improved with the use of micro and nanostructures. Some of the improvements include controlled and extended therapeutic effects along with reduced toxicity. However, the advent of a new procedure does not come without problems such as low efficiency of drug delivery and burst release of drugs at the beginning of the treatment. Due to the exponential increase in nanotechnology research, many structures have been developed to

carry drugs to their respective targets. One of the obvious nanostructured forms is the sphere, sometimes also called particle or vesicle. The efficiency of micro and nanoparticles is too low and sometimes hard to impregnate with the desired drug.

Recent developments in electrospinning research have lead to the ability to capsulate therapeutic drugs directly into electrospun fibers. Zeng et al showed that poly(L-lactic acid) (PLLA) could be electrospun in presence of typical commercial drugs such as Triethyl benzyl ammonium chloride (TEBAC), sodium dodecyl sulphate (SDS), aliphatic PPO-PEO ether (AEO10), rifampicin (a drug for tuberculosis), and paclitaxel (an anti-cancer drug).[133] The drugs where found to have been completely encapsulated and the system showed nearly zero-order kinetics. This and other recent studies are showing that drugs are successfully being encapsulated inside electrospun fibers with predictable degradation models. This is very promising for future biomedical applications, especially postoperative local chemotherapy.

Thanks to its inherent technique, electrospinning is one of the few processes that results in production of long fibers of diameters ranging from the micro to the nanoscale. The great progress that has been made in recent years does not necessarily translate into the development of electrospun-fiber carriers for drug delivery. This area is still in its infancy and thus is very limited. Kenawy et al.[8] studied the release of 5% tetracycline hydrochloride from electrospun poly (ethylene-co-vinyl acetate), poly (lactic acid), and their blends. The initial rate of release of all formulations was high during the first 10–12 h, due to burst release of drug from the sample surface. Zong et al[129]. also prepared

PDLLA electrospun fibers containing Mefoxin, but observed complete release of Mefoxin within 48 h and a bad burst release in the first 3 h, because a great deal of drug molecules were on or near the fiber surface. So it is desirable to capsulate a drug inside the fibers in addition to controlling the fiber diameter. It is possible to solve this problem by controlling both the biodegradable polymeric substance, and the distribution of the drug to be delivered within the fiber matrix.

2.5.3 Porous Silicon Nanostructures for Biosensor Applications

Silicon is a great semiconducting material, which lead to the exponential development of a multifunctional semiconducting industry during the previous 50 years. This industry was one of the main driving forces in the discovery of many processes that alter the silicon surface structure to enhance its electronic, optical, or mechanical properties. Silicon etching has been well studied. Table 2 showed a few of the etching agents used to obtain a multitude of porous structures. One of the main advantages of porous silicon is the large increase in its surface area, which provides numerous sites for many potential species to attach. This makes it an ideal host for sensing applications. In addition, the pore size and porosity factor could by adjusted by tuning etching parameter, which leads to great flexibility in the dimensions of molecules to be interfaced with the biomaterial. Porous silicon has been used as an optical interferometric transducer for detecting small organic molecules (biotin and digoxigenin), 16-nucleotide DNA oligomers, and proteins (streptavidin and antibodies) at pico- and femtomolar analyte concentrations[135]. Microcavity resonators made of porous silicon have been used in biosensors. These resonators possess the unique characteristics of line narrowing and luminescence

enhancement. Chan et al. (2000) fabricated a DNA biosensor based on a porous silicon microcavity structure[51].

Recent use of porous silicon as a DNA based biosensors have increased due to the use of novel interfacial binding methods. There exist several methods have been used to bind single strand DNA to the porous silicon base[52]. Silanization has been a commonly used method to bind DNA to porous silicon. This method is based on the function of silane as a coupling agent by providing a stable interfacial bonding molecule between an inorganic surface (porous silicon) and an organic nanostructure (DNA). 3-glycidoxypropyltrimethoxy silane is commonly used as the chemical compound to silanize the oxidized porous silicon. By lowering the pH to about 4 using HF, silane is converted to silanol, which is more reactive[136]. The mechanism of attachment between silanol and the organic end of the interface is accomplished through the covalent bonding of the silanized surface with the nucleophillic amine group. A different method is detailed in chapter 5 regarding the fabrication of mesocavities on silicon wafer for the immobilization of RSV F gene specific ssDNA with sol-gel coating over the silicon surface to develop a probe for the recognition of cDNA of the attached ssDNA. This dissertation presents a novel optical and mechanical approach to detect DNA hybridization by properly coating over the surface of PS mesocavities with highly selective receptor molecules ssDNA using TEOS to quickly determine the presence of complementary (cDNA). This novel approach is part of the global theme of developing interfaces for biomedical applications –in this case biosensing application- using fabricated nanostructures.

CHAPTER 3: SYNTHESIS AND CHARACTERIZATION OF COLLAGEN-SINGLE WALL CARBON NANOTUBES NANOCOMPOSITE INTERFACES FOR ORTHOPAEDIC AND TISSUE ENGINEERING APPLICATIONS

3.1 Introduction

One of the remaining and still significant challenges for orthopaedic surgery is to insure competent bonding between implants (especially soft implants) and the surrounding musculoskeletal tissues. The ideal fixation strategy would provide immediate mechanical competency to allow early mobilization followed by long-term biological integration of the implant within the musculoskeletal structure. This is done through a well designed biocompatible interface between the bio insert and the native tissue. The surface morphology of the bio insert or implant that is presented to the neo-surfaces created in surgery and the regenerating native tissue that ensues is of principal importance when designing biologic-inorganic interfaces. There is a growing realization that integration of and attachment between artificial orthopaedic devices and native tissues can be optimized by using a rapidly emerging class of materials in the nanometer size. The structural size of nanomaterials is less than 100 nm, and they can be designed and manufactured with surface roughness similar to the biological environment. Furthermore, nanomaterials provide a high surface to volume ratio when produced in rod like shapes called nanowires or nanotubes, thereby providing an increase in the surface area to which the native tissue can bind and attach while at the same time retain their extraordinary mechanical properties. It is expected that nanomaterial-based fabrications

will simultaneously provide optimal mechanical strength at the interface immediately after surgery.

The discovery in the early 1990s of carbon nanotubes has given scientists and engineers a new horizon to a material (carbon) that is as old as planet Earth or even older. The wide range of novel physical properties is paving the way for a wide range of applications spanning many cutting edge technologies such as bio and nanotechnologies. These outstanding physical properties are a direct result of the near-perfect microstructure of the nanotubes, which at the atomic scale can be thought of as a hexagonal sheet of carbon atoms rolled into a seamless, quasi-one-dimensional cylindrical shape. Besides their extremely small size (in the range of several nanometers), it has been suggested that carbon nanotubes are even less dense than aluminum, have tensile strengths twenty times that of high strength steel alloys, have current carrying capacities 1000 times that of copper, and transmit heat twice as well as pure diamond[137]. To take advantage of this unique combination of size and properties, a wide variety of applications have been proposed for carbon nanotubes, including: chemical and genetic probes, field emission tips, mechanical memory, supersensitive sensors, hydrogen and ion storage, scanning probe microscope tips, and structural materials[137]. The continual increase in nanotechnology focus on nanowires and nanotubes due to their remarkable properties is providing new alternatives to the more traditional technologies such as microelectronics which are based on the silicon revolution in the twentieth century.

This chapter outlines the design and development results of nano-scale inserts and nanocomposites from an artificial but biologically compatible material and a naturally derived material, namely: carbon nanotubes and collagen. The synthesized nanocomposite was applied to designed collagenous materials for enhanced fixation and osteointegration. A systematic investigation of the use of a nanocomposite composed of single-wall carbon nanotubes and solubalized type I collagen as a potential orthopaedic implantable device was conducted. Fiber of roughly 150 μm in diameter and 30 to 40 cm in length were synthesized and crosslinked by Nordihydroguaiaretic acid (NDGA) to form a material with mechanical characteristics similar to native human tendon. A second method based on electrospinning a novel nanocomposite using type I collagen and SWCNT for tissue engineering applications is also presented in this chapter. The electrospinning method yields fibers ranging in diameter from several tens of nanometers to several micrometers. The wide range of fiber diameters that are produced by electrospinning is a clear advantage in scaffold production for tissue engineering applications.

3.2 Materials and Methods

3.2.1 Materials

SWCNT produced via high-pressure carbon monoxide conversion synthesis (HiPCO) was used. Different purifications of SWCNT were also purchased from Sigma Aldrich to study *in vitro* impact of the different grades. Post-processing of as-grown SWCNT was conducted by applied repetitive cycles of acid cleaning and annealing to eliminate any

residual metal catalysts and amorphous carbon. The applied post-process yielded different purity levels reaching up to 99% pure SWCNT. The efficiency of this process did not prove to be crucial for biocompatibility.

Type I collagen was derived from a fetal bovine tendon according to established protocols. Human osteoblasts, obtained from American Tissue Type Culture (hFOB 1.19, ATTC), were used for *in vitro* studies. These are SV40 transfected cells that retain their phenotype in expressing alkaline phosphatase *in vitro*. These cells were used in the experiments described below. They are simple to culture and expand well in DMEM/F12 medium supplemented with fetal bovine serum albumen. Cell culture dishes with a 0.2% fibrillar collagen gel containing various amounts of uniformly dispersed SWCNTs (0.5 – 20%) were prepared. Osteoblasts were plated out at a cell density of 50,000 units per well directly onto the gel. The number of attached osteoblasts was measured 24 hours after plating.

3.2.2 Fabrication of Collagen-SWCNT Nanocomposite for Orthopaedic Applications

Processing temperature is one of the challenges in developing collagen-based nanocomposites. Carbon nanotubes require relatively high temperatures during the growth process. For this reason, CNT's have to be collected into a powder form and dispersed into a soluble form of collagen. All physical and chemical characterizations (described later in this chapter) were performed on soluble type I collagen/SWCNT composite.Two distinct processing techniques are used to develop nanocomposites with

different physical characteristics. The first processing technique follows the geletion route to a drying process that yields a hair like structure that is referred to as a fiber. Throughout this technique, type I collagen was derived from a fetal bovine source. After extracting the extensor and flexor tendons from the animal's hooves, a series of acid and pepsin digestion treatments were carried on for 48 hours. The resulting solution was then centrifuged and the pellet extracted. This pellet was then diluted into 3% acetic acid to obtain a 0.2% collagen solution. Single wall carbon nanotubes were produced via high pressure carbon monoxide conversion synthesis (HiPCO, carbon Nanotechnologies, Houston, TX). SWCNT were mixed at 0.5, 1, 2, 5, 10 and 20 weight percent and sonicated in the collagen solution for 1.5 hours. This was sufficient for the SWCNT's to stay homogeneously suspended for longer than 4 days. This was crucial to the fiber process since it takes 2 days for fibril formation and drying process. The sonicated solution was then poured into 4 mm diameter (15000MW cutoff) dialysis tubes to dialyze against acetic acid. This process takes 6 hours with water being changed every half an hour. The dialysis tubes are then transferred to a phosphate buffer (7.4 pH) over night. At the end of this process the solution has gelled and fibrillogenesis has occurred. A drying process follows by pulling the fibers at a rate of 5 cm/hour. A solution is prepared to crosslink the dried fiber. This solution is prepared by oxygenating a 0.1M sodium phosphate ($NaPO_4$) that has a pH equal to 7. A 90mg of NDGA is then dissolved into 3 ml of 0.4M sodium hydroxide and the two solutions combined are used to crosslink the dried fibers for at least 6 hours (figure 16).

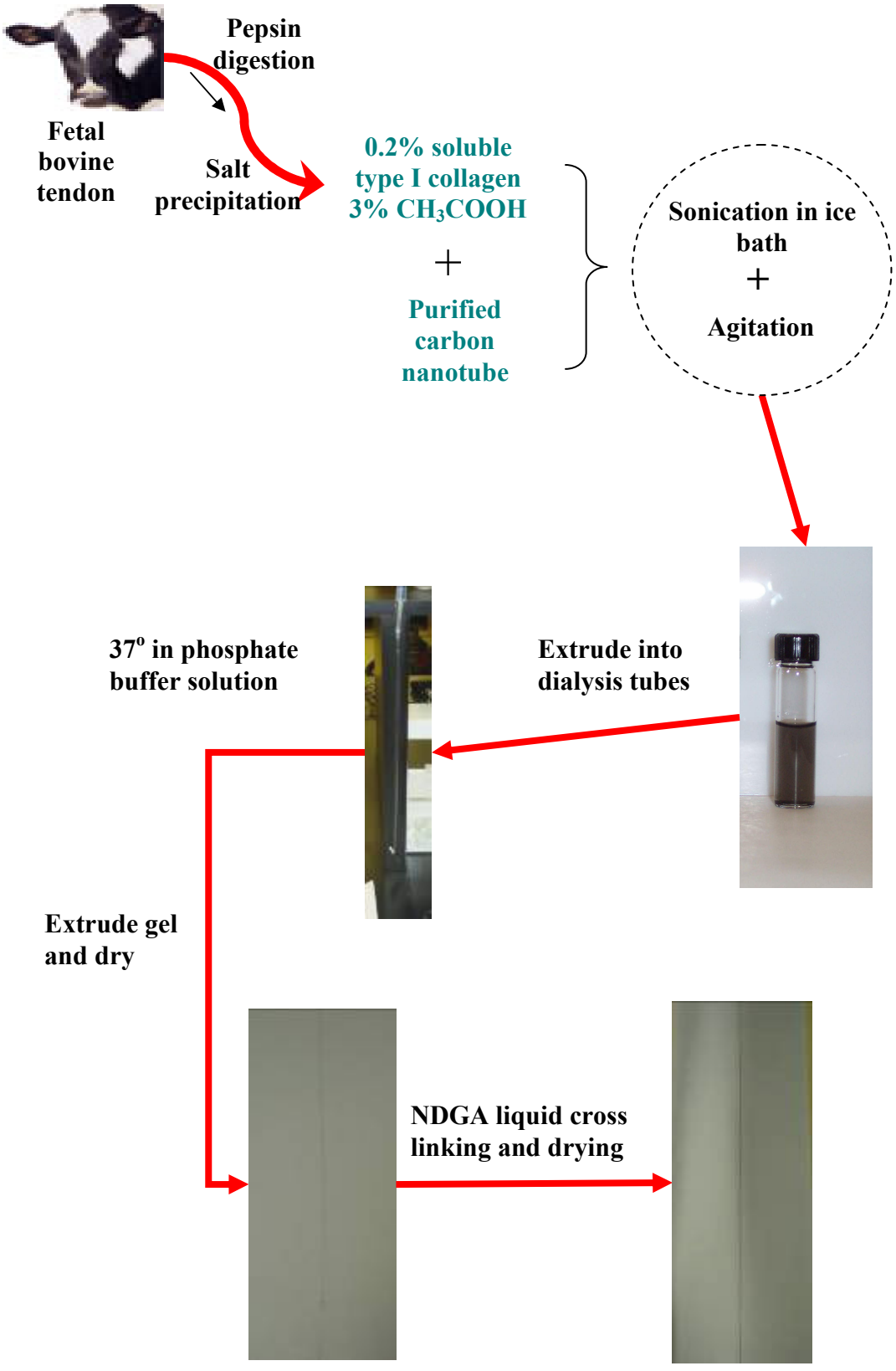

Figure 16: Process flow of the collagen/SWCNT composite fabrication for orthopaedic applications.

3.2.3 Fabrication of Collagen-SWCNT Nanocomposite for Tissue Engineering Applications

A second fabrication technique was implemented, which yielded electrospun collagen/SWCNT fibrils with diameter in the nanometer to micrometer range. Electrospinning the nanocomposite solution into self assembled biopolymeric fibrils, thanks to the liquid crystal structure of collagen, provides an ideally suited technique for osteoblast cell alignment and proliferation. The self assembled nanocomposite represents a building block for constructing an extra cellular matrix like functional material for optimized cellular proliferation. The broad range of fiber diameters in conjunction with the use of SWCNT yields an ideal scaffolding structure for tissue engineering applications.

Electrospinning requires high DC voltage that is applied to a metallic tip of a syringe. This voltage acts as a catalyst that breaks the surface tension at the tip and a jet of very fine- self assembled collagen fibrils that deposit on a grounded target at a distance far enough from the syringe tip to allow for the solvent to completely evaporate. A basic electrospinning setup is depicted in figure 17. The spinneret needle is metallic and is connected to a syringe where the collagen-SWCNT melt is located. The spinneret is connected to a pump that controls the ejection rate. The DC voltage supply is connected to the metallic tip. When a threshold voltage value is reached, the pendant drop of polymer at the end of the syringe becomes highly electrified. The induced charges evenly distribute themselves over the droplet, and that combined with the Coulombic forces from the applied electric field creates the Taylor cone[138-140]. The distance between the

spinneret and the collector is another parameter is has to be optimized based on the processing conditions and material type, but is usually on the order of tens or hundreds of millimeters[141]. The diameter of the aperture on most spinnerets used for electrospinning is around several tenths of a millimeter[129,141]. At that diameter, gauge numbering is often used. Applied voltage varies greatly amongst different materials, but normally higher viscosity melts will require higher voltages to be electrospun. With this setup, fibers can be produced from a host of materials including ceramics, polymers, and biological molecules with diameters at the nano range [141].

The specific process flow for producing electrospun collagen-SWCNT fibers is detailed in figure 18. The initial steps to obtain the electrospun nanocomposite are identical to the gelation route described in figure 16. Collagen is pepsin digested and salt precipitated three times before a pure form of soluble type I collagen is obtained. After sonication and agitation in an ice bath for an hour and a half, the solution is dipped in liquid nitrogen and frozen. These two processes are very important because the rapid freezing after proper dispersion of the SWCNT prevents the carbon nanotubes from progressing towards the initial agglomeration stage. It is then lyophilized until all water has sublimated. The resulting material is a sponge like substance that is dissolved back into 1,1,1,3,3,3 Hexafluoro, 2, Propanol. The ratio of collagen weight to solvent volume is crucial in yielding high quality electrospun fibers. The final two steps have been designed further preserve the dispersion of SWCNTs into the collagen matrix thanks to the high polarity of the molecules 1,1,1,3,3,3 Hexafluoro, 2, Propanol.

(A)

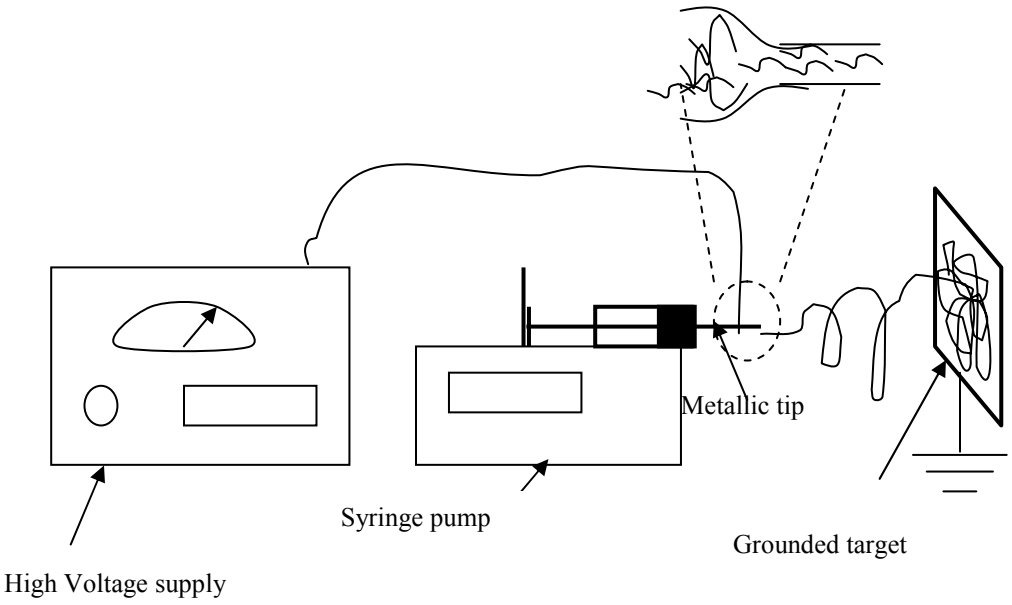

(B)

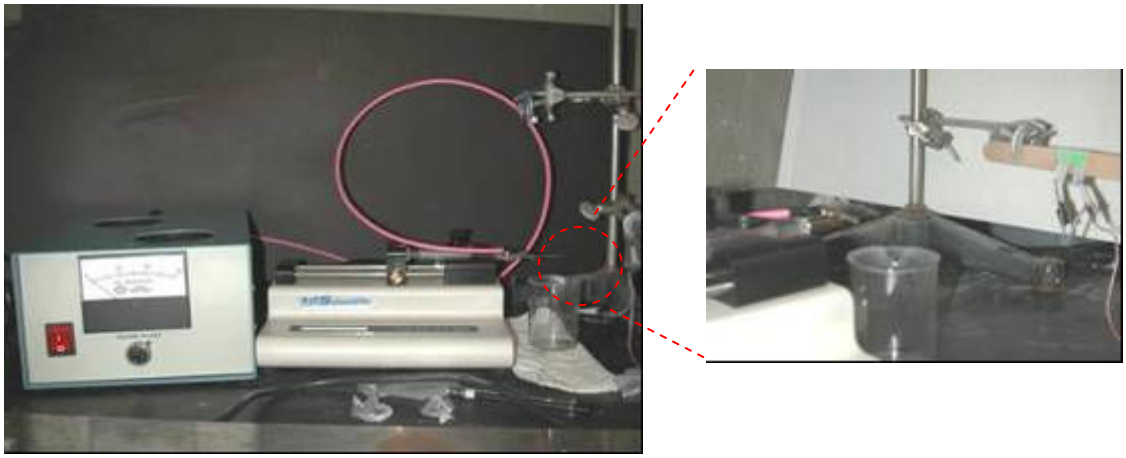

Figure 17: (A) Schematic of a basic electrospinning setup. (B) Actual setup used for collagen-SWCNT nanocomposite synthesis.

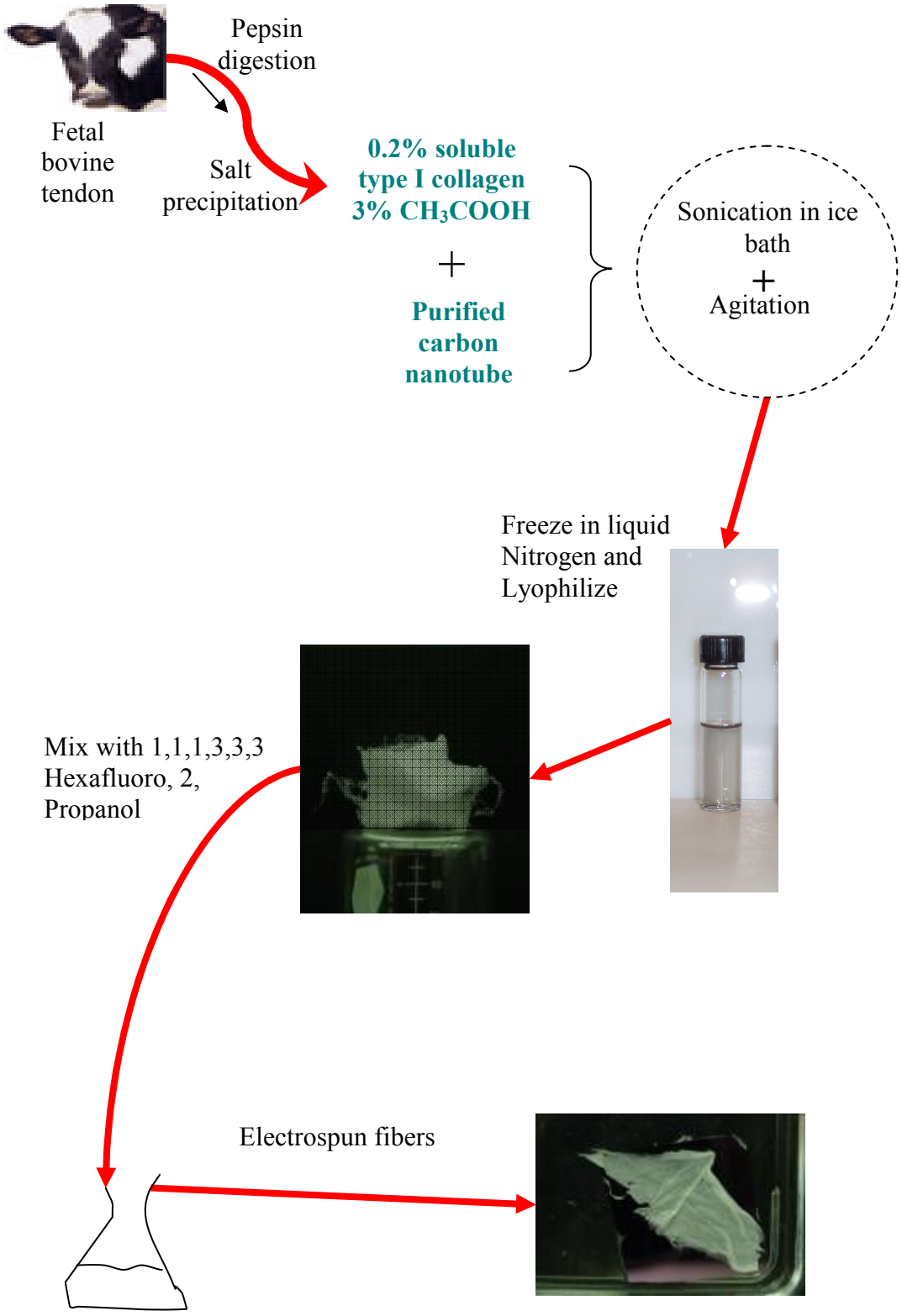

Figure 18: Process flow of the electrospinning collagen/SWCNT composite for tissue engineering applications.

3.3 Characterization Techniques

Working with nanostructures such as the gelation processed and electrospun collagen-SWCNT nanocomposite fibers requires sophisticated tools to mainly characterize three inherent properties; surface morphology, molecular arrangements, and mechanical competency. Diameter variations and surface structures are examples of morphological characteristics. The molecular make up and arrangement within the developed fibers is of great influence on the fiber's thermal and mechanical characteristics. Certain chemical post production treatments such as NDGA crosslinking change the intra and inter-molecular makeup of the fibers and thus need to be evaluated to determine the impact on the final characteristics. Mechanical properties of gelation processed fibers as well as electrospun fibers are of great importance in applications that require the supporting of other biological structures such as tendons, ligaments, and other connective tissues. This section introduces the reader to various characterization techniques that were performed to derive detailed information about the morphology, molecular structure, and mechanical competency of collagen-SWCNT fibers obtained by the aforementioned processing techniques.

The potential biomedical applications that could benefit form the developed collagen-SWCNT nanocomposite require a large battery of characterization techniques to be applied in order to assess the molecular structure, mechanical integrity, biocompatibility, and cytotoxicity. As a result, a multitude of microscopy, spectroscopy, and mechanical characterization techniques have been conducted. Scanning electron microscopy (SEM), Transmission Electron Microscopy (TEM) and High Resolution TEM (HRTEM) were

used to observe the general structure of the nanocomposite produce by the aforementioned methods. Both gelation processed and electrospun fibers were imaged by a Hitachi 800 SEM tool.

Cross sectional TEM images of individual collagen-SWCNT gelation processed fibers were obtained after the following processing steps: 5 mm long cuts were taken and dehydrated into 70% then 95% and 100% ethanol for 1 hour each. The cuts then were put into a transition solvent (100% propylene oxide) for 1 hour. The resulting cuts were then infiltrated with propylene oxide and resin (Epon 812) in a ratio of 1:1 overnight, then into the same mixture at a ratio of 1:2 for 5 hours. Embedding into a polymer resin followed at 45 ^{o}C for 3 days. The sectioning was accomplished using a semi-thin sectioning followed by an ultra thin sectioning using Reichert Ultracut E ultra microtome. Sections varying between 80 and 130 nm were finally obtained for TEM analysis. The resulting sections were stained with uranyl acetate and lead citrate. An FEI Technai F30 HRTEM was used to observe the interaction between collagen molecules and the SWCNT. It is important to mention that cross sections of the nanocomposites were taken along the fiber axes and also perpendicular to the fibers. As for the electrospun fibers, direct deposition was accomplished on TEM copper grids to make preserve the quality and alignment of the nanocomposite.

Fourier Transform Infra Red (FTIR) and Raman spectroscopy were used to characterize the molecular structure of the collagen/CNT nanocomposite. A PerkinElmer 100 series with wavelength range between 7800 and 350 cm^{-1} was used to determine the

molecular structure of the type I collagen derived from fetal bovine source. Raman spectroscopy was acquired using a Renishaw Micro-Raman with an Argon ion laser (514.5 nm). All spectroscopy data was collected using dry samples. An Asylum MFP-3D atomic force microscope (AFM) was used to study the surface topography of the collagen/SWCNT nanocomposite. Thermal Gravimetric Analysis (TGA) and Differential Scanning Calorimetry (DSC) were used to determine the impact of a change in temperature on the physical characteristics of the gelation processed fibers. Finally, a bulk and surface mechanical characterization was carried out using an MTS mini Bionix 858 materials testing system and MTS NanoIndenter XP respectively. All bulk mechanical characterization techniques used 5 specimens for each conducted experiment. Furthermore, a phosphate buffer was used to simulate a realistic biological environment during all bulk tensile testing. As for nanoindentation, duplicates were used to determine the surface characteristics of the geletion processed fibers with 25 indentations programmed per tested fiber.

3.4 Results and Discussions

3.4.1 Electron Microscopy Analysis

SWCNT were readily dispersed in 0.2% type I collagen at concentrations up to 20% (w/w of collagen). Proper dispersion of SWCNTs into Type I collagen solution was achieved by optimizing the sonication time and agitation speed. One hour and half were needed in an ice bath to achieve proper dispersion that held for over 4 days. It is important to mention that first sonication trials at room temperature resulted in a large

amount of denatured collagen and subsequently inhibited fibrillogenesis. This was due to a transfer of energy from the sonicator to the solution, thus increasing its temperature to 45 ^{o}C.

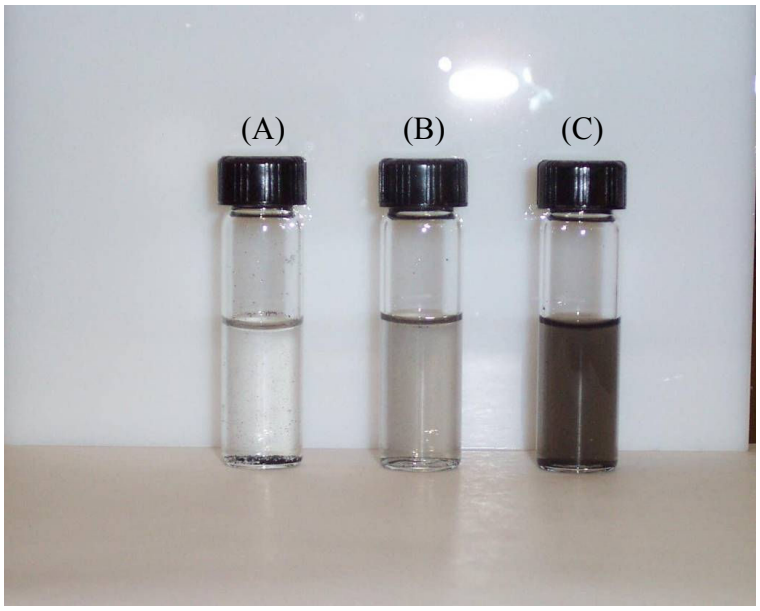

Figure 19: Dispersion of single wall carbon nanotubes in water and soluble type I collagen. (A) 1% SWCNT in water. (B) 1% SWCNT in 0.2% solubalized type I collagen. 5% SWCNT in 0.2% solubalized type I collagen.

To demonstrate the dispersion behavior of SWCNT in collagen, figure 19 (B) and (C) clearly show that carbon nanotubes are well distributed within collagen at 1 and 5 % respectively. Figure 19 (A) shows the contrasting agglomeration of SWCNT in water due to the overcoming Van der Waal forces. Collagen thus is a highly polar medium that readily disperses carbon nanotubes under the proper processing conditions.

The three dimensional appearance of both gelation processed and electrospun collagen-SWCNT nanocomposites were extensively studied using electron microscopy images. SEM images of an NDGA crosslinked type I collagen fiber and collagen-SWCNT fiber are shown in figure 20 and 21 respectively.

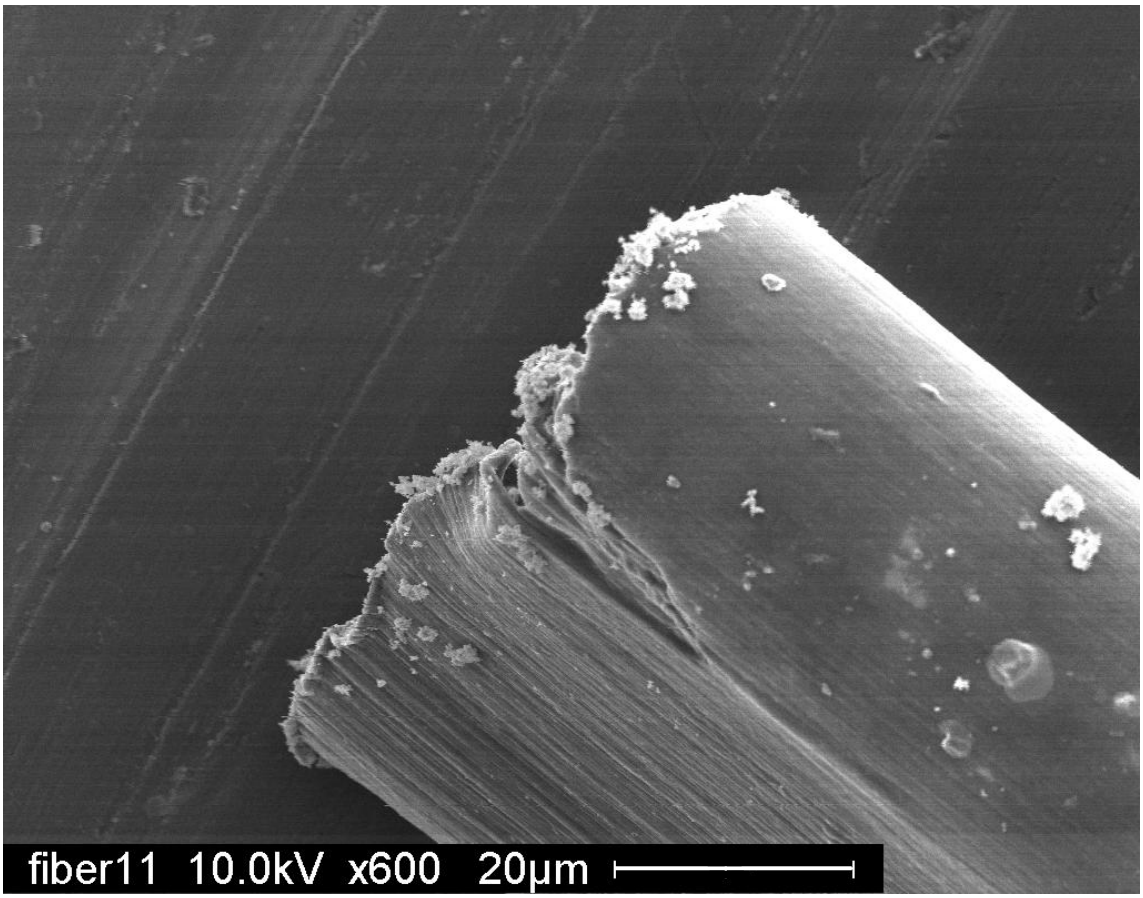

Figure 20: SEM image of a type I collagen gelation processed fiber after rupturing during tensile testing.

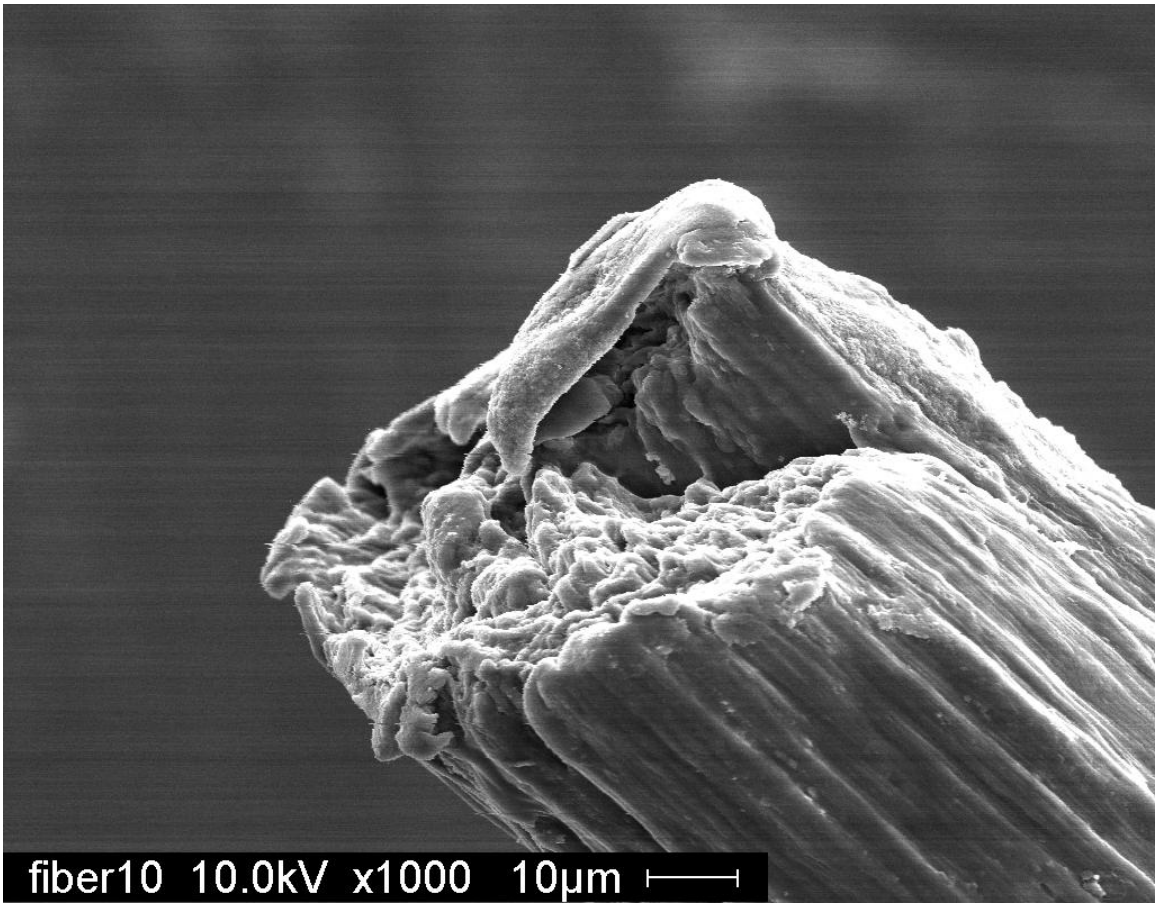

Figure 21: SEM image of a type I collagen with 5% SWCNT gelation processed fiber after rupturing during tensile testing.

SWCNT have a clear impact on the surface morphology of the nanocomposite as shown figures 20 and 21. Further mechanical characterization using a nanoindenter will quantitatively show the impact of SWCNT on the surface modulus and hardness.

A TEM image of gelation processed type I collagen fiber obtained by along the fibril axis cross section is shown in figure 22. The characteristic banded appearance of collagen fibrils a clear in the TEM picture. Although there is little understanding of the exact process by which collagen fibrillogenesis occurs, the banding structures has been attributed to tropocollagen packing. This molecular packing yields an alternative stacking

of an overlap zone and a gapped zone. The resulting staggered crystalline arrangement was found to yield a 68 nm distance between striations, which is discernable from the TEM picture in figure 22.

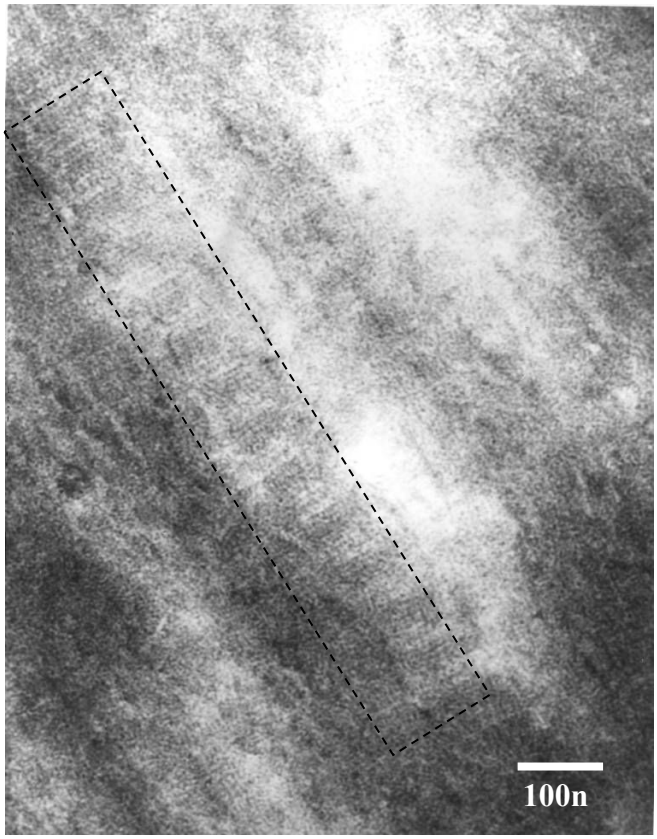

Figure 22: TEM image of longitudinal cross section of NDGA crosslinked type I collagen.

Further investigation was performed using an HRTEM to observe the interaction of single wall nanotubes with the collagen fibrils. The result is shown in figures 23 (A) and (B). One can deduce from part A of the figure that the cross section used for this image was taken perpendicular to the direction of fibrils. This is shown but the dark disk shaped marks that are thought to be cross sections of individual collagen fibrils.

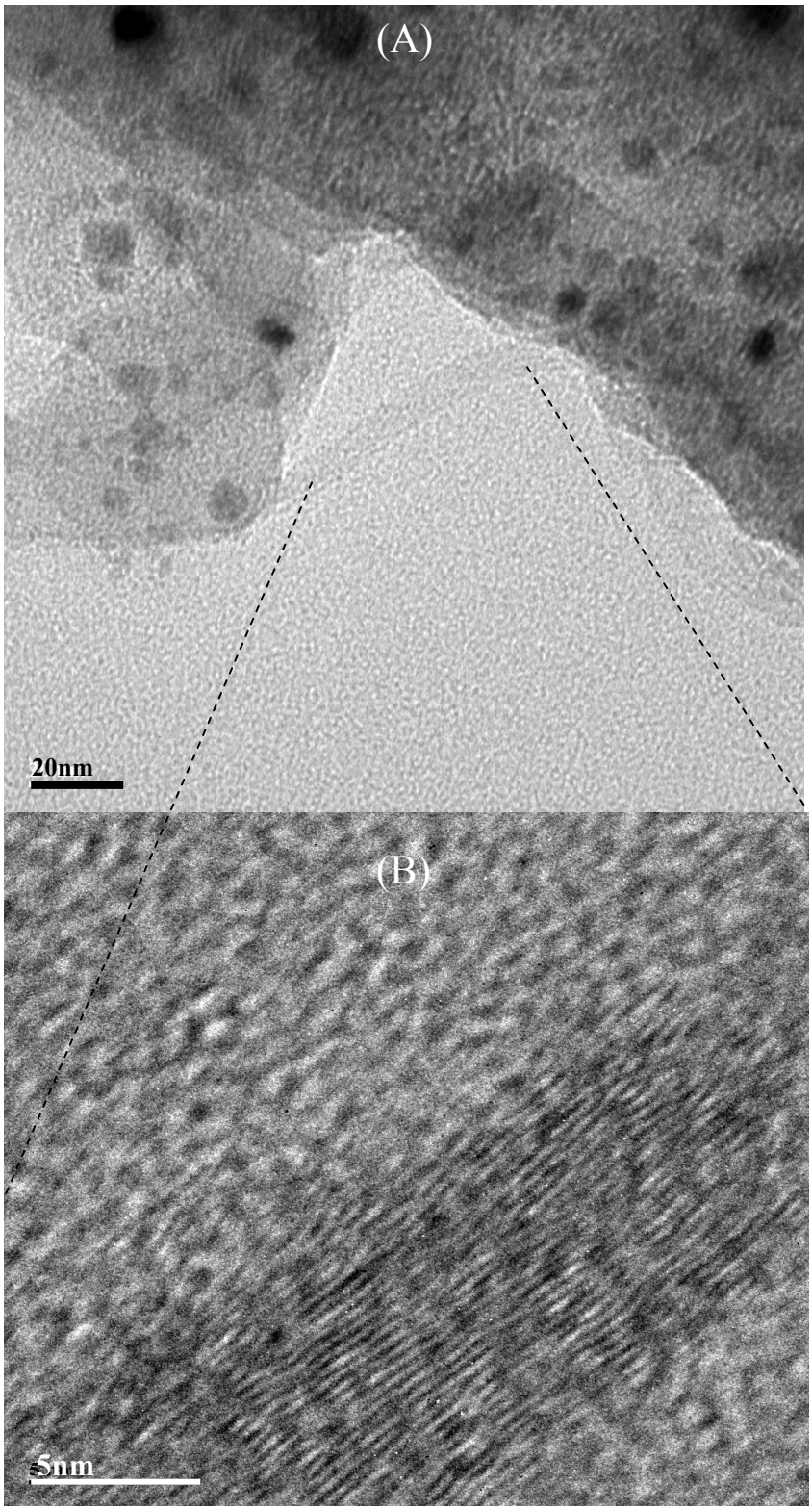

Figure 23: (A) HRTEM image of a collagen-SWCNT cross section. (B) Magnification showing a small bundle of aligned single wall carbon nanotubes.

Figure 23 (B) shows the characteristic carbon walls found in nanotubes, were close to a width of 5 or 6 single wall nanotube are held together by Van der Waal forces.

After discussing the electron microscopy analysis of gelation processed collagen-SWCNT nanocomposite, it is imperative to examine the methodology taken to optimize the electrospun nanofibers using the scanning electron microscopy. Before displaying the images, however, it is necessary to discuss the influential parameters that need to be considered. As discussed in chapter 2, electrospinning is a process that directly results from an imbalance of forces. The cohesive forces which retain the fluid's viscosity and "shape" are mainly due to surface tension characteristics. As the voltage applied to the solution increases, the electrostatic forces become larger than the surface tension forces, which eject the polymeric solution towards the grounded target. The cohesive strength of the solution is characterized by two interactions: the interaction of the solvent particles with other solvent particles (in this case 1,1,1,3,3,3 hexafluoro-2-propanol) and the interaction of the solvent particles with polymer molecules (or dissolved collagen molecules). Since the polymers tend to be longer than the solvent, hydration of the polymer molecules ends up to be the primary interaction. The interactions between solvent particles are characterized by surface tension, while the interactions between solvent and polymer molecules are characterized by viscosity. Figures 24 through 27 show the impact of collagen concentration on the quality of electrospun fibers. One could clearly notice the "beading" effect of viscosity and surface tension ratios. Solutions with collagen concentrations above 20% (w/v) or 20 g per 100 ml of solvent did not yield any nanofibers. Concentrations between 20 and 10% had large amounts of beads.

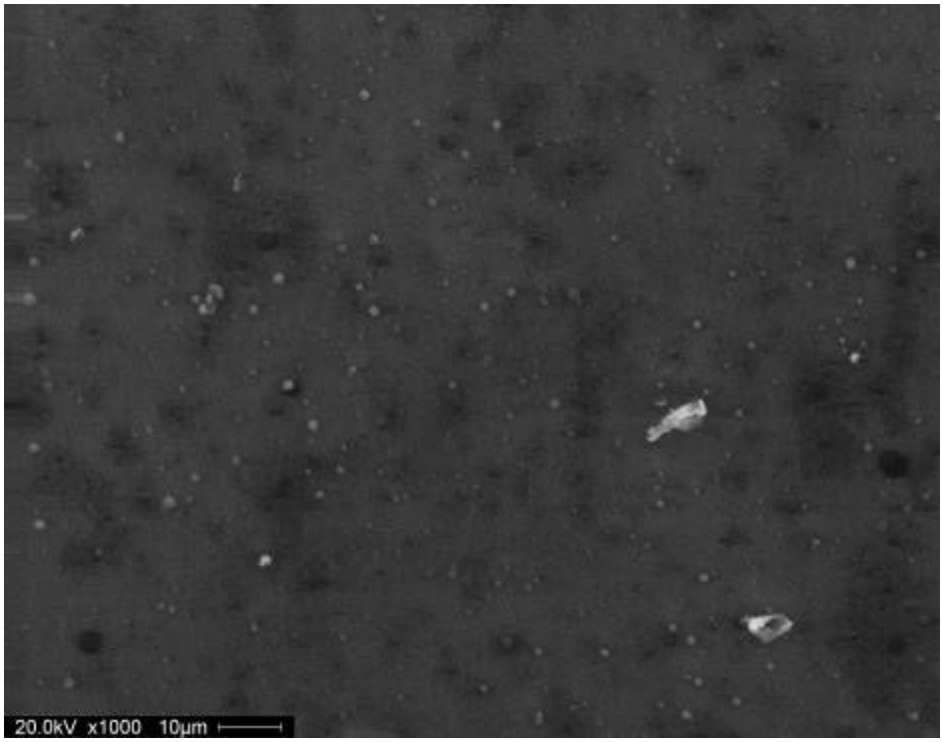

Figure 24: Electrospun collagen at 20% (w/v).

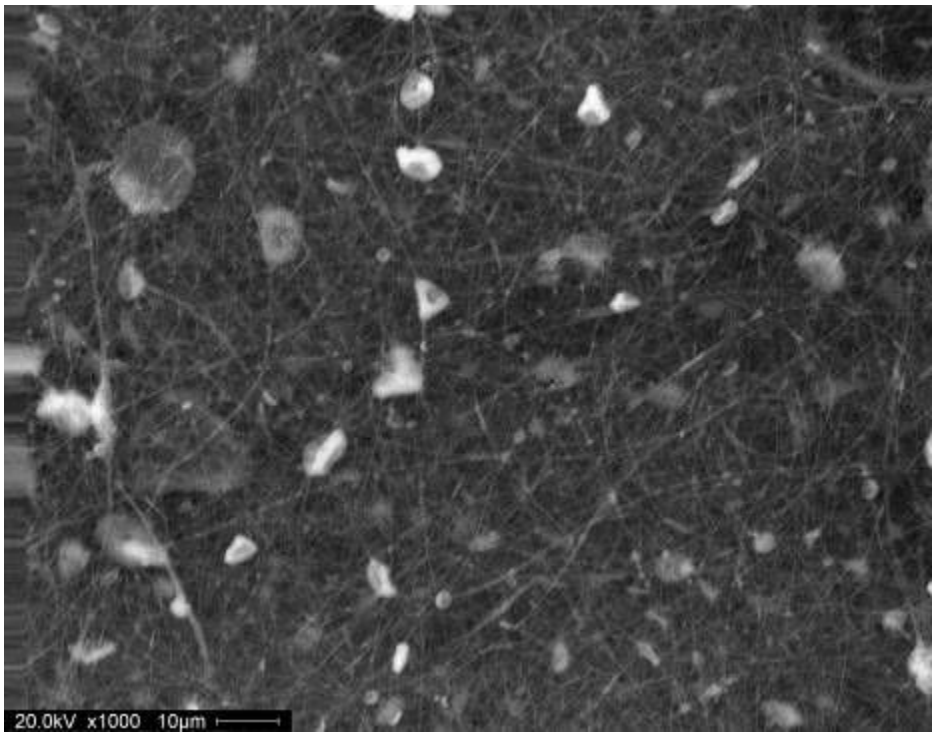

Figure 25: Electrospun collagen at 15% (w/v).

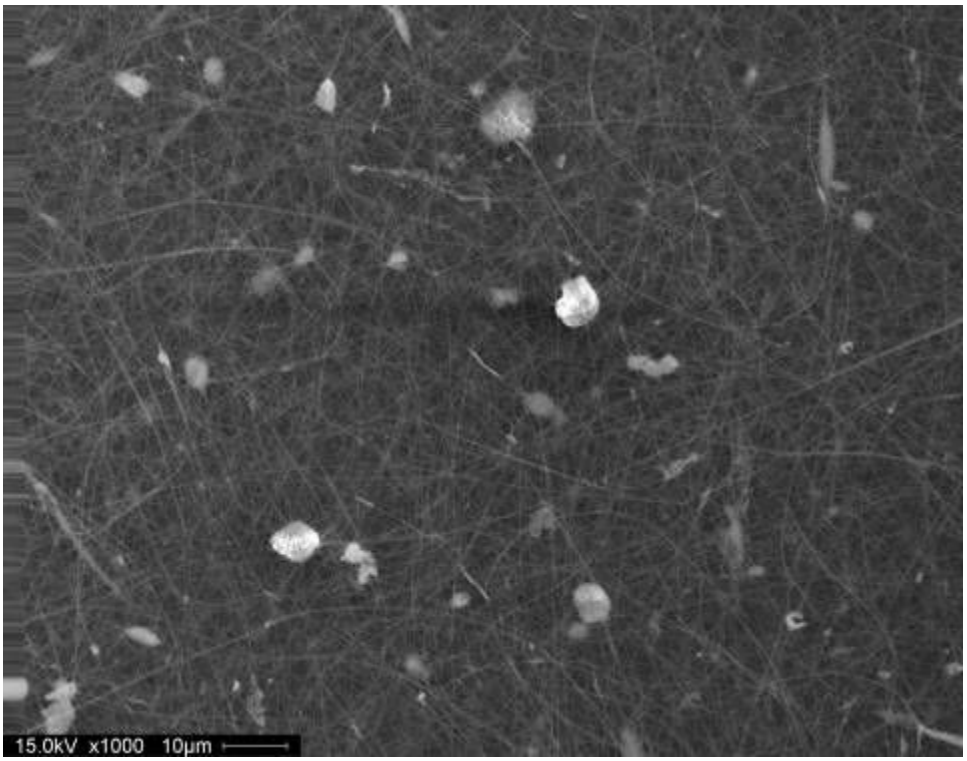

Figure 26: Electrospun collagen at 10 (w/v).

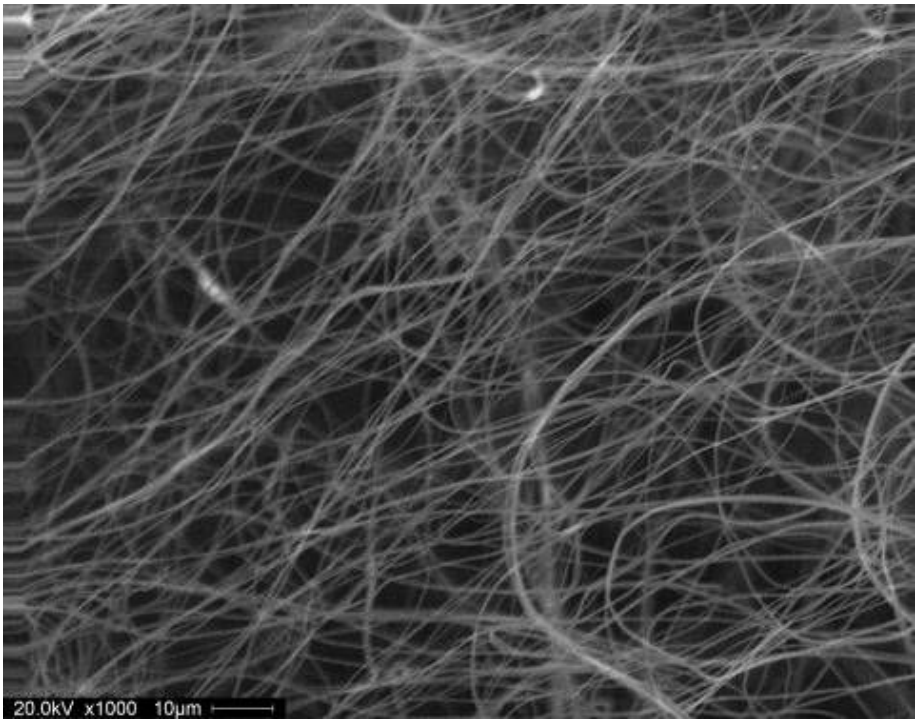

Figure 27: Electrospun collagen at 8 (w/v).

These beads are agglomerations of fibrils due to increase in the applied voltage needed to overcome the surface tension forces at the tip. It is also important to notice that over 20% collagen concentration entrains saturation of the polymer solubility. This situation contributes to the entanglement of collagen fibrils and increases the beading effect. As bead formation decreases, more uniform nanofiber formation increases. The optimized concentration of collagen was determined to fall in the range between 8 and 10% (w/v). The DC voltage needed to overcome the surface tension at the optimized concentration was found to range between 15 and 17 kV.

The effect of spinneret to target distance was also studied and optimized at 22 cm. This is an important parameter in electrospinning nanocomposites for biomedical applications. This is due to the need for the solvent to evaporate before reaching the target. It is well known that 1,1,1,3,3,3 hexafluoro-2-propanol is a highly toxic solvent and any trace of its existence within the electrospun fiber could be detrimental to the subsequent use of fiber to grow any biological tissue. Optimization of the spinneret to collector distance was done in parallel with the concentration adjustment process. Figure 28 and 29 show two SEM images with different magnifications detailing the effect of electrospinning at close range (in this case 8 cm between spinneret and target.) Figure 28 clearly shows the large solvent spots along with large structures of unorganized collagen fibrils due to the high concentration used in this case (25% w/v). Figure 29 shows the effects of the close distance with a lower collagen concentration (20% w/v). Figures 30 and 31 show the non-aligned and aligned fibers respectively. The ability to align electrospun fibers is essential in guiding cell proliferation during tissue engineering.

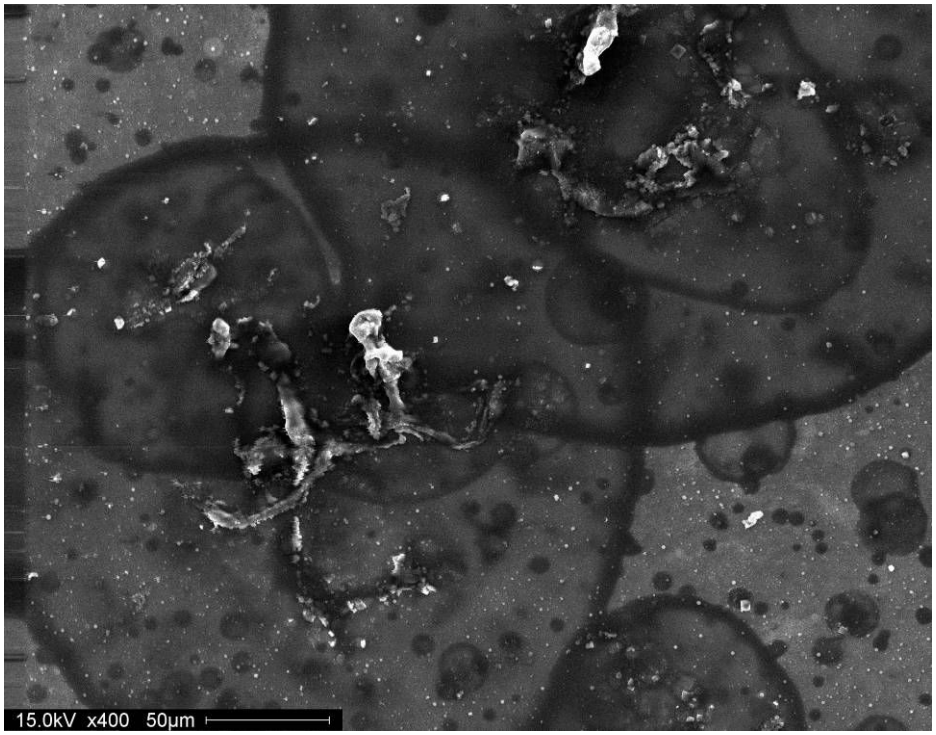

Figure 28: Low magnification SEM image showing the large solvent spots.

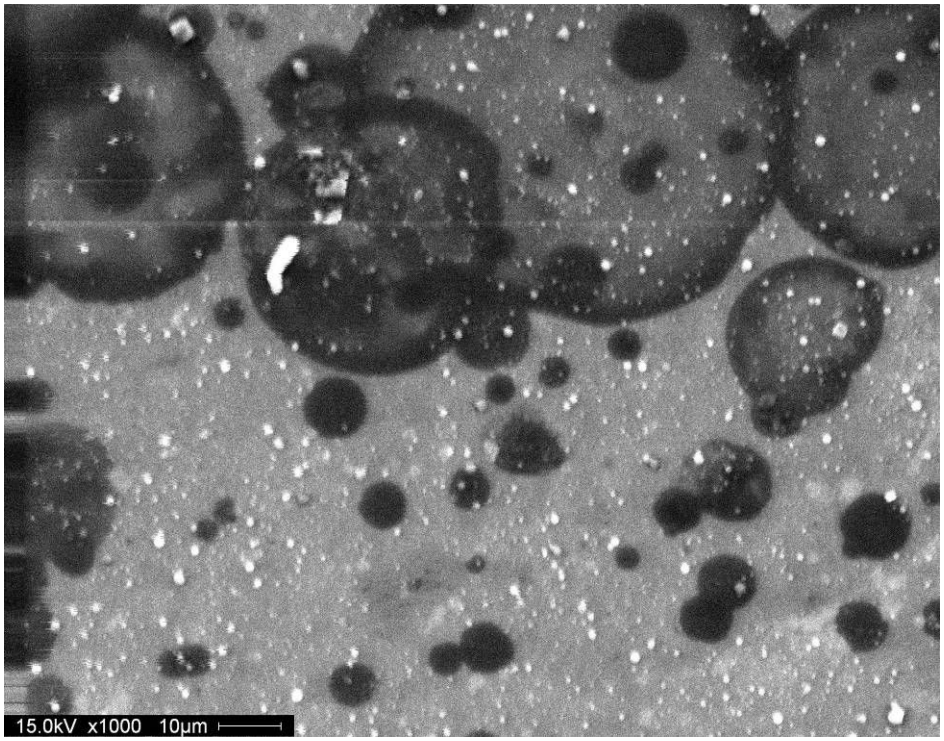

Figure 29: Higher magnification SEM image showing the large solvent spots.

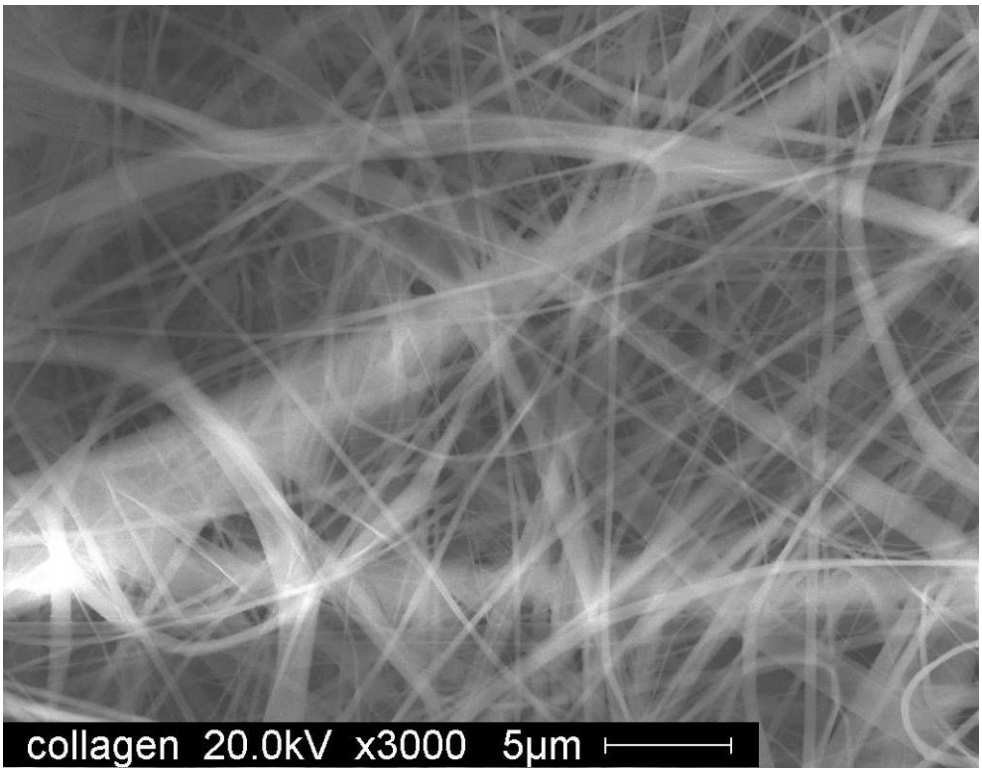

Figure 30: SEM image of non aligned electrospun collagen.

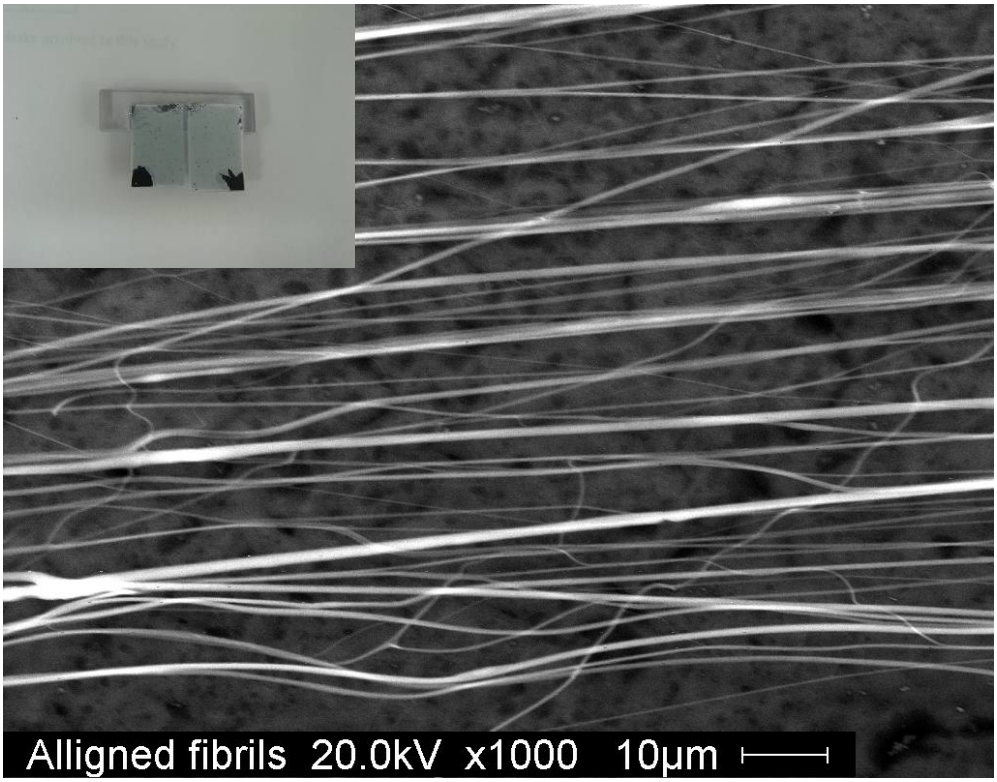

Figure 31: SEM image of aligned electrospun collagen. Onset shows the setup used to obtain aligned fibers.

Further microscopy analysis of electrospun collagen-SWCNT nanocomposite was conducted using HRTEM. Figure 32 shows a low magnification HRTEM image of collagen mixed with 5% single wall carbon nanotubes. Some agglomeration is clearly seen in this low magnification image. This is thought to be due to the relaxation time that carbon nanotubes go through when they are dissolved in the 1,1,1,3,3,3 hexafluoro-2-propanol. Thus electrospinning the nanocomposite immediately after mixing is necessary to obtain more uniform nanofibers. This condition is not necessarily disadvantageous because there single wall nanotubes could be extremely useful on the surface of the fibers. The usefulness is related to the ability to be recognized by communication specific proteins found on the surface of mammalian cells such as integrin.

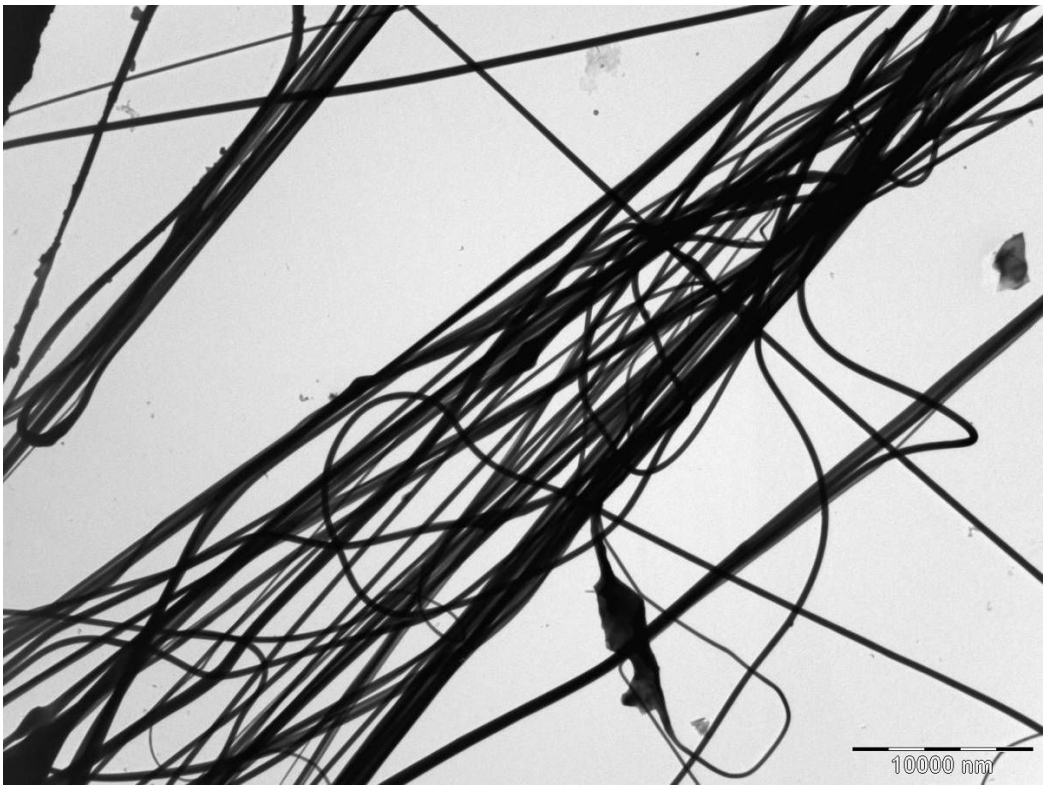

Figure 32: Low magnification HRTEM image of electrospun collagen- 5% SWCNT.

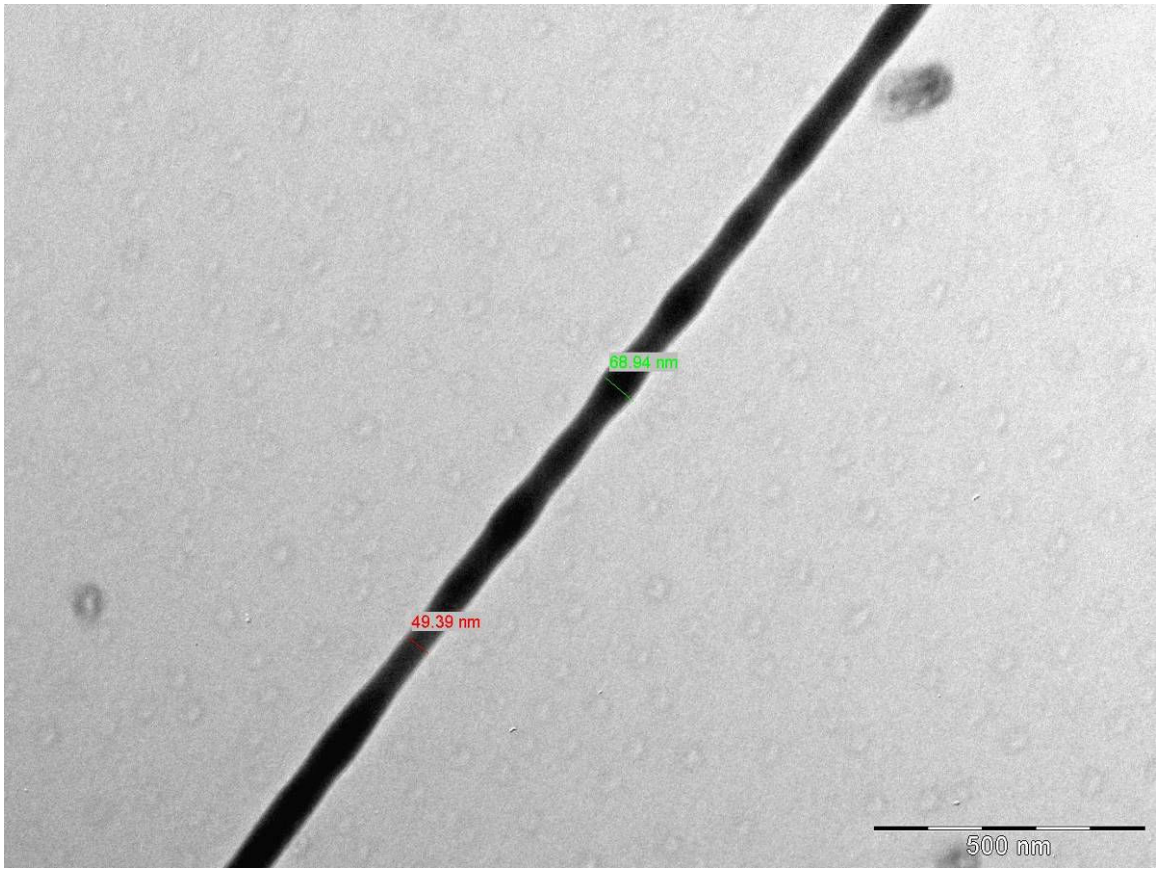

Figure 33: Higher magnification HRTEM image of electrospun collagen- 5% SWCNT.

Figure 33 shows a higher magnification of one of the electrospun collagen fibers containing 5% SWCNT. The effect of carbon nanotubes is shown in this picture as period conglomerates. Measurements shown on the picture depict the swelling effect caused by the SWCNTs from 49 to 59 nm. The variations in fiber diameter are a definite advantage in designing electrospun micro and nanofiber mats for use in biomedical engineering applications such as tissue engineering.

3.4.2 Atomic Force Microscopy Analysis

Atomic force microscopy (AFM) is a great tool to observe topographies of different nanostructures and thin films with angstrom precision. Figure 34 and 35 show a surface

topography and a three dimensional image respectively of the gelation processed collagen fiber with no imbedded carbon nanotubes. The fiber was immersed in a sample holder containing a phosphate buffer solution and a high stiffness AFM cantilever tip was used. The imaged surface shows a high degree of alignment of collagen fibrils in the longitudinal axis, which is supported by the SEM image in figure 20. This explains the relatively high tensile strength exhibited by the collagen fiber, as shown in Koob et al[69].

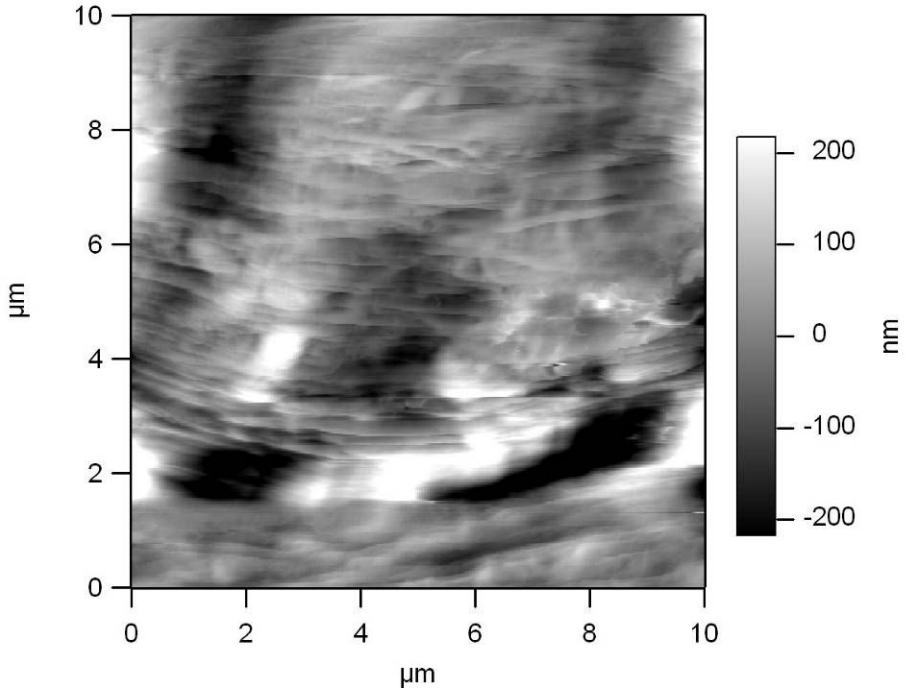

Figure 34: Atomic force microscopy images showing a 2D surface distribution of gelation processed fiber.

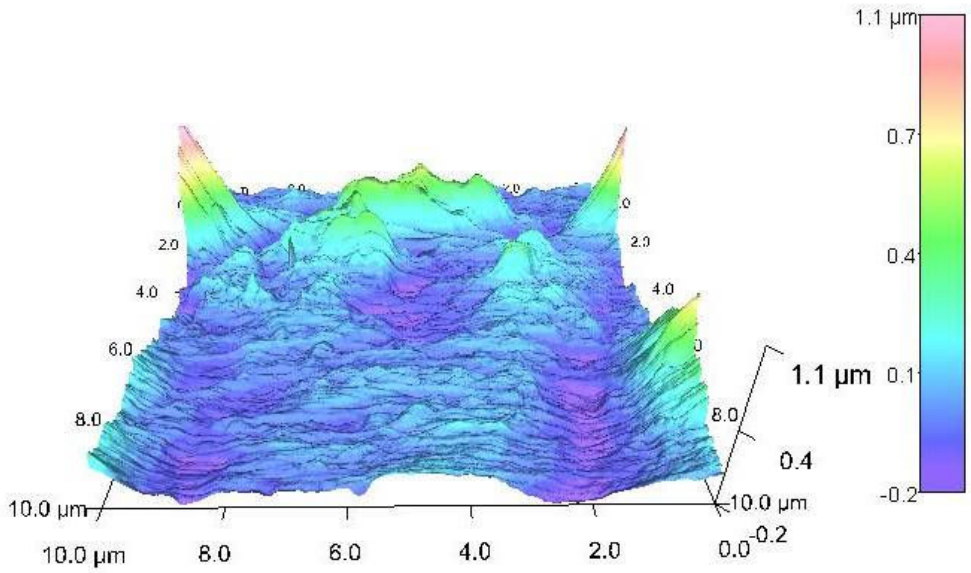

Figure 35: AFM representation of a 3D surface distribution of the same fiber as in figure 34.

Electrospun collagen-SWCNT nanofibers where also studied using AFM. Figure 36 shows a surface image of the nanocomposite immersed in a phosphate buffer solution. The novel approach used to collect the AFM image shows with high clarity the different between the highly stiff single wall carbon nanotubes and much softer collagen matrix. Carbon nanotubes are represented by thin white lines. The black arrows shown in figure 36 highlight one long bundle of single wall carbon nanotubes.

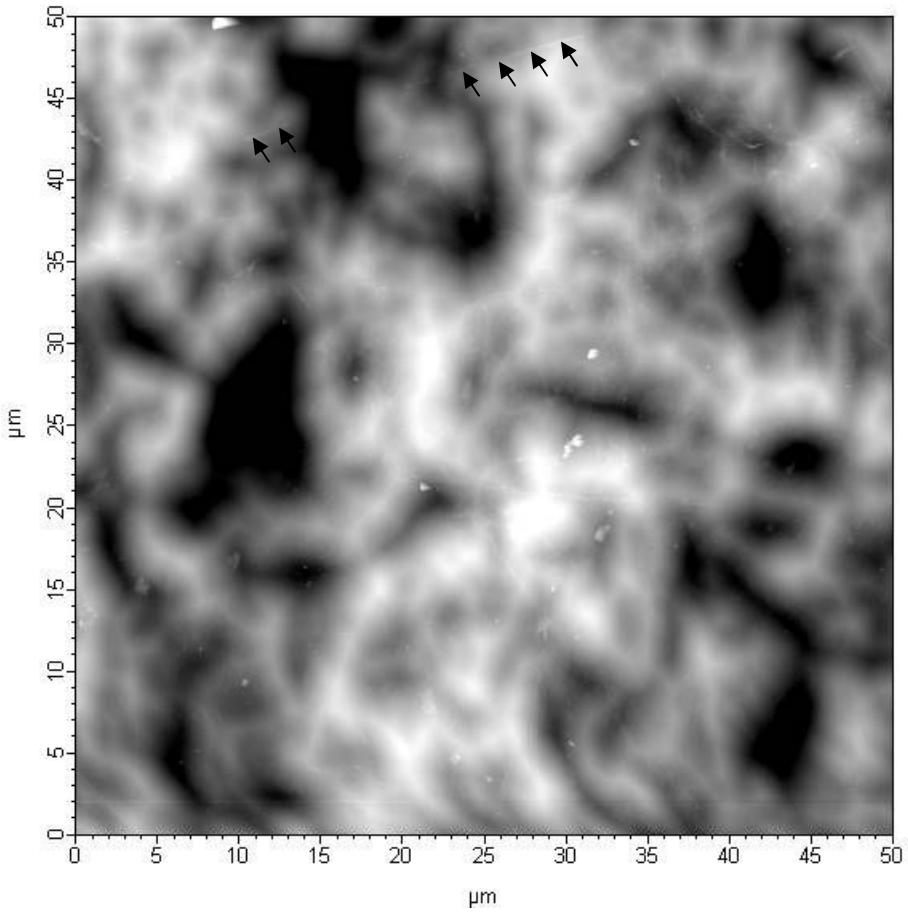

Figure 36: AFM image of electrospun collagen-5%SWCNT in phosphate buffer.

3.4.3 Spectroscopy Analysis

FTIR and Raman spectroscopy were the main two spectroscopic characterization techniques used to validate the existence of type I collagen and single wall carbon nanotubes. Characteristic peaks were observed in both spectroscopy measurements that provide proof for the existence of type I collagen and SWCNT. Figure 37 shows FTIR spectra of the collagen/SWCNT nanocomposite. Characteristic peaks of main amide groups were observed and matched current literature[8]. This clearly demonstrate the existence of type I collagen in the nanocomposite. All FTIR spectra showed the same

collagen characteristic peaks. The percentage of carbon nanotubes used in the nanocomposite sample was not enough to show characteristic peaks.

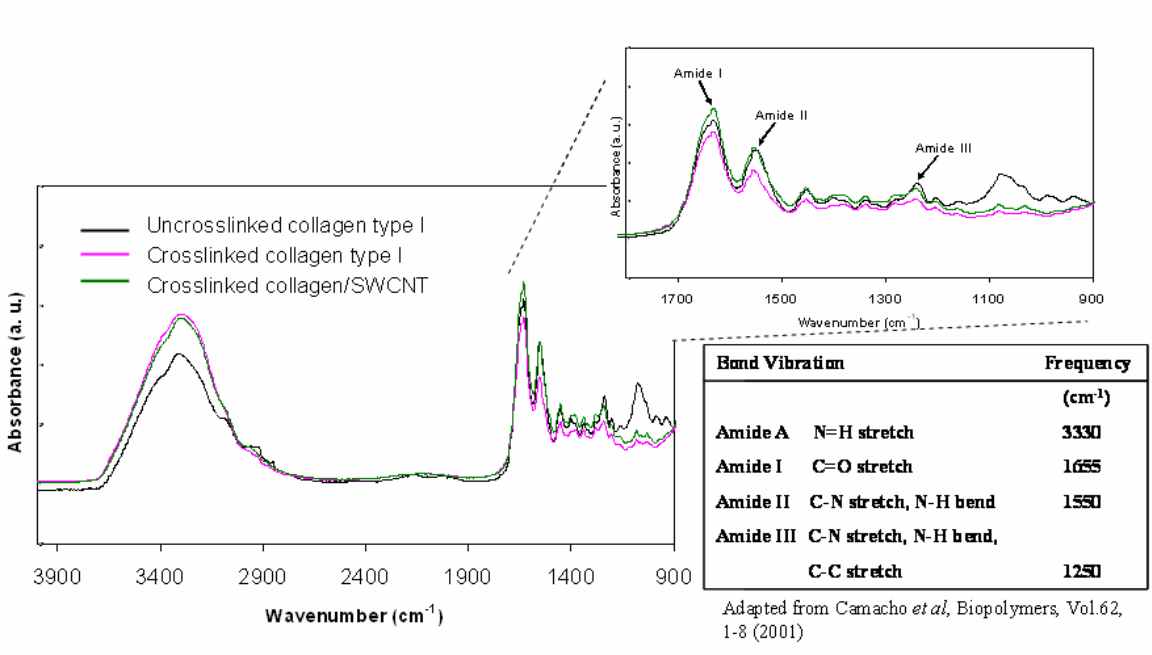

Figure 37: FTIR spectra of collagen and nanocomposite (5%SWCNT w/w).

Raman spectroscopy was used to confirm the presence of SWCNT within the nanocomposite. Figure 38 shows distinct peaks in the G band (1580-1590 cm^{-1}) and D band (1550-1565 cm^{-1}). These two peaks are characteristic of carbon nanotubes. Notice the small shift in from 1582 to 1587 cm^{-1} between pure carbon nanotubes and collagen composite. This is due to damping that collagen provides in the axial vibration of the carbon nanotubes during laser excitation[142, 143]. Furthermore, the vibration peak at 180 cm^{-1} proves the existence of SWCNT due to the distinct radial breathing mode effect, which is a radial expansion of single walls as a result of the exciting laser[144].

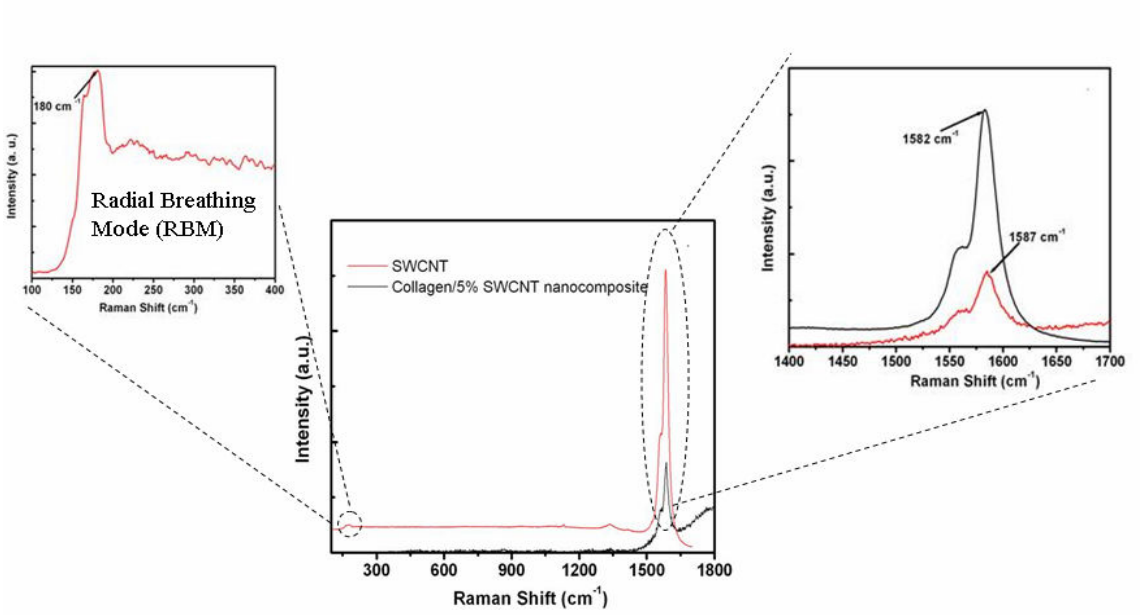

Figure 38: Raman Spectroscopy of collagen-SWCNT (5% w/w) nanocomposite.

3.4.4 Bulk Mechanics

Mechanical testing of the fibers showed strength at failure (between 90 and 140 MPa) and Young's modulus (between 850 and up to 1200 MPa) values that were comparable to native tendon values. Figure 39 shows a representation of the mechanical characterizations of the nanocomposite versus control fibers. Uniaxial tensile tests to failure at a strain rate of 1% per second were performed on the collagen based nanocomposite fibers. Results in figure 39(A) showed strength at failure between 0.09 and 0.14 GPa and part (B) shows a Young's modulus between 0.85 and up to 1.2 GPa that were comparable to native tendon values. At high concentrations of SWCNT, a gradual increase in stiffness was observed. A net decrease in mechanical integrity was observed in nanocomposites with SWCNT weight percentage of 10 and 20%. This is thought to be due to large increase in segregation of carbon nanotubes within the biomatrix thus decreasing the alignment of collagen fibrils along the longitudinal axis.

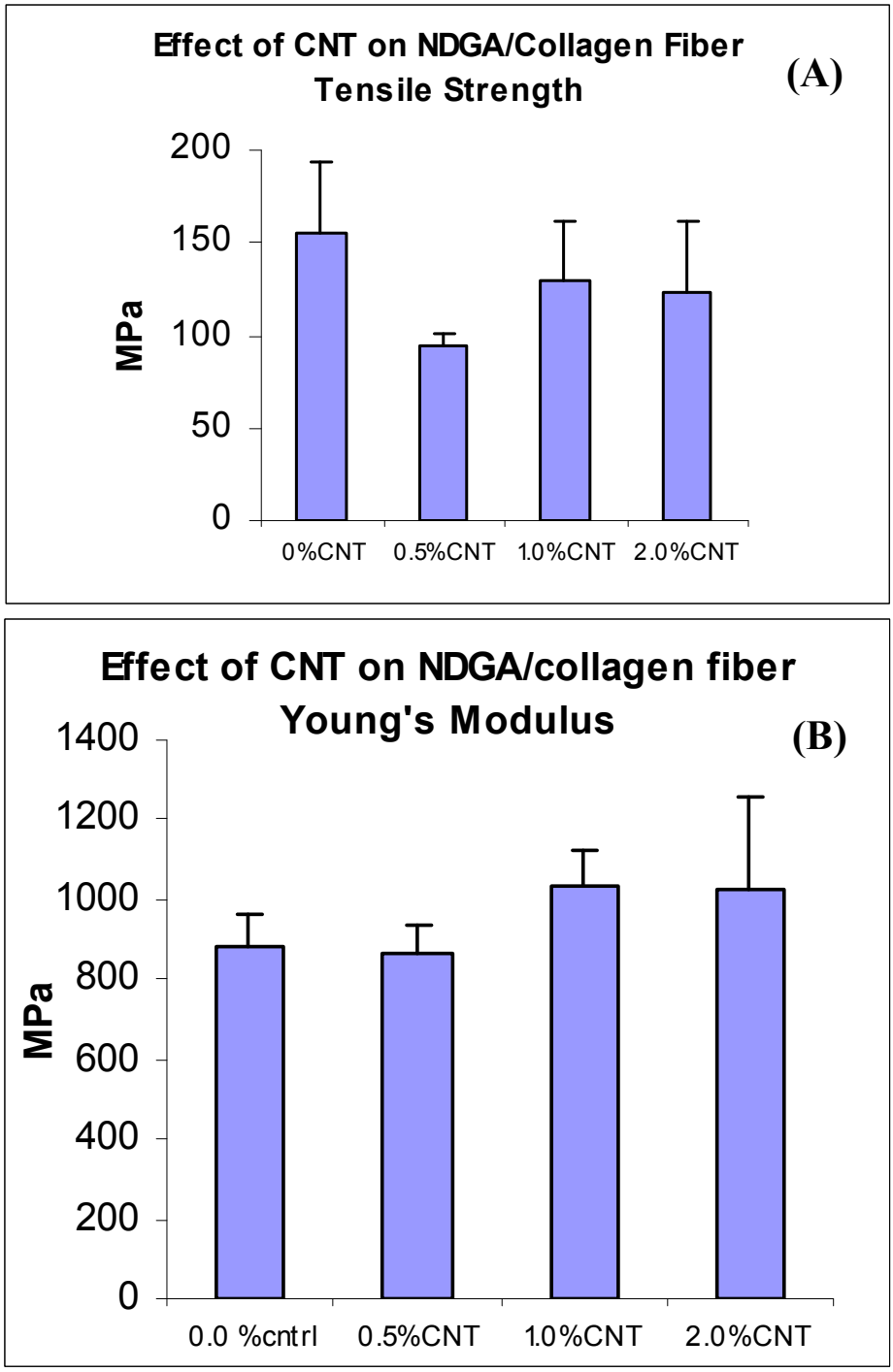

Figure 39: Mechanical characteristics of collagen and nanocomposite fibers. (A) Variation in ultimate tensile strength with percent SWCNT. (B) Variation in bulk stiffness with percent SWCNT.

The nanocomposite provides stiffness tunability which is crucial in designing material for tendons and ligaments. Improved spinning fiber techniques are expected to increase the isotropic alignment of carbon nanotubes, which will dramatically increase the stiffness of the fiber composite[145]. The decrease in ultimate strength is thought to be due to problems with segregation in SWCNT. This has plagued carbon nanotube research and efforts are made to optimize the dispersion techniques at different carbon nanotube concentrations. It is important to note that the increase in stiffness is a necessary mechanical characteristic during the fixation of the fiber composite into bone tunnels due to the compounded effect on the interfacial shear stress. This may prove to be an instrumental advantage that could solve the fixation challenges faced by existing materials and devices.

3.4.5 Nanoindentation

Nano scale indentation testing is a method that was developed as a thin film surface characterization tool. This method was developed as a refinement technique to the already established Brinell, Knoop, Vickers, and Rockwell indentation procedures. Nanoindentation requires the use of an indenter tip with a known geometry. This tip is driven into the material to be tested by applying an increasing normal load. Apart from the nanoscale displacement of displacement of the tip, the distinguished feature involved is the indirect measurement of the contact area between the tip and the specimen. As a result, at each stage of the experiment the position of the indenter relative to the sample surface is precisely monitored with a sensor. Data is obtained by graphing each loading and unloading cycle. A typical load-unloading curve is depicted in figure 40. Notice that

the calculated stiffness S is directly proportional to the change in unloading force and inversely proportional to the change in unloading displacement as shown in the following equation; were P is the load, h is the tip displacement, and E_r is the reduced modulus.

$$S = \frac{dP}{dh} = 2 \cdot \sqrt{A} \frac{E_r}{\sqrt{\pi}}$$ Equation 6

To obtain the reduced modulus equation 7 is used were E_r is the reduced (combined) modulus of the system composed of the indenter (E_i) and the sample (E_s) moduli.

$$\frac{1}{E_r} = \frac{1-\upsilon_i^2}{E_i} + \frac{1-\upsilon_s^2}{E_s}$$ Equation 7

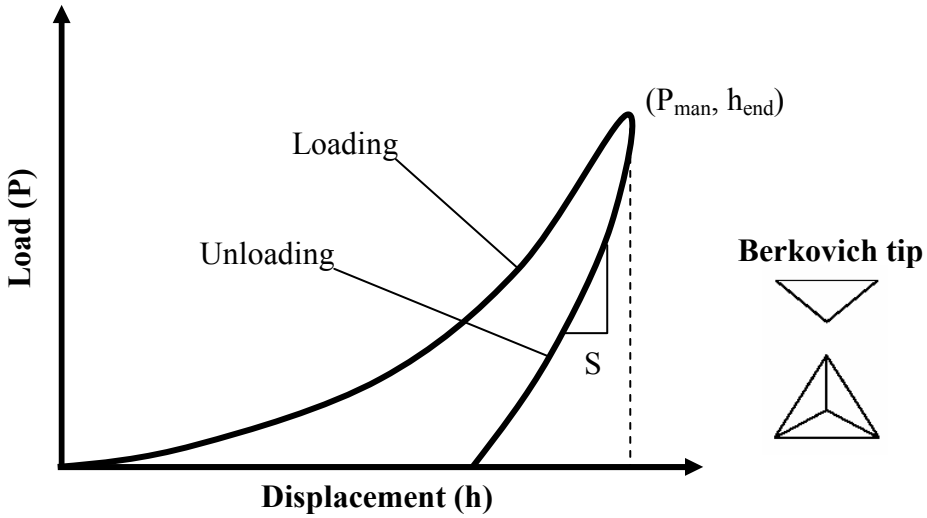

Figure 40: Typical load-unload nanoindentation curve[47]. Schematic of a Berkovich indenter tip (onset)

Load versus displacement curves are the result of downward and then upward movement of the nanoindenter. A schematic illustration of a Berkovich indenter is shown as an onset in figure 40. Because the hardness and modulus calculations, derived from the nanoindentation process, are related to the indenter tip geometry and the apparent contact

area, it is important to account for non ideal situations. To account for non ideal geometric deformities at the tip of the indenter, it is crucial to perform a calibration process using a sample with well know surface characteristics prior to conducting an experiment. To account for initial disparities in the apparent contact area, the author disregarded data points collected from initial contact to an indentation depth of 50 nm as suggested by literature.[47] One of the challenges in designing a nanoindentation experiment on the gelation processed fibers is the geometric shape of these fibers. Nanoindentation is usually carried on smooth thin films to characterize the film and its interfacial properties. Due to the cylindrical shape of the fibers, precise alignment and shallow indentations are necessary for accurate measurement of the mechanical surface properties. Figure 41 shows the geometrical schematics of the indenter-fiber surface interface.

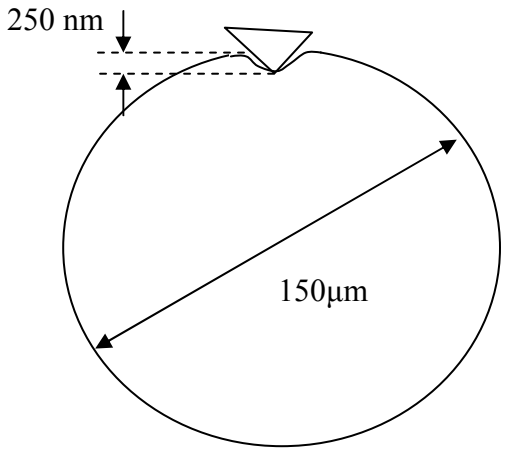

Figure 41: Schematic representation of maximum indentation depth with respect to fiber total diameter.

Figure 42 shows a load versus displacement curves of 16 indentations performed on a crosslinked collagen fiber. As mentioned in the characterization section of the chapter, 25

indentations were performed on duplicates of each specimen to validate the collected data. Due to a relatively high surface roughness however, certain indentation sites did not yield completed data because errors in the software calculation procedure. Different indentation values were collected for different specimen with the lowest being 3 indentations for crosslinked collagen with 10% SWCNT.

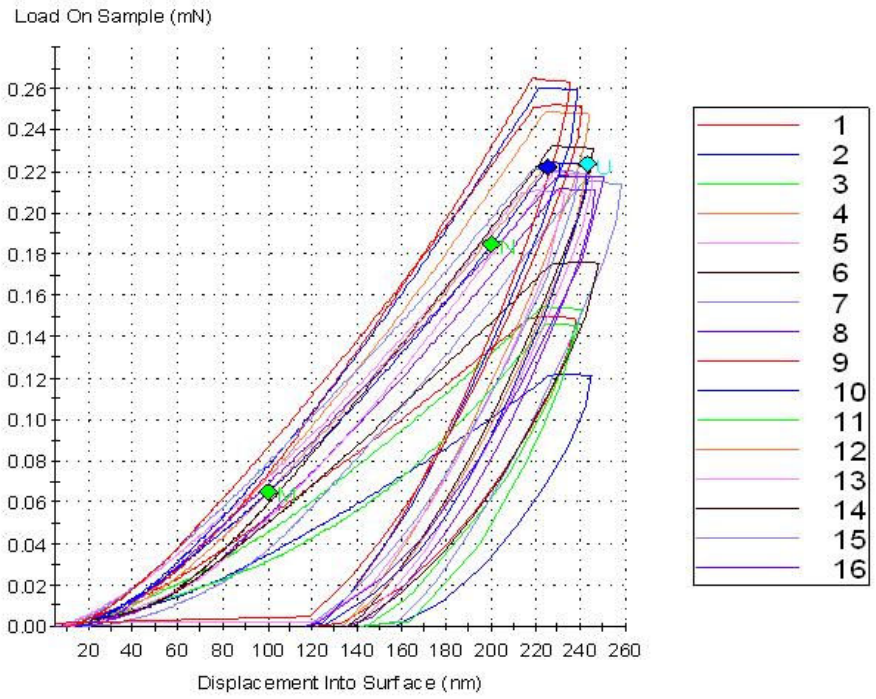

Figure 42: Load vs. Displacement of cross-linked collagen fibers.

Modulus and hardness data was derived from the load versus displacement curves. Figures 43 and 44 show the modulus and hardness values respectively for uncross linked and crosslinked collagen along with different percent SWCNT nanocomposites.

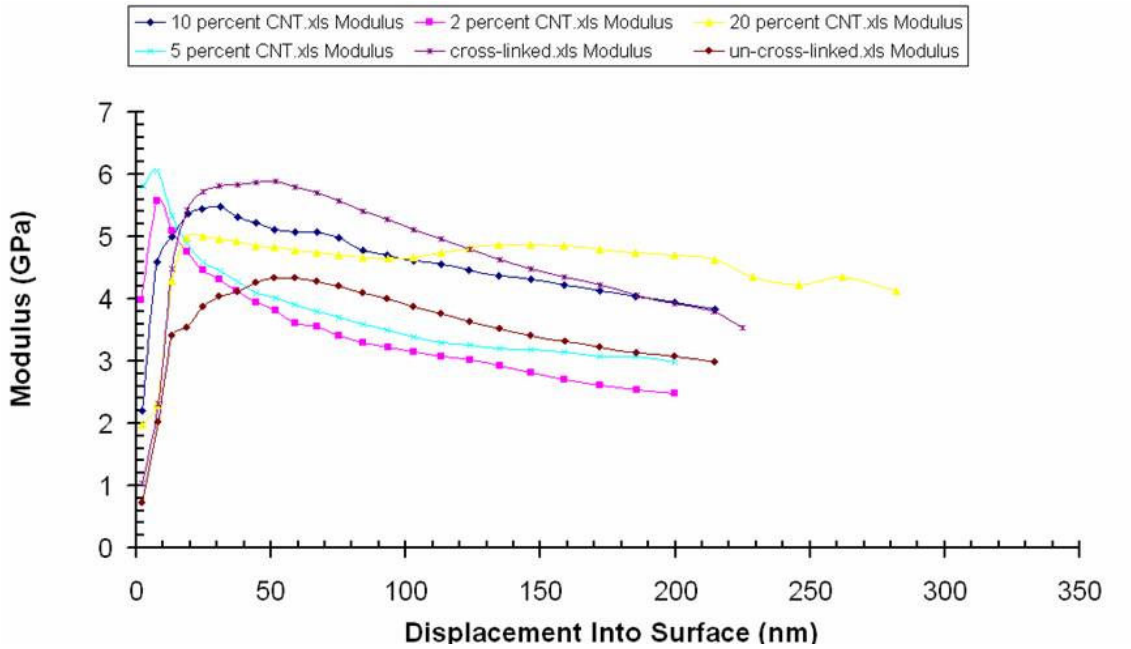

Figure 43: Modulus versus displacement graphs of gelation processed fibers.

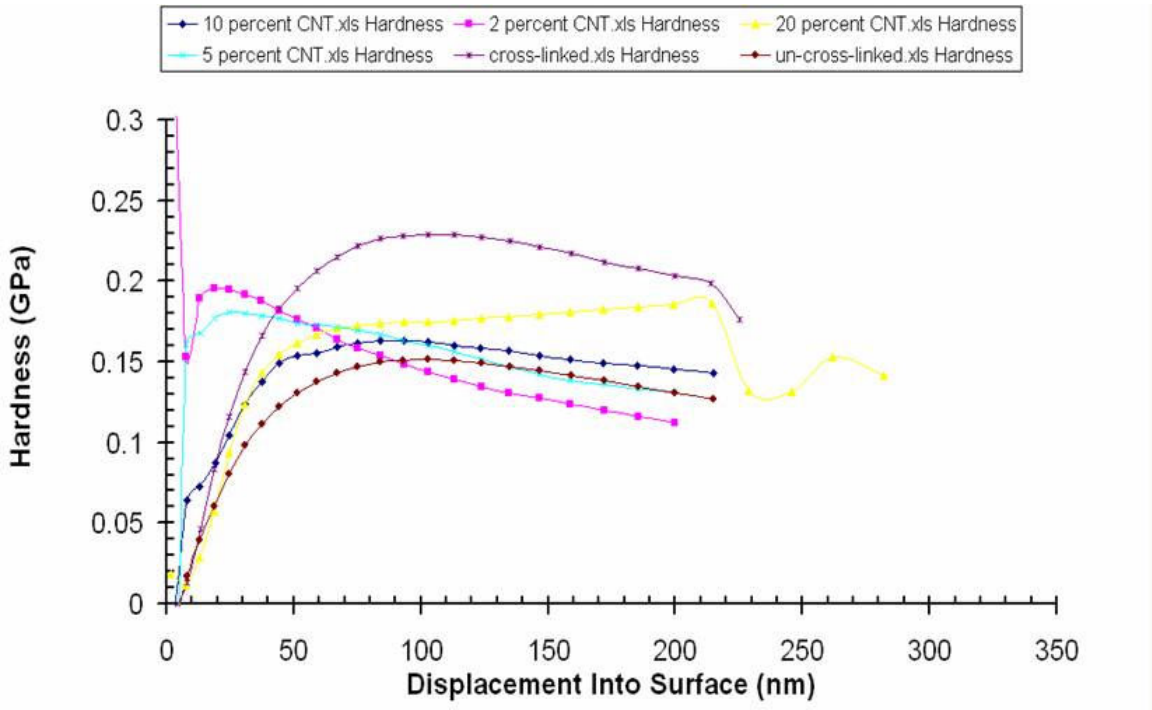

Figure 44: Hardness versus displacement graphs of gelation processed fibers.

Two main important observations could be deduced from figure 43. Crosslinking has definite effect on the surface modulus as has been noticed in the bulk mechanical characterization. The second observation relates to the proportional increase in surface modulus with increase in SWCNT percent content. Finally, 20% SWCNT registered a higher surface modulus than crosslinked collagen. This data is contradictory to the bulk mechanics values that suggest decrease in bulk modulus with increase carbon nanotube content. This is due to the nature of the forces applied in both characterization techniques and the behavior of collagen and SWCNT with respect to the applied forces. In bulk mechanics, tensile force was applied along the major axis of the collagen fibrils and SWCNTs. This has entrained slipping effects magnified by certain conglomeration effects of carbon nanotubes in between fibrils. Nanoindentation, on the other hand provides an inherent compressive force that is perpendicular to the major fibril and SWCNT axes. The carbon nanotubes thus, play a reinforcing role regardless of agglomeration effects. Similarly, hardness values increase with both crosslinking and percent SWCNT increase as shown in figure 44.

3.4.6 In Vitro Analysis

A cell line was derived from human osteoblast transfected with SV40 T antigen was used to study the biocompatibility of the nanocomposite. Cells grew around control and nanocomposite fibers to confluence after 1 day and osteocalcin production increased from day 1 to day 4 after culture with no significant difference between control and nanocomposite. Figure 45 shows the clear increase in osteocalcin count after 4 days in all 3 samples with the highest increase registered with the carbon nanotubes containing

specimen. Figure 46 shows a CyQuant assay conducted using the derived osteoblast cells in media containing collagen films with different purification % of SWCNT.

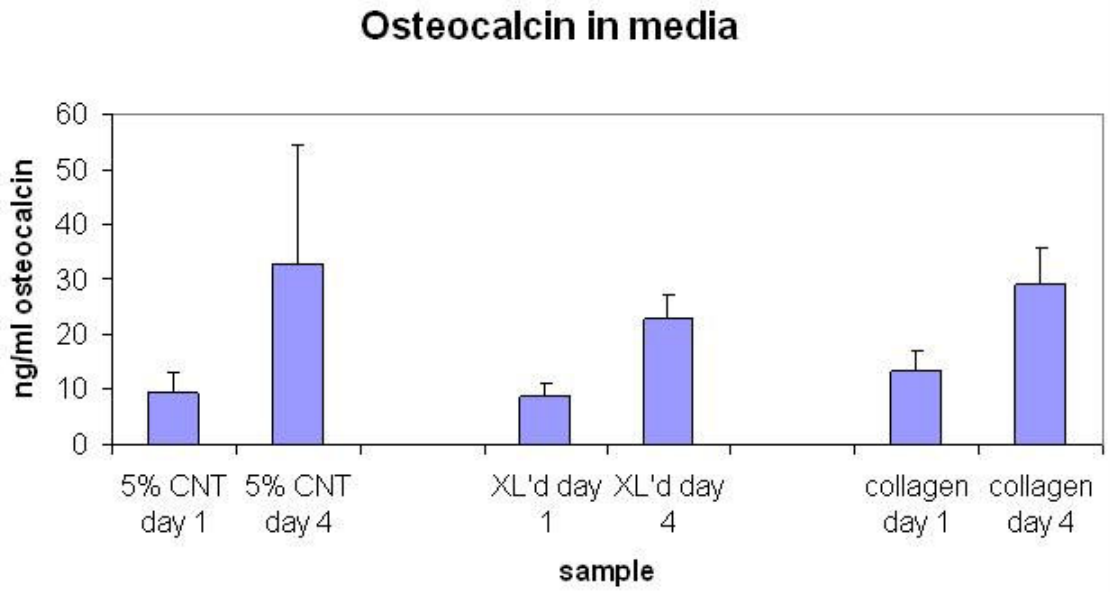

Figure 45: Osteocalcin count in un-crosslinked, crosslinked, and 5%SWCNT containing gelation processed collagen fibers.

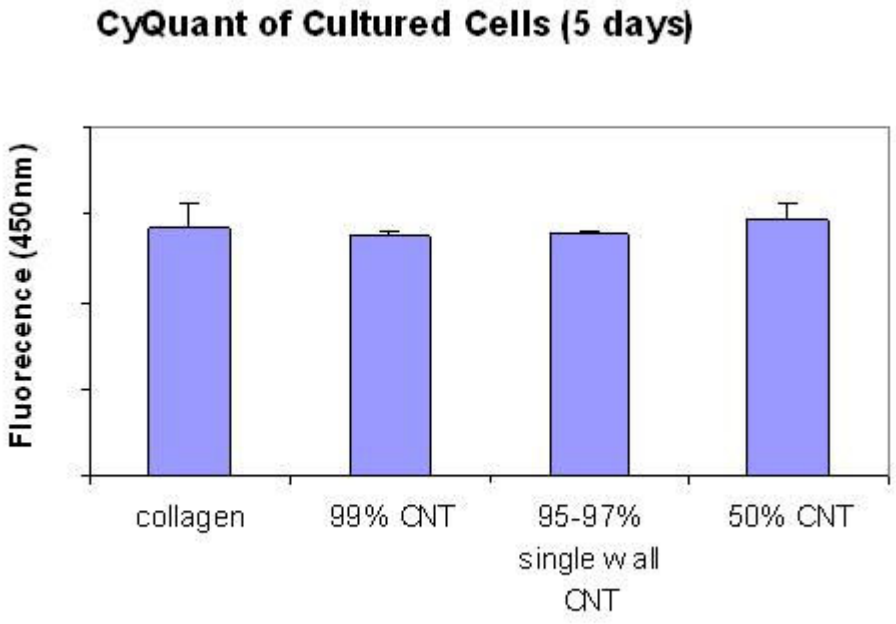

Figure 46: Osteoblast cell count 5 days after culture.

There was no significant variation in the cell count and osteoblast cells were found to be confluent after one day in culture, indicating good biocompatibility of this specific composite. Figures 47 (A) and (B) respectively show light microscopy images of good osteoblast cell population around NDGA-collagen fibers (control) and NDGA crosslinked nanocomposites fibers with 2% content of SWCNTs.

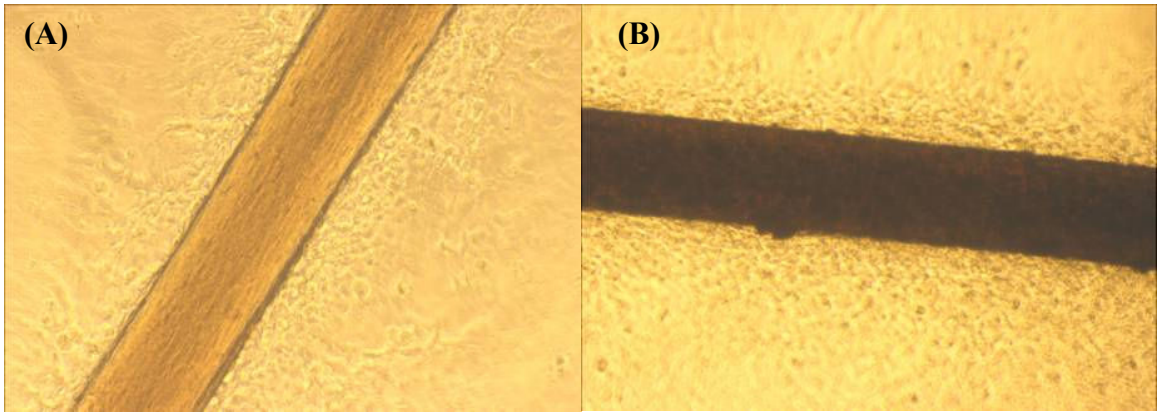

Figure 47: Optical microscopy image of (A) crosslinked collagen and (B) crosslinked collagen-2% SWCNT nanocomposite.

Due to the inherent partial biodegradability of the collagen fibers, it is expected that the carbon nanotubes will play a mediation role in new bone formation around the implant, thereby increasing the mechanical strength of the interface. Furthermore, we expect to use the ability to tailor the stiffness of the nanocomposite to develop bone-like mechanical properties that can be used for bone augmentation and replacement. The properties of this composite can be adjusted by varying the relative proportions of the constituents and the fiber formation processes. Further investigation into the biocompatibility of the developed collagen/SWCNT nanocomposite was conducted. After growing osteoblast cells were confluent in culture, samples were collected and

stained with Alizarin red to observe the osteocalcin activity after contact with control and nanocomposite fibers. All samples (un-crosslinked, crosslinked collagen, and crosslinked nanocomposite with 5% SWCNT) displayed similar increases in osteocalcin activity from day 1 to day 4. The nanocomposite, however, did show larger fluctuations in osteocalcin activity particularly in day 4. This is mainly due to large differences in surface morphology between different nanocomposite samples.

3.4.7 Thermal Analysis

Thermal analysis such as Differential Scanning Calorimetry (DSC) and Thermal Gravimetric Analysis (TGA) are important characterization tools to investigate polymer's intrinsic molecular rearrangements as a result of a change in temperature.

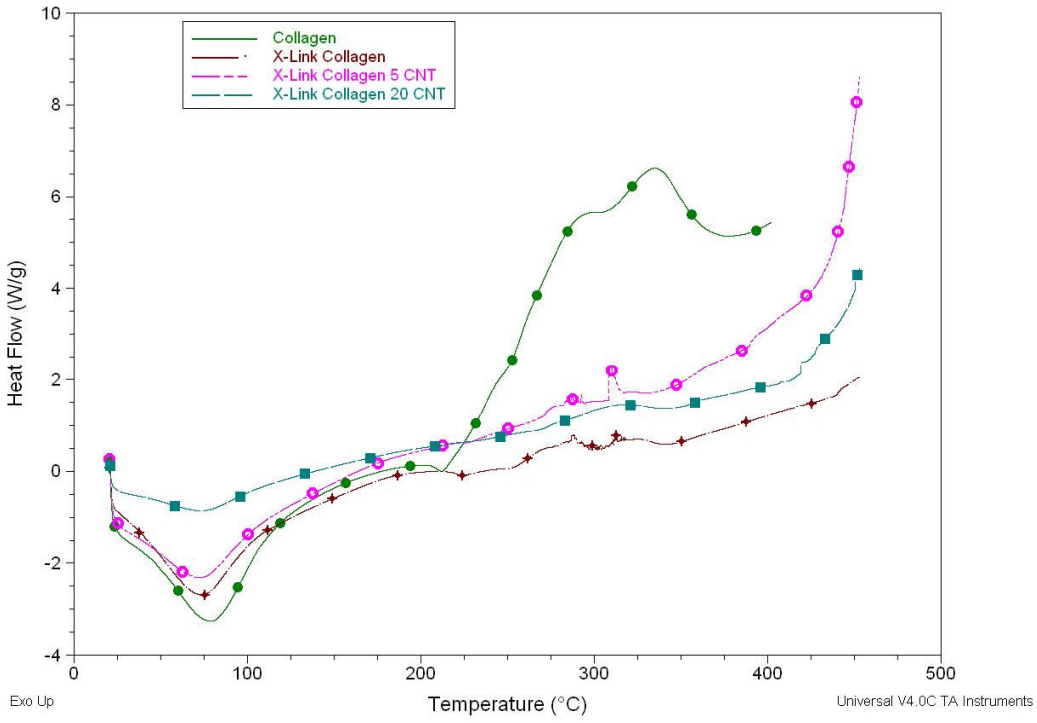

Figure 48: DSC spectra of un-crosslinked, crosslinked and SWCNT containing collagen nanocomposites.

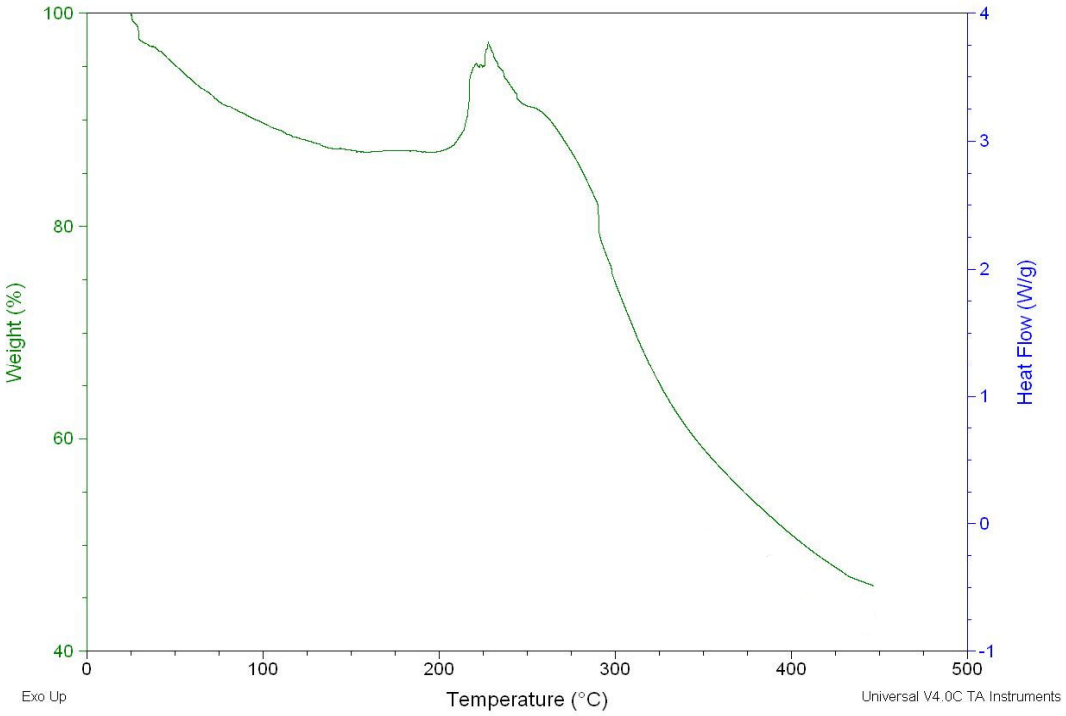

Figure 49: TGA spectrum of un-crosslinked collagen.

TGA data (figure 49) showed that these fibers are hydrophilic which is in support of previous research by Koob et al which argued that gelation processed fibers have cross-sectional diameter increases by an average 41%. The initial analysis of the DSC spectra shown in figures 48 suggest that the endothermic reaction shown by the dipping effect around 82 ^{o}C corresponds to the glass transition temperature of the collagenous fibers. TGA data however refute this hypothesis because of the early loss of mass that started around 80 ^{o}C and continued until beyond 200 ^{o}C where decomposition is though to have occurred. The initial loss of mass is then attributed to the loss of water originally absorbed by the fibers. It is interesting to notice the effect of SWCNT on the water absorption of the fibers. The increase to 5 then 20 % SWCNT content showed proportional decrease of water content, which is thought to be due to the inherent hydrophobicity of carbon nanotubes.

3.5 Conclusions

This chapter demonstrates a process by which a collagen/SWCNT composite was synthesized into fibers that could be combined to form a material with similar mechanical characteristics to tendon or ligament. SWCNT (0.5, 1, 2, 5, 10, and 20 weight percent) was successfully dispersed in as little as 0.13% of type I solubalized collagen solution without need for additional solvents. Raman and Fourier transform infrared (FTIR) spectroscopy were used to characterize the intermolecular interactions within the nanocomposite. Transmission and scanning electron microscopy, light, and atomic force microscopy (AFM) were used to study the surface topography and cross sections of the fibers. Micro tensile testing and nanoindentation were used to characterize the bulk and surface mechanical properties of the nanocomposite. A 31% stiffness increase in the nanocomposite fiber has been observed with 5% SWCNT content. Furthermore, an increase in surface stiffness that was proportional to the increase in SWCNT was observed. The water absorbance capacity of the collagen-SWCNT fibers was characterized by Differential Scanning Calorimetry (DSC) and Thermal Gravimetric Analysis (TGA). Carbon nanotubes were found to control the water content in the collagenous fibers thanks to their inherent hydrophobicity. A Human osteoblast cell line transfected with SV40 T antigen was used to study the biocompatibility of the nanocomposite. These cells were confluent in media after one day in culture. Osteocalcin was also monitored as a precursor for osteoblast formation and was found to have the highest increase on average around the collagen-SWCNT fibers.

The single wall carbon nanotubes added to form the composite provided for tunability of the stiffness in tensile testing. Furthermore, the mechanical characteristics of the nanocomposite were similar to native human tendon. Finally, there was no toxicity in presence of carbon nanotubes and preliminary cell culture data show no loss of osteoblast phenotype. Future work will further examine the interaction between the SWCNT and collagen fibrils with the biomatrix. Functionalization of SWCNT and use of multi-wall carbon nanotubes (MWCNT) should be incorporated as fillers into solubalized type I collagen. Similar physical characterization should be conducted and a comparative study should follow to determine an optimized composition for use in orthopaedic inserts and coatings[146].

This chapter also details the fabrication and characterization of a novel collagen-SWCNT nanocomposite by Electrospinning. The obtained fibers ranged from several tens of nanometers to a few microns. Single wall carbon nanotubes were successfully integrated in the collagen biomatrix and HRTEM images showed that these SWCNTs were present both within and on the surface of the electrospun fibers. The dispersion of SWCNT has great benefits in future use of this nanocomposite as scaffolding material for tissue engineering applications.

CHAPTER 4: DEVELOPMENT AND CHARACTERIZATION OF A MESOCAVITY DNA BIOCHIP FOR RESPIRATORY SYNCYTIAL VIRUS (RSV) DIAGNOSIS

4.1 Introduction

DNA plays an important role in many cellular processes like replication, homologous recombination and transcription. Besides its genomic information, DNA exhibits very interesting biophysical and physicochemical properties, which are essential for proper functioning of the biomolecular processes involved. Human respiratory syncytial virus (RSV) is a negative sense, single-stranded RNA virus of the family Paramyxoviridae, which includes common respiratory viruses such as those causing measles and mumps. A negative-sense viral RNA is complementary to the messenger RNA (mRNA) and thus must be converted to positive-sense RNA by an RNA polymerase before translation. Biochips, particularly those based on DNA are powerful devices that integrate the specificity and selectivity of biological molecules with electronic control and parallel processing of information. This combination will potentially increase the speed and reliability of biological analysis. Microelectronic technology is especially suited for this purpose since it enables low-temperature processing and thus allows fabrication of electronics devices on a wide variety of substances like glass, plastic, stainless steel and silica wafer. Ultra-high micro-cavities on a silicon wafer chip using an electrochemical etching technique and a dry silicon-etching process can be used to fabricate the DNA biochip. Fundamental phenomena like molecular elasticity, binding to protein; super-

coiling and electronic conductivity also depend on the numerous possible DNA confirmations and can be investigated nowadays on a single molecule level.

Fluorescently labeled oligonucleotide probes are nowadays in much regular use for nucleic acid sequencing[147], sequencing by hybridization[25] (SBH), fluorescence in situ hybridization[148](FISH), fluorescence resonance energy transfer[149] (FRET), molecular beacons[150], Taqman probes[29]. and chip-based DNA arrays[151]. This has made fluorescent probes an important tool for clinical diagnostics and made possible real-time monitoring of oligonucleotide hybridization. Furthermore, fluorescent-based diagnostics avoids the problem of storage, stability, and disposal of radioactive label[152,153,32], DNA nucleotide sequence can be labeled with fluorescence at 5′ and monitored. Experiments with single DNA were reported with scanning tunneling microscopy[154], fluorescence microscopy[34], fluorescence correlation spectroscopy[155], optical tweezers[156], bead techniques in magnetic fields[35], optical micro fibers[157], electron holography[158] and atomic force microscopy[159-161]. All these methods provide direct or indirect information on molecular structure and function.

Knowledge of structural and physical properties in microbial cells and microbial cell components is required to obtain a comprehensive understanding of cellular process and their dynamics. The need for a nondestructive method was satisfied with the development of the Atomic Force Microscope (AFM). The last 15 years have witnessed the extraordinary growth of structural studies in biology, and the impact is being felt in almost all areas of biological research. Several groups have used AFM for the analysis of

DNA, protein, and DNA–protein interactions[162]. AFM has been demonstrated to be a powerful and sensitive method for detecting surface-confined DNA molecules at molecular levels[42].

Until recently, electron microscopy was used as the main tool for imaging DNA. However, this technique can be harsh on biological samples, making successful analysis extremely difficult. AFM allowed the analysis of biological molecules to be performed faster, easier and more accurately yielding successful characterization of biological specimens.

Various methods can be employed to bind DNA to different hosts. An array of substances, including catalytic antibodies, DNA, RNA, antigens, live bacterial, fungal, plant and animal cells, and whole protozoa, have been encapsulated in silica, organosiloxane and hybrid sol-gel materials. Sol-gel immobilization leads to the formation of advanced materials that retain highly specific and efficient functionality of the guest biomolecules within the stable host sol-gel matrix[163]. The protective action of the sol-gel cage prevents leaching and enhances their stability significantly. The advantages of these 'living ceramics' might give them applications as optical and electrochemical sensors, diagnostic devices, catalysts, and even bio-artificial organs. With rapid advances in sol-gel precursors, nano engineered polymers, encapsulation protocols and fabrication methods, this technology promises to revolutionize bio-immobilization. Biosensors using immobilized receptors are finding ever-increasing application in a wide variety of fields such as clinical diagnostics, environmental

monitoring, food and drinking water safety, and illicit drug monitoring[164]. One of the most challenging aspects in development of these sensors is immobilization and integration of biological molecules in the sensor platform. Numerous techniques, including physical covalent attachment, entrapment in polymer and inorganic matrices, have been explored over the past decade. Sol-gel process are promising host matrices for encapsulation of biomolecules such as enzymes, antibodies, and cells[165].

Porous silicon (PS) was discovered in 1956 by Uhlir[48] while performing electro polishing experiments on Silicon wafers using an HF-containing electrolyte. He found that increasing the current over a certain threshold, a partial dissolution of the silicon wafer started to occur. PS formation is then obtained by electrochemical dissolution of silicon wafers in aqueous or ethanoic HF solutions. Micro and mesocavities are of interest for a wide range of fundamental and applied studies, including investigations of cavity quantum electrodynamics[166], optical elements for telecommunications[50], single-photon sources[51], and chemical or biological sensors[167]. Micro-fabrication techniques allow reproducible fabrication of resonators with lithographically controlled dimensions.

Biological sensors fabricated on the nanoscale offer new ways to explore complex biological systems because they are responsive, selective and inexpensive. Two primary advantages make nanoscale PS based DNA biochips a very attractive option: (i) enormous surface area ranges from 90 to 783 m^2/cm^3, which provide numerous sites for potential species to attach. (ii) Its room temperature luminescence spans the visible spectrum, which makes it an effective transducer. In case of PS the most commonly used

method for binding DNA involves coating of sol-gel material containing DNA on an oxidized silicon surface. The function of tetra-ethyl-ortho-silicate (TEOS) is to provide a stable coupling between two non-bonding surfaces: an inorganic surface to a biomolecule. The most interesting feature of PS is its room temperature visible luminescence. PS mesocavity resonators possess the unique characteristics of line narrowing and luminescence enhancement[168]. The emission peak position is completely tunable by modifying the coating over the surface of porous silicon[169]. The direct Epifluorescent Filter Technique (DEFT) is a rapid method for enumerating bacteria. Used widely in the dairy industry for milk and milk products, it has also been applied to beverages, foods, clinical specimens and in environmental research. A mesocavity DNA biosensor was chosen to diagnose RSV virus because by nature, DNA is highly selective as ssDNA strand pairs only bind to its complementary strand. When two non-complementary strands of DNA are exposed together no binding will occur[170]. In this study, mesocavities on silicon wafer are used for immobilization of RSV F gene specific ssDNA with sol-gel coating over silicon surface to develop the probe for the recognition of cDNA of the attached ssDNA. We present a novel optical and mechanical approach to detect DNA hybridization by properly coating over the surface of PS mesocavities with highly selective receptor molecules ssDNA using TEOS to quickly determine the presence of complementary (cDNA). The DNA biochip has been characterized by a Digital Instruments Atomic Force Microscope (AFM) with nanoscope dimension 3000 software, a Hitachi S800 Scanning Electron Microscope (SEM), a Vanox research grade optical microscope, and an SPEX 500M temperature stabilization Photoluminescence (PL) spectrometer.

4.2 Materials and Methods

4.2.1 Materials

A crystalline n-type silicon wafer with resistivity ranging between 0.4 and 0.6 Ωcm was used for developing porous silicon (PS) layers by dipping in a solution of hydrogen fluoride (HF) and ethanol, tetra-ethyl-ortho-silicate (TEOS), HCl, and HNO_3. DNA Nucleotides: The DNA sequence corresponding to 1241 to 1335 base pair of original RSV F gene (MDN-1335=5′ATA ATC GCA CCC GTT AGA AAA TGT CTT TAT GAT TCC ACG ATT TTT ATT GGA TGC TGT ACA TTT AGT TTT GCC ATA GCA TGA CAC AAT GGC TCC TAG) and the probe cDNA (MDN-1241FL=5′ CTA GGA GCC ATT GTG TCA TGC TAT GGC AAA ACT AAA TGT ACA GCA TCC AAT AAA AAT CGT GGA ATC ATA AAG ACA TTT TCT AAC GGG TGC GAT TAT) labeled with a guanosine cyanoethyl phosphoramidite molecule at 5' were synthesized and column purified. The maximum absorption wave length of the fluorescent molecule is 494nm and the maximum emission is 520nm. The MDN-1241-FL oligonucleotide was used to visualize the hybridization of ssDNA. A total of 2 µg of DNA diluted in distilled water was used to coat the surface of 1 mm x 1mm silicon wafer. After adding the DNA, silicon wafers were dried at 30 ^{o}C in an oven and used for AFM studies. For DNA hybridization studies, 2 µg of probe cDNA was mixed in distilled water and applied to the silicon wafers attached with ssDNA.

4.2.2 Preparation of Mesocavities on a Silicon Wafer

Anodic etching was used to prepare PS wafers using a solution containing 49% high purity aqueous HF and 50% ethanol. A 14.4 cm^2 exposed area of the polished, crystalline n-type silicon wafer was etched for 5 minutes in a Teflon cell (figure 50) at a constant anodic current of 40.3 mA/cm^2.

A 200 nm gold layer was deposited by sputtering at the bottom of the wafer to insure ohmic contact. The cathode contact was made using a platinum mesh that is in contact with the solution. After achieving the etching process, the wafer was rinsed in ethanol and blown dry in a nitrogen environment. The advantage of this cell geometry is the simplicity of equipment as shown in figure 50. The presence of a difference in the potential between the top and the bottom electrodes of such a cell, leads to different values of the local current density[171].

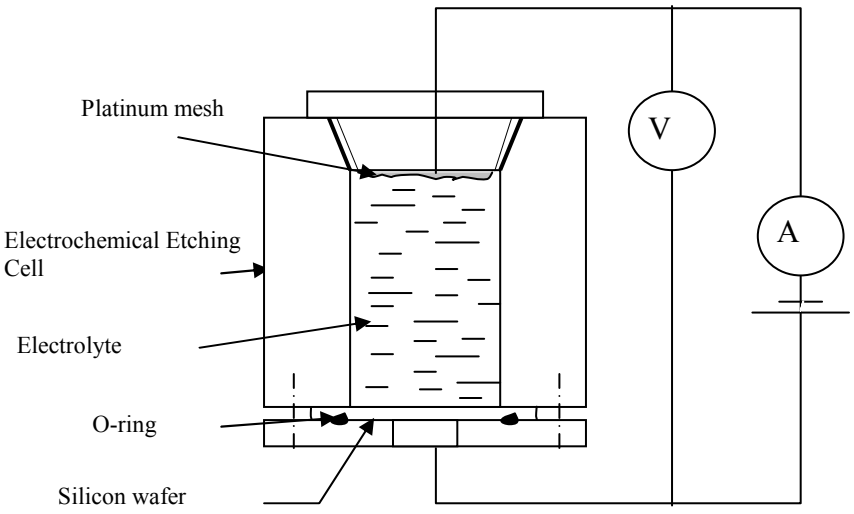

Figure 50: Schematics of Electrochemical Etching of Silicon Wafer.

4.2.3 Immobilization of ssDNA onto Porous Silicon and DNA Hybridization

The method used for binding DNA involves coating of a sol-gel material on an oxidized surface of porous silicon for immobilization of single-strand DNA. Sol-gel is a colloidal suspension of silica particles that is gelled to form a solid. The resulting porous gel can be chemically purified and consolidated at high temperatures into high purity silica. The idea behind the sol-gel optical sensors is based on changes in optical parameters of active sensing molecules physically entrapped in sol-gel thin films. Those changes are induced by changing external physico-chemical parameters such as temperature, hydrostatic pressure or presence of analyte molecules. There are several kinds of optical signals which could be used as analytical response of such sensors, for instance: intensity of light absorbed or emitted by the sensing molecules, and time of luminescence decay[172]. This paper uses the intensity of fluoresced light to determine the sensing capability of the biochip.

The 96 base pairs RSV F MDN-1335 Oligonucleotides 5′ ATA ATC GCA CCC GTT AGA AAA TGT CTT TAT GAT TCC ACG ATT TTT ATT GGA TGC TGT ACA TTT AGT TTT GCC ATA GCA TGA CAC AAT GGC TCC TAG were immobilized using TEOS spreading over the surface of the silicon wafer to immobilize DNA in the mesocavities. A mixture of 25µL of TEOS, 5 µL of 0.1 M HCl and 25µL of de-ionized water (DI) were mixed in a vial and further diluted at 50% (solution A). The last step involved mixing 2 µg of DNA and 3µL DI water in 5 µL of solution A. The pH was controlled near 7 during the mixing procedure described above.

The schematic diagrams in figure 51 show the steps taken to immobilize ssDNA and attach the cDNA on PS. Part (a) of figure 51 shows the procedure for immobilizing the ssDNA using TEOS, figure 51 (b) shows the immobilized ssDNA on porous silicon and figure 51 (c) represents the hybridization of fluorescence labeled cDNA to the corresponding RSV F genome already attached to the porous silicon.

DNA hybridization of ssDNA attached to mesocavity and cDNA was performed by using MDN-1241-FL oligonucleotide which was labeled with a dual emission (blue and green) guanosine cyanoethyl phosphoramidite molecule. 5µL of MDN-1241-FL in de-ionized water was dispensed on the DNA chip for 30 min at 25 ^{o}C. The biochips were washed with de-ionized water after each step to deactivate and remove any un-reacted cross linker and any non-hybridized DNA. Three sets of PS, ssDNA, and hybridized DNA chips with DNA concentrations of were then taken to be analyzed using epifluorescence microscopy, AFM, and PL.

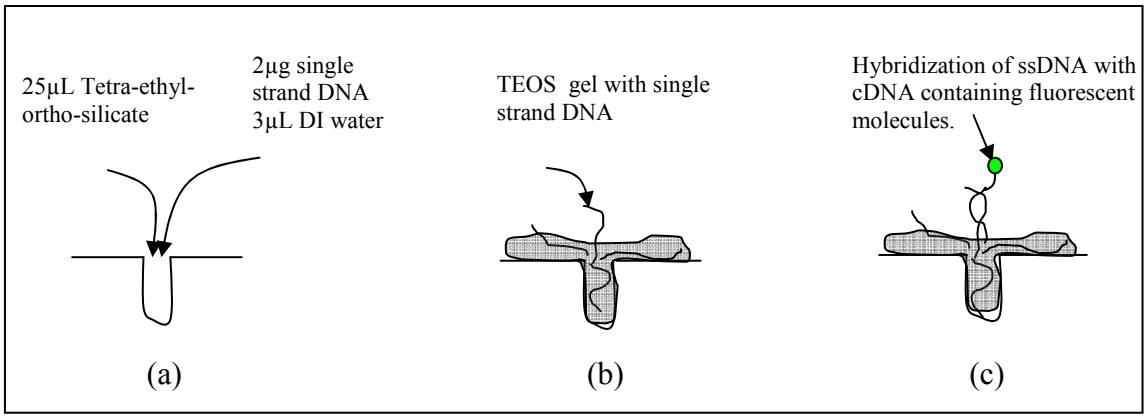

Figure 51: Schematic process of DNA attachment and hybridization with fluorescent molecules on PS using TEOS.

4.2.4 AFM Characterization

There are various modes of AFM operation, the most common are: non-contact mode, contact mode, and tapping mode. Tapping mode was the preferred technique of operation for this study since it has features that allow better quality imaging with little deleterious effects on the sample. Digital Instruments Atomic Force Microscope (AFM) with nanoscope dimension 3100 software, and a scan size varying from 50 nm by 50 nm to 100 μm by 100 μm was used to obtain quantitative, two and three-dimensional images of surface topographies of DNA on bare and porous silicon with ultra-high resolution. All analyses were conducted in air and the samples were brought to room temperature before AFM analysis.

4.2.5 Epifluorescence Microscopy Analysis

The optical microscopy pictures were recorded on porous silicon wafers without any DNA, porous silicon attached with ssDNA and after hybridization of ssDNA with its cDNA using a Vanox research grade optical microscope. Two dry objectives were used to collect images at 10x and 40x magnifications. The third objective offers oil immersed 100 x magnifications. The transverse mode profile for the disk and evanescent field used for sensing is equivalent to that of a slab waveguide with the same thickness and refractive indices. A ccd camera was used to collect the pictures showed in figure 53. Therefore, one can take advantage of enhanced power at the surface of the porous silicon containing mesocavities, having the same penetration depth and relative cladding power as in the straight waveguide structure.

4.2.6 SEM Analysis

The two inch wafer porous silicon was cut into 2 by 2 centimeter areas. Three samples were taken and prepared for SEM study. A Hitachi S800 was used for the analysis. A 25 kV source was applied to obtain the images shown in figure 52 (A) (3000 X) and (B) (6000 X).

4.2.7 Photoluminescence Analysis

Two samples of non-hybridized DNA and two hybridized DNA on PS were dried in an incubator for 1 hour at 32 ^{o}C before use in photoluminescence study. A SPEX 500M spectrometer was used for this study. All samples were illuminated with a helium cadmium (He Cd) laser at 325 nm and 55mW. The laser beam was kept at 1.5 mm in diameter to minimize the damage to the DNA molecules. Variation in the wavelength due to the hybridization of RSV complementary strand to the DNA single strand was investigated.

4.3 Results and Discussions

4.3.1 SEM Characterization of Mesocavity

Surface and cross sectional SEM images of porous silicon were obtained after etching (as shown in figure 52 (A) and (B). Part (A) of the figure clearly shows the pattern of well dispersed cavities. Pores with diameters varying 150 and 650 nm were observed. A distribution of pore diameters throughout a representative area of about 1400 μm^2 is shown in part (C) of figure 52. An imaging software was used to calculate the pore

diameter and general porosity. A porosity of 9% was estimated by dividing the sum of the pore areas by the total area of the sample. It is important to notice the high number of pores available for attachment even for 9% porosity. Branching of different pores throughout the depth was also observed (figure 52 (B)). This is typical of n-type silicon porosity formation. More specifically, nucleation of porous structures in n-type silicon takes place during the first minutes of the anodization (pore incubation stage) and detectable because it dominates over the pore propagation. Later, the dissolution of silicon mass takes place through two competitive processes: some part gets lost through electrochemical etching and the remaining part gets dissolved chemically[173]. This is the main reason for the branching in pores that happens as anodization time increases.

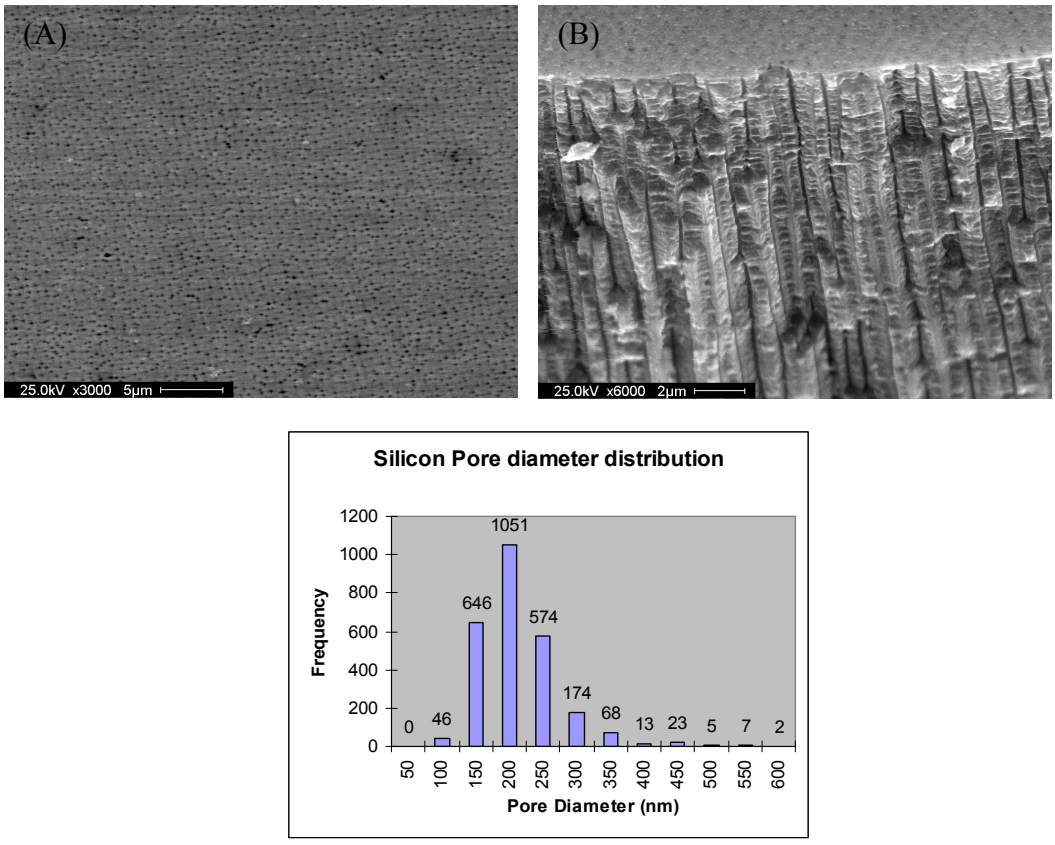

Figure 52: SEM picture of n-type porous silicon surface, (A) surface image, (B) cross section, and (C) distribution of pore diameters throughout a representative area.

4.3.2 Epifluorescence Microscopy Studies

Epifluorescence microscopy was used in this study to collect fluorescent light from PS, ssDNA attachment, and cDNA hybridization on PS. Epifluorescence is an optical set-up for a fluorescence microscope in which the objective lens is used both to focus ultraviolet light on the specimen and collect fluorescent light from the specimen. The pictures show a clear indication of DNA hybridization as the cDNA molecule was tagged with fluorescence molecule. Epifluorescence is more efficient than transmitted fluorescence, in which a separate lens or condenser is used to focus ultraviolet light on the specimen. Epifluorescence also allows fluorescence microscopy to be combined with an optical microscope used to achieve fluorescence-aided molecule sorting (FAMS) and enable simultaneous analysis of DNA interaction at the level of single strands. The mesocavity design has an advantage over the single layer structure as the refractive index of the surrounding material increases the reflectivity spectrum and causes it to shift. This is further demonstrated during the optical microscopy studies. This was performed by labeling corresponding RSV F genome cDNA (MDN-1241-FL) with fluorescein at 5′ and used for hybridization. The fluorescent molecule serves as donor-acceptor pairs for Forster resonance energy transfer. FAMS permits equilibrium and kinetic analysis of macromolecule-ligand interactions; this was validated by measuring with ssDNA and cDNA. FAMS is a general platform for ratio metric measurements that report on structure, dynamics, stoichiometries, environment, and interactions of diffusing or immobilized molecules, thus enabling detailed mechanistic studies and ultra sensitive diagnostics[174].

Epifluorescence microscopy was used in this study to collect fluorescent light from PS, ssDNA attachment, and cDNA hybridization on PS. Figures 53 (a) through 53 (c) show the PS surface under three different magnifications (10 X, 40 X, and 100 X). Figures 53 (d) through 53 (f) show the TEOS and ssDNA mixture on the PS surface, and figures 53g through i show the hybridization effect on the surface. The hybridization is visually discernable in figure 53 (i) by observing the green color spots. This finding is later confirmed by PL spectra.

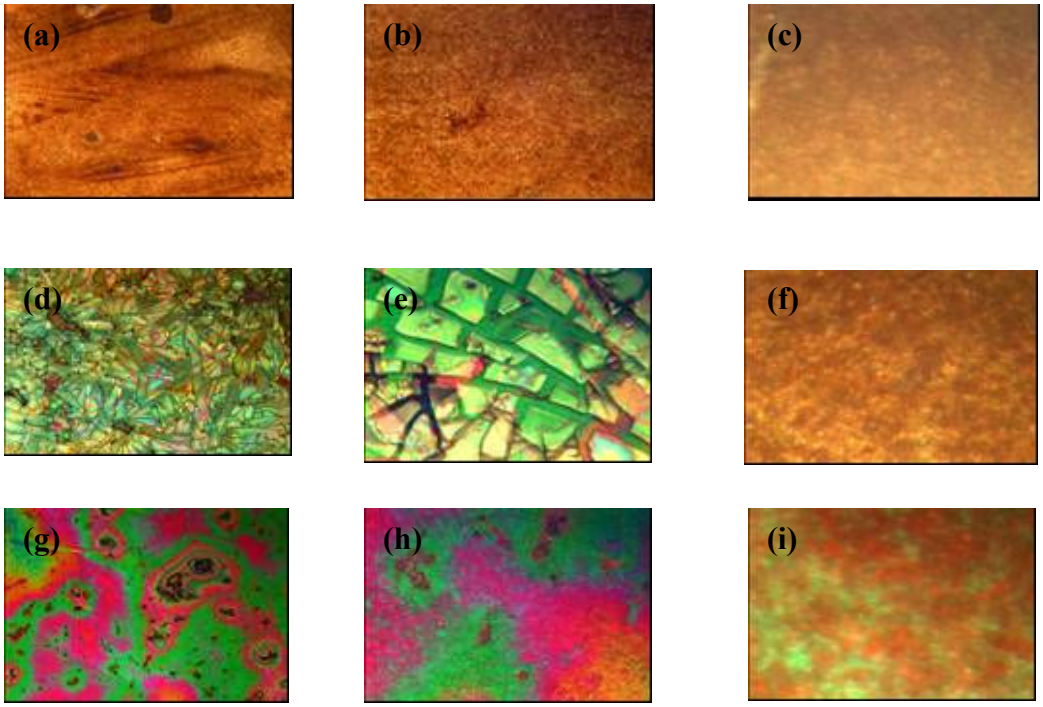

Figure 53: Epifluorescence images of DNA biochip. (a) (10X), (b) (40X) and (c) (100X) shows images of porous silicon with mesocavities only, (d) (10X), (e) (40X) and (f) (100X) porous silicon mesocavities treated with TEOS and attached with ssDNA and (g) (10X), (h) (40X) and (i) (100X) of DNA hybridization with fluorescence attached cDNA molecule with ssDNA on TEOS treated porous silicon.

Further UV-spectra have shown the retention of the fluorophore in the modified cDNA. The absorbance at 333-340 nm and at 260 nm due to fluorophore and DNA

respectively and fluorescence emission spectra at 500-520 nm wavelengths clearly confirmed the retention of the chromophore in the oligonucleotides. The relative enhancement in the intensity of peak is due to the fluorescence molecule attached to the cDNA. A fluorophore layer placed on top of the porous silicon will experience an enhancement of the input optical signal. The effect of field enhancement in mesocavities can be interpreted as an increase of absorption efficiency of the fluorophore due to increased interaction length of the incident field with an absorbing molecule. Therefore, an increase in amount of fluorescent photons generated from the molecule at the mesocavities versus the linear waveguide is proportional to a number of fluorescence molecule or hybridization with cDNA. Therefore the advantage of the mesocavity format versus waveguide format for analytical applications is the amount of fluorescence molecules present at surface of porous silicon or hybridization. This could be a powerful technique to detect the hybridization analysis even at very low concentration.

4.3.3 AFM Studies

AFM studies were conducted on polished and porous silicon surfaces to understand the effect on the geometrical orientation of the ssDNA molecules. The effect of the cross linking chemistry was also studied by observing ssDNA with and without TEOS on a polish silicon surface. Figure 54 (a) shows ssDNA adsorbed on a polished silicon surface. Notice the rope like structure randomly coiled on the silicon surface. The familiar DNA organization on a very smooth surface changed dramatically when the ssDNA was cross linked within the TEOS sol-gel matrix as shown in figure 54 (b). Although intermolecular electrostatic forces are thought to constitute a major source of interactions between the

ssDNA molecules and the TEOS, additional factors which may contribute to the intermolecular interactions include Coulombic, hydrophobic, and hydrogen- bonding interactions. The forces involved resulted in an increase in polarity of the biomelocules thus increasing the surface tension between the ssDNA and the silicon. This phenomenon resulted in periodic cleavages in the ssDNA molecules and the circular shapes formation shown in figure 54 (b).

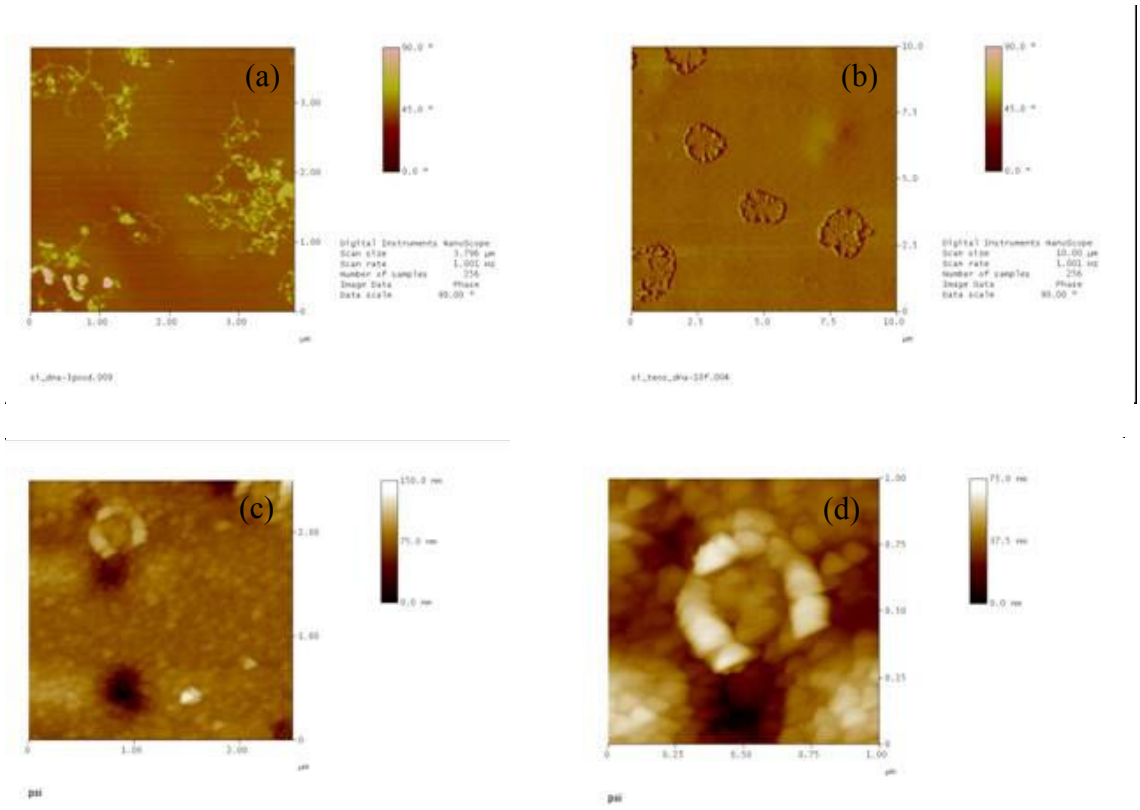

Figure 54: Atomic force micrographs showing: (a) ssDNA on silicon; (b) cross linked ssDNA on silicon; (c) 2.5 µm and (d) 1 µm scans of non-hybridized DNA on porous silicon.

Figure 5-c shows a two dimensional picture of a section of the mesoporous silicon wafer with an ssDNA bundle attached to a cavity. A “horse shoe” like structure coming out of the mesocavity is now visible. The novel cross linking procedure combined with

the use of porous silicon introduced in this paper is though to have generated this repeating structure. Figure 54 (d) is a close-up AFM image showing detailed features from the ssDNA bundle shown in figure 54 (c). Further surface analysis of this image provides more information about the dimensions and the form of the ssDNA bundle. The ssDNA structure, as shown in figure 54 (c), has a 29 nm pitch. This value is fairly high compared with published AFM studies that show ssDNA pitch ranging between 1 and 10 nm.[175,176] This is though to be due to the cross linking effects on the surface tension which may have increased the intermolecular attraction between individual ssDNA ropes. Further calculations were carried out to determine the exposure efficiency of ssDNA after crosslinking. Following a systematic number of scans (10 μm X 10 μm) throughout the sensing area, the number of exposed ssDNA molecules with attachments to cavities was counted. An efficiency coefficient was measured by dividing the number of exposed molecules by the number of cavities available. The efficiency was found to be equal to 34.5%. This value does not account for the number of molecules embedded into the sol gel.

4.3.4 Photoluminescence Studies Before and After Hybridization

Photoluminescence (PL) was used to study the change in reflected intensity after the cDNA hybridization. Four samples were used for this study; two with ssDNA immobilized on the mesocavity and two hybridized DNA samples. A clear increase in the PL intensity was observed after hybridization of the ssDNA with cDNA (Figure 55). Close to 9 fold increase in the luminescence spectra was registered after hybridization. A significant change in the intensity was clearly perceived between ssDNA and hybridized

DNA samples. While ssDNA samples did not show any significant peak, the hybridized samples did show two peaks. The smaller peak was registered at 382 nm which corresponds to the color blue. The peak with higher intensity corresponds to the green color with a wavelength of 508 nm. This clearly demonstrates a noticeable change that could be used to quantify the extent of hybridization on the surface. Furthermore, the PL spectra are in concordance with the images obtained by fluorescent microscopy, where bright blue and green areas were observed on the hybridized surface of the PS. Table 3 summarize the PL and fluorescence microscopy findings.

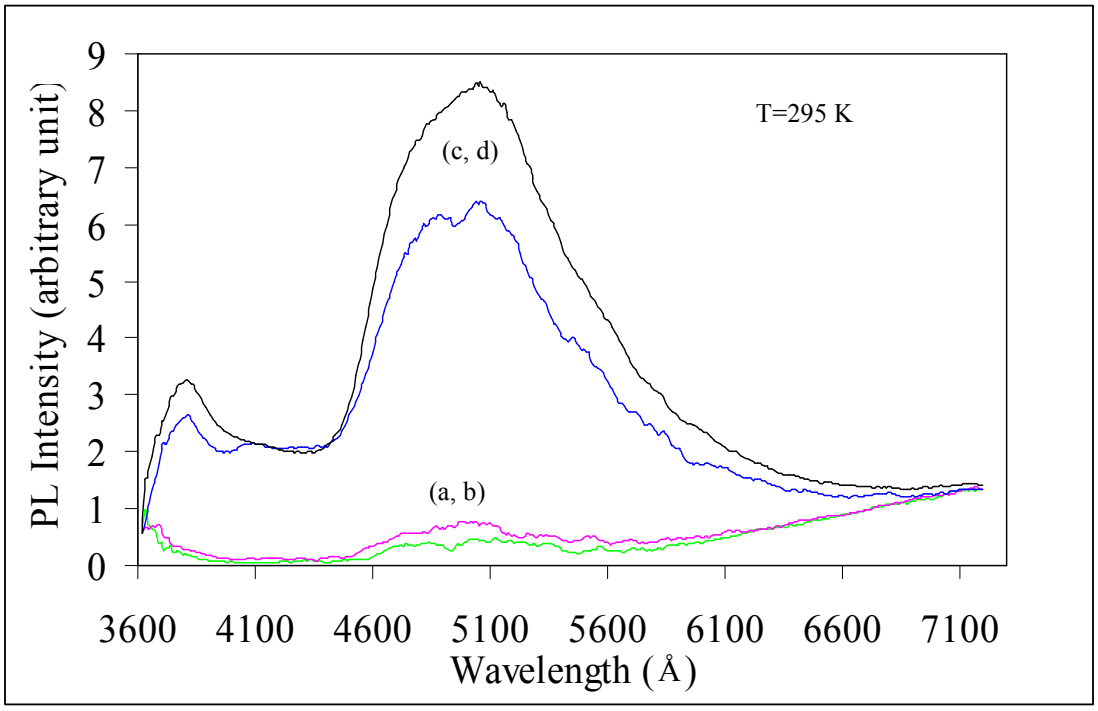

Figure 55: PL spectra of: (a, b) two ssDNA on porous silicon spectra , (c, d) two hybridized DNA on porous silicon spectra.

Table 3: Fluorescence and optical microscopic studies of DNA biochip.

Technique	**ssDNA**	**Hybridized**
Optical Microscopic studies	Dark green color was observed with very little fluorescence	Bright blue and green fluorescence observed
Photoluminescence Studies (PL)	No significant photoluminescence was observed	Relatively high intensity spectra with blue peak (382 nm) and green peak (508nm)

4.4 Conclusions

An RSV virus sensor was fabricated using porous silicon. The mechano-chemical approach provides many advantages including high sensitivity, specificity and cost-effectiveness. Furthermore, the compatibility of the silicon mesocavity fabrication process with the usual silicon technology makes this material a very interesting candidate for DNA biochip fabrication. Highly specific ssDNA were immobilized corresponding to RSV F gene on silicon mesocavities. The addition of fluorescein at 5' of cDNA provided the confirmation method for the hybridization of ssDNA using photoluminescence technique. The function of the present DNA biochip sensor is based on the hybridization process, which involves the pairing of a single strand of nucleic acid with a complementary sequence. The underlying porous silicon structure was used to increase the attachment sites for the DNA sensor. AFM images showed the nature of the interaction between ssDNA molecules within the cross-linking matrix.

Since RSV is a negative sense RNA virus and there is no PCR or RT-PCR required processing the samples for its use in the sensor, the present technology is uniquely suitable for diagnosis of RNA (negative as well positive sense) viruses. Application of the mesocavity attached ssDNA biochip is highly customizable for diagnosis of other DNA viruses, bacteria, and genetic diseases since preparation of complementary strand DNA requires hybridization process to be performed at high temperature (70-80 ^{o}C). The technology presented in this chapter provides the basic building blocks for the integration of nanochip fabrication for biological applications[177].

CHAPTER 5: CONCLUSIONS

A systematic study has been carried out on the synthesis, characterization, of two interfaces between naturally derived and synthetic nanostructures. Carbon nanotubes and porous silicon represent the synthetic nanostructures that were developed for the purpose of interfacing with the naturally derived bovine type I collagen and respiratory syncytial virus DNA respectively.

A novel process was demonstrated by which a collagen/SWCNT composite was synthesized into fibers that could be combined to form a material with similar mechanical characteristics to tendon or ligament. SWCNT (0.5, 1, 2, 5, 10, and 20 weight percent) was successfully dispersed in as little as 0.13% of type I solubalized collagen solution without need for additional solvents. Raman and Fourier transform infrared (FTIR) spectroscopy were used to characterize the intermolecular interactions within the nanocomposite. Transmission electron microscopy (SEM), light, and atomic force microscopy (AFM) were used to study the surface topography and cross sections of the fibers. Micro tensile testing and nanoindentation were used to characterize the bulk and surface mechanical properties of the nanocomposite. A 31% stiffness increase in the nanocomposite fiber has been observed with 5% SWCNT content. Furthermore, an increase in surface stiffness that was proportional to the increase in SWCNT was

observed. The water absorbance capacity of the collagen-SWCNT fibers was characterized by Differential Scanning Calorimetry (DSC) and Thermal Gravimetric Analysis (TGA). Carbon nanotubes were found to control the water content in the collagenous fibers thanks to their inherent hydrophobicity. A Human osteoblast cell line transfected with SV40 T antigen was used to study the biocompatibility of the nanocomposite. These cells were confluent in media after one day in culture. Osteocalcin was also monitored as a precursor for osteoblast formation and was found to have the highest increase on average around the collagen-SWCNT fibers.

The single wall carbon nanotubes added to form the composite provided for tunability of the stiffness in tensile testing. Furthermore, the mechanical characteristics of the nanocomposite were similar to native human tendon. Finally, there was no toxicity in presence of carbon nanotubes and preliminary cell culture data show no loss of osteoblast phenotype. Future work will further examine the interaction between the SWCNT and collagen fibrils with the biomatrix. Functionalization of SWCNT and use of multi-wall carbon nanotubes (MWCNT) should be incorporated as fillers into solubalized type I collagen. Similar physical characterization should be conducted and a comparative study should follow to determine an optimized composition for use in orthopaedic inserts and coatings.

Details of the fabrication and characterization of a novel collagen-SWCNT nanocomposite by Electrospinning were demonstrated. The obtained fibers ranged from a few microns in diameter to several tens of nanometers. Single wall carbon nanotubes

were successfully integrated in the collagen biomatrix and HRTEM images showed that these SWCNTs were present both within and on the surface of the electrospun fibers. The dispersion of SWCNT has great benefits in future use of this nanocomposite as scaffolding material for tissue engineering applications.

An RSV virus sensor was fabricated using porous silicon. The mechano-chemical approach provides many advantages including high sensitivity, specificity and cost-effectiveness. Furthermore, the compatibility of the silicon mesocavity fabrication process with the usual silicon technology makes this material a very interesting candidate for DNA biochip fabrication. Highly specific ssDNA were immobilized corresponding to RSV F gene on silicon mesocavities. The addition of fluorescein at 5' of cDNA provided the confirmation method for the hybridization of ssDNA using photoluminescence technique. The function of the present DNA biochip sensor is based on the hybridization process, which involves the pairing of a single strand of nucleic acid with a complementary sequence. The underlying porous silicon structure was used to increase the attachment sites for the DNA sensor. AFM images showed the nature of the interaction between ssDNA molecules within the cross-linking matrix.

Since RSV is a negative sense RNA virus and there is no PCR or RT-PRC required processing the samples for its use in the sensor, the present technology is uniquely suitable for diagnosis of RNA (negative as well positive sense) viruses. Application of the mesocavity attached ssDNA biochip is highly customizable for diagnosis of other DNA viruses, bacteria, and genetic diseases since preparation of complementary strand

DNA requires hybridization process to be performed at high temperature (70-80C). Furthermore, the immobilization technique used to fixate RSV single strand DNA is both biocompatible and offer stability of extended periods of time thus providing potentially long shelf life when used as part of a commercial device. The technology presented provides the basic building blocks for the integration of nanochip fabrication for biological applications.

REFERENCES

1. Hastings GW. Biomedical engineering and materials for orthopaedic implants J. Phys. E: Sci. Instrum. 1980;13:599-607.

2. Butler DL JN, Dressler MR. . Functional Efficacy of Tendon Repair Processes. Annu. Rev. Biomed. Eng. 2004;6:303-329.

3. McClatchey K D. Musculoskeletal Conditions Affect Millions. Arch. Pathol. Lab. Med. 2004;128(4):480-488.

4. Leitinger B, Hohenester E. Mammalian collagen receptors. Matrix Biology;In Press, Corrected Proof.

5. Barbara Brodsky AVP. Molecular Structure of the Collagen Triple Helix Advances in Protein Chemistry 2005;70:301–339.

6. Horbett TA. Proteins: structure, properties, and adsorption to surfaces. San Diego: Academic Press; 1996. 133.

7. Schakenraad J M. Cells: Their surface and interactions with materials New York, NY.: Academic Press; 1996.

8. Brunetter D M. The effect of surface topography on cell migration and adhesion. Int. J. Oral Maxillofac. Implants 1988;3:231–246.

9. K. Bordji, J. M. Jouzeau, D. Mainard, E. Payan, P. Netter, K. T. Rie, T. Stucky, Hage-Ali M. Cytocompatibility of Ti-6Al-4V and Ti-5Al-2.5Fe alloys according to three surface treatments, using human fibroblasts and osteoblasts. Biomaterials 1996;17:929.

10. Grimes CA, Mungle C, Kouzoudis D, Fang S, Eklund PC. The 500 MHz to 5.50 GHz complex permittivity spectra of single-wall carbon nanotube-loaded polymer composites. Chemical Physics Letters 2000;319(5-6):460-464.

11. Higashi S, Yamamuro T, Nakamura T, Ikada Y, Hyon SH, Jamshidi K. Polymer-hydroxyapatite composites for biodegradable bone fillers. Biomaterials 1986;7(3):183-187.

12. Ito M. In vitro properties of a chitosan-bonded hydroxyapatite bone-filling paste. Biomaterials 1991;12(1):41-45.

13. Harris PJF. Carbon Nanotubes and Related structures: New Materials for the Twentieth Century. New York: Cambridge University Press; 1999.

14. Saito R, Dresselhaus, G., Dresselhaus, M.S. . Physical Properties of Carbon Nanotubes. London: Imperial College Press; 1998.

15. Meincke O, Kaempfer D, Weickmann H, Friedrich C, Vathauer M, Warth H. Mechanical properties and electrical conductivity of carbon-nanotube filled polyamide-6 and its blends with acrylonitrile/butadiene/styrene. Polymer 2004;45(3):739-748.

16. Koerner H, Price, G., Pearce, N. A., Alexander, M., Vaia, R. A. . Remotely actuated polymer nanocomposites - stress-recovery of carbon-nanotube-filled thermoplastic elastomers. Nat. Mater. 2004;3:115-120.

17. Thostenson ET, Chou, T. W. Aligned Multi-Walled Carbon Nanotube-Reinforced Composites: Processing and Mechanical Characterization. Phys D Appl Phy 2002;35:L77-L80.

18. Colbert D. Single Wall Nanotubes: A New Option for Conductive Plastics and Engineering Polymers. Plast. Addit. Compound 2003;5:12.

19. Huczko A LH, Calko E, Grubek-Jaworska H, Droszcz P. Physiological testing of carbon nanotubes: are they asbestos like? Fullerene Sci. Tech. 2001;9(2):251–254.

20. Lam C-W, James JT, McCluskey R, Hunter RL. Pulmonary Toxicity of Single-Wall Carbon Nanotubes in Mice 7 and 90 Days After Intratracheal Instillation. Toxicol. Sci. 2004;77(1):126-134.

21. Webster TJ, Waid MC, McKenzie JL, Price RL, JU E. Nano-biotechnology: carbon nanofibres as improved neural and orthopaedic implants Nanotechnology 2004;15:48-54.

22. Price RL, Waid MC, Haberstroh KM, Webster TJ. Selective bone cell adhesion on formulations containing carbon nanofibers. Biomaterials 2003;24(11):1877-1887.

23. Elias KL, Price RL, Webster TJ. Enhanced functions of osteoblasts on nanometer diameter carbon fibers. Biomaterials 2002;23(15):3279-3287.

24. A.D.Mirzabekov. DNA sequencing by hybridization a mega sequencing method and a diagnostic tool. TIBTECH 1994;12:27-32.

25. Speel EJM, Hopman AHN, Komminoth P. Amplification Methods to Increase the Sensitivity of In Situ Hybridization: Play CARD(S). J. Histochem. Cytochem. 1999;47(3):281-288.

26. Wennmalm S, Edman L, Rigler R. Conformational fluctuations in single DNA molecules. PNAS 1997;94(20):10641-10646.

27. Smith SB, Cui Y, Bustamante C. Overstretching B-DNA: The Elastic Response of Individual Double-Stranded and Single-Stranded DNA Molecules. Science 1996;271(5250):795-799.

28. Yashveer Singh, Archana Pandey, Krishna K. Dubey, Geeta Watal, Misra K. Fluorescence resonance energy transfer: A diagnostic tool in oligonucleotide therapy. Curr. Sci 2000 78:487-492.

29. N.E. Broude. Stem-loop oligonucleotides: a robust tool for molecular biology and biotechnology. Trends in Biotechnology 2002;20:249-256.

30. Carl T. Wittwer, Mark G. Herrmann, Alan A. Moss, Rasmussen RP. Continuous Fluorescence Monitoring of Rapid Cycle DNA Amplification. Biotechniques 1997;22:130-139.

31. Schena M. Microarray Biochip Technology: Eaton Publishing Company/Biotechniques Books; 2000. 298.

32. Drobyshev A, Mologina N, Shik V, Pobedimskaya D, Yershov G, Mirzabekov A. Sequence analysis by hybridization with oligonucleotide microchip: identification of [beta]-thalassemia mutations. Gene 1997;188(1):45-52.

33. Guckenberger R, Heim M, Cevc G, Knapp HF, Wiegrabe W, Hillebrand A. Scanning tunneling microscopy of insulators and biological specimens based on lateral conductivity of ultrathin water films. Science 1994;266(5190):1538-1540.

34. M. Yanagida, Y. Hiraoka, Katsura I. Dynamic behaviors of DNA molecules in solution studied by fluorescence microscopy. Cold Spring Harbor Symp.Quant .Biol. 1983;47:177.

35. Wang MD, Yin H, Landick R, Gelles J, Block SM. Stretching DNA with optical tweezers. Biophys. J. 1997;72(3):1335-1346.

36. Strick TR, Allemand JF, Bensimon D, Bensimon A, Croquette V. The Elasticity of a Single Supercoiled DNA Molecule. Science 1996;271(5257):1835-1837.

37. Smith SB, Finzi L, Bustamante C. Direct mechanical measurements of the elasticity of single DNA molecules by using magnetic beads. Science 1992;258(5085):1122-1126.

38. Cluzel P, Lebrun A, Heller C, Lavery R, Viovy J-L, Chatenay D, Caron F. DNA: An Extensible Molecule. Science 1996;271(5250):792-794.

39. Fink H-W, Schonenberger C. Electrical conduction through DNA molecules. Nature 1999;398(6726):407-410.

40. Hansma HG, Sinsheimer RL, Li M-Q, Hansma PK. Atomic force microscopy of single-and double-stranded DNA. Nucl. Acids Res. 1992;20(14):3585-3590.

41. Dario Anselmetti JFBSXF-B. Single Molecule DNA Biophysics with Atomic Force Microscopy. Single Molecules 2000;1(1):53-58.

42. H. G. Hansma , Hoh JH. Biomolecular imaging with the atomic force microscope. Annu Rev Biophys Biomol Struct. 1994;23:115-139.

43. Hansma HG, Sinsheimer RL, Groppe J, Bruice TC, Elings V, Gurley G, Bezanilla M, Mastrangelo IA, Hough PV, PK H. Recent advances in atomic force microscopy of DNA. Scanning 1993 15(5):296-299.

44. Hench LL, West JK. The sol-gel process. Chem. Rev. 1990;90(1):33-72.

45. C.J. Brinker, Scherer GW. SOL-GEL-Glass:I. Gelation and Gel Structure. J. Non-Crystalline Solids 1985;70:301-322.

46. Kumar A, Malhotra R, Malhotra B.D, Grover S.K. Co-immobilization of cholesterol oxidase and horseradish peroxidase in a sol-gel film Analytica Chimica Acta 2000;414(1):43-50.

47. Fisher-Cripps AC. Nanoindentation. New York: Springer- Verlag; 2002.

48. Uhlir A. Electrolytic shaping of germanium and silicon. Bell Syst.Tech.J 1956;35:333.

49. Smith RL, Collins SD. Porous silicon formation mechanisms. Journal of Applied Physics 1992;71(8):R1-R22.

50. Goryachev DN, Belyakov LV, Sreseli OM. Electrolytic fabrication of porous silicon with the use of internal current source. Semiconductors 2003;37(4):477-481.

51. S.Chan, P.M.Fauchet, Y. Li, L.J.Rothberg, B.L.Miller. Porous Silicon Microcavities For Biosensing Applications. Phys. Sta.Sol 2000;182:541.

52. Isola NR, Stokes DL, Vo-Dinh T. Surface-Enhanced Raman Gene Probe for HIV Detection. Anal. Chem. 1998;70(7):1352-1356.

53. Iijima S. Helical microtubules of graphitic carbon. Nature 1991;354(6348):56-58.

54. LT Canham. Silicon quantum wire array fabricated by electrochemical and chemical. dissolution of wafers. Appl Phys Lett 1990;57(10):1046-1048.

55. Lauerhaas JM, Sailor MJ. Chemical Modification of the Photoluminescence Quenching of Porous Silicon. Science 1993;261(5128):1567-1568.

56. Janshoff A, Dancil KPS, Steinem C, Greiner DP, Lin VSY, Gurtner C, Motesharei K, Sailor MJ, Ghadiri MR. Macroporous p-Type Silicon Fabry-Perot Layers. Fabrication, Characterization, and Applications in Biosensing. J. Am. Chem. Soc. 1998;120(46):12108-12116.

57. Tsakalakos T, Ovid'ko I, K V. Electroplating and Electroless Deposition of Nanostructured Magnetic Thin Films. Nanostructures: Synthesis, Functional Properties and Applications. II. Mathematics, Physics and Chemistry, Nato Science Series 2003;128:511-532.

58. Z.R. Dai, Z. W. Pan, Wang ZL. Novel Nanostructures of Functional Oxides Synthesized by Thermal Evaporation. Advanced Functional Materials 2003;13(1):9-24.

59. Maria G. Patino, Mirdza E. Neiders, Andreana S. Collagen: An Overview. Implant Dentistry 2002;11(3):280-284.

60. H. Beard, Faulk W. Page, Conoche L. Some immunological aspects of collagen. Prog Allergy 1977;22:45-106.

61. Eyre DR. Collagen: molecular diversity in the body's protein scaffold. Science 1980;207(4437):1315-1322.

62. Donald Voet, Voet JG. Biochemistry, Vol. 1: Biomolecules, Mechanisms of Enzyme Action, and Metabolism Wiley; 3 edition 2003.

63. Hulmes DJ, Wess TJ, Prockop DJ, Fratzl P. Radial packing, order, and disorder in collagen fibrils. Biophys. J. 1995;68(5):1661-1670.

64. E Vuorio, Crombugghe Bd. The family of collagen genes. Annu. Rev. Biochem 1990;59(837-872).

65. D. Hulmes. The collagen superfamily- Diverse structures and assemblies. Essays Biochem 1995;27:49-67.

66. S. Seyedin, Rosen D. Matrix protein of the skeleton. Curr. Opin. Cell. Biol 1990;2:914-919.

67. Harkness R. Treatise on collagen. New York: Academic Press; 1968. 248-253.

68. Cowin R. Handbook of Bioengineering. New York: McGraw Hill; 1987.

69. T. J. Koob, D. H. Hernandez. Mechanical and thermal properties of novel polymerized NDGA-gelatin hydrogels. Biomaterials 2002;24:1285-1292.

70. Mandl L. Collagenase. New York: Gordon Breach; 1970. 1-16.

71. Kroto HW, Heath JR, O'Brien SC, Curl RF, Smalley RE. C60: Buckminsterfullerene. Nature 1985;318(6042):162-163.

72. Kratschmer W, Lamb LD, Fostiropoulos K, Huffman DR. Solid C60: a new form of carbon. Nature 1990;347(6291):354-358.

73. Zhang D, Shi L, Fang J, Li X, Dai K. Preparation and modification of carbon nanotubes. Materials Letters 2005;59(29-30):4044-4047.

74. Department of Materials Science and Engineering, Pen State, http://www.seas.upenn.edu/mse/research/nanotubes.html.

75. Kanzow H, Ding A. Formation mechanism of single-wall carbon nanotubes on liquid-metal particles. Physical Review B 1999;60(15):11180.

76. Cassell AM, Verma S, Delzeit L, Meyyappan M, Han J. Combinatorial Optimization of Heterogeneous Catalysts Used in the Growth of Carbon Nanotubes. Langmuir 2001;17(2):260-264.

77. Kiichiro K, Tohru I, Ken-ichi S, Hidetoshi S, Kazunori M. Effect of negative dc bias voltage on mechanical property of a-C:H films deposited in electron cyclotron resonance plasma. Journal of Applied Physics 1995;78(2):1394-1396.

78. Young Chul C, Young Min S, Seong Chu L, Dong Jae B, Young Hee L, Byung Soo L, Dong-Chul C. Effect of surface morphology of Ni thin film on the growth of aligned carbon nanotubes by microwave plasma-enhanced chemical vapor deposition. Journal of Applied Physics 2000;88(8):4898-4903.

79. Delzeit L, Chen B, Cassell A, Stevens R, Nguyen C, Meyyappan M. Multilayered metal catalysts for controlling the density of single-walled carbon nanotube growth. Chemical Physics Letters 2001;348(5-6):368-374.

80. Li J, Papadopoulos C, Xu JM, Moskovits M. Highly-ordered carbon nanotube arrays for electronics applications. Applied Physics Letters 1999;75(3):367-369.

81. Ashbee KHG. Fundamental Principles of Fiber Reinforced Composites: Lancaster: Technomic.; 1993.

82. Andrews R, Jacques D, Rao AM, Rantell T, Derbyshire F, Chen Y, Chen J, Haddon RC. Nanotube composite carbon fibers. Applied Physics Letters 1999;75(9):1329-1331.

83. Yu M-F, Lourie O, Dyer MJ, Moloni K, Kelly TF, Ruoff RS. Strength and Breaking Mechanism of Multiwalled Carbon Nanotubes Under Tensile Load. Science 2000;287(5453):637-640.

84. Wagner HD, Lourie O, Feldman Y, Tenne R. Stress-induced fragmentation of multiwall carbon nanotubes in a polymer matrix. Applied Physics Letters 1998;72(2):188-190.

85. Lourie O, Cox DM, Wagner HD. Buckling and Collapse of Embedded Carbon Nanotubes. Physical Review Letters 1998;81(8):1638.

86. Shanmugharaj AM, Bae JH, Lee KY, Noh WH, Lee SH, Ryu SH. Physical and chemical characteristics of multiwalled carbon nanotubes functionalized with aminosilane and its influence on the properties of natural rubber composites. Composites Science and Technology 2007;67(9):1813-1822.

87. P. Nikolaev, M.J. Bronikowski, R.K. Bradley, F. Rohmund, D.T. Colbert, K.A. Smith, Smalley RE. Gas-phase Catalytic Growth of Single-Walled Carbon Nanotubes from Carbon Monoxide. Chem. Phys. Lett. 1999;313:91.

88. Garg A, Sinnott SB. Effect of chemical functionalization on the mechanical properties of carbon nanotubes. Chemical Physics Letters 1998;295(4):273-278.

89. Schadler LS, Giannaris SC, Ajayan PM. Load transfer in carbon nanotube epoxy composites. Applied Physics Letters 1998;73(26):3842-3844.

90. Qian D, Dickey EC, Andrews R, Rantell T. Load transfer and deformation mechanisms in carbon nanotube-polystyrene composites. Applied Physics Letters 2000;76(20):2868-2870.

91. A Huczko, H Lange, E Calko, H Grubek-Jaworska, Droszcz P. Physiological testing of carbon nanotubes: are they asbestos like? Fullerene Sci Tech 2001;9(2):251-254.

92. P. R. Hunziker, Stolzb M, Aebib U. Nanotechnology in Medicine: moving from the bench to the bedside. Chimia 2002;56:520-526.

93. Canham LT. Silicon quantum wire array fabrication by electrochemical and chemical dissolution of wafers. Applied Physics Letters 1990;57(10):1046-1048.

94. F. Ronkel, Schultze JW. Electrochemical Aspects of Porous Silicon Formation. Journal of Porous Materials 2000;7(1):11-16.

95. Pascual A, Fernandez JF, Sanchez CR. Nucleation and growth of pores and photoluminescence in p-type porous silicon. Journal of Applied Physics 2002;92(2):866-869.

96. Lehmann V, Foll H. Formation Mechanism and Properties of Electrochemically Etched Trenches in n-Type Silicon. Journal of The Electrochemical Society 1990;137(2):653-659.

97. Brumhead D, Canham LT, Seekings DM, Tufton PJ. Gravimetric analysis of pore nucleation and propagation in anodised silicon. Electrochimica Acta 1993;38(2-3):191-197.

98. A. Pascual, J.F. Fernández, C.R. Sánchez, S. Manotas, Agulló-Rueda F. Structural Characteristics of p-Type Porous Silicon and their Relation to the Nucleation and Growth of Pores. Journal of Porous Materials 2002;9(1): 57-66.

99. Duk Ryel Kwon, Subhankar Ghosh, Lee C. Growth and nucleation of pores in n-type porous silicon and related photoluminescence. Materials Science and Engineering B 2003 103:1-8.

100. Xiaoge Gregory Zhang. Electrochemistry of Silicon and its Oxide: Springer; 2001.

101. Eddowes MJ. Anodic dissolution of p- and n-type silicon : Kinetic study of the chemical mechanism. Journal of Electroanalytical Chemistry 1990;280(2):297-311.

102. C Pickering, M I J Beale, D J Robbins, P J Pearson, R Greef. Optical studies of the structure of porous silicon films formed in p-type degenerate and non-degenerate silicon. Journal of Physics C: Solid State Physics 1984;17(35):6535-6552.

103. Lehmann V, Gosele U. Porous silicon formation: A quantum wire effect. Applied Physics Letters 1991;58(8):856-858.

104. Henglein A. Physicochemical properties of small metal particles in solution: "microelectrode" reactions, chemisorption, composite metal particles, and the atom-to-metal transition. J. Phys. Chem. 1993;97(21):5457-5471.

105. Philip Moriarty. Nanostructured materials. J Reports on Progress in Physics 2001;3(297).

106. Sergeev GB, Shabatina TI. Low temperature surface chemistry and nanostructures. Surface Science 2002;500(1-3):628-655.

107. N.P. Balsara, H. Hahn. Block copolymers in nanotechnology. New Jersey: World Scientific Publishing; 2003.

108. Salata OV. Applications of nanoparticles in biology and medicine. Journal of Nanobiotechnology 2004;2(1):3.

109. Bordji K, Jouzeau JY, Mainard D, Payan E, Netter P, Rie KT, Stucky T, Hage-Ali M. Cytocompatibility of Ti-6Al-4V and Ti-5Al-2.5Fe alloys according to three surface treatments, using human fibroblasts and osteoblasts. Biomaterials 1996;17(9):929-940.

110. A. Regalado. Nanotechnology Patents Surge As Companies Vie to Stake Claim. The Wall Street Journal 2004;A1.

111. Seeram Ramakrishna KF, Wee-eong Teo, Teik-cheng Lim, Zuwei Ma. An Introduction to Electrospinning and Nanofibers: World Scientific.

112. TEO W RS. A review on electrospinning design and nanofibre assemblies. Nanotechnology 2006;17:R89-R106.

113. Kataryzna. Electrospun composite nanofibers for fundamental applications. Journal of Nanoparticle Research 2005.

114. Gupta B. KV. Manufactured Fibre Technology. London: Chapman and Hall; 1997.

115. Thandavamoorthy. Electrospinning of Nanofibers. Applied Polymer Science 2005(96):557-569.

116. Doshi. Electrostatics 1995(35).

117. R. Langer, J. P. Vacanti. Tissue engineering. Science 1993;260(5110):920-926.

118. Darrell H. Reneker, Haoqing Hou. Electrospinning: Informa Healthcare 2004.

119. Eugene D. Boland, Gary E. Wnek, David G. Simpson, Kristin J. Pawlowski, Gary L. Bowlin. Tailoring Tissue Engineering Scaffolds Using Electrostatic Processing Techniques: A Study of Poly(Glycolic Acid) Electrospinning. Journal of Macromolecular Science—Pure and Applied Chemistry 2001;38(12):1231.

120. Zheng-Ming Huang, Yanzhong Z. Zhang, S. Ramakrishna. Double-layered composite nanofibers and their mechanical performance. Journal of Polymer Science Part B: Polymer Physics 2005;43(20):2852-2861.

121. Ito Y, Hasuda H, Kamitakahara M, Ohtsuki C, Tanihara M, Kang I-K, Kwon OH. A composite of hydroxyapatite with electrospun biodegradable nanofibers as a tissue engineering material. Journal of Bioscience and Bioengineering 2005;100(1):43-49.

122. HJ Gong, XP Yang, GQ Chen, TQ Liu, SM Zhang, XL Deng, XY Hu. Study on PLA/MWNT/HA hybrid nanofibers prepared via electrospinning technology. Acta Polym. Sin. 2005;2:297-300.

123. Riboldi SA, Sampaolesi M, Neuenschwander P, Cossu G, Mantero S. Electrospun degradable polyesterurethane membranes: potential scaffolds for skeletal muscle tissue engineering. Biomaterials 2005;26(22):4606-4615.

124. MacDonald RA, Laurenzi BF, Viswanathan G, Ajayan PM, JP S. Collagen-carbon nanotube composite materials as scaffolds in tissue engineering. Journal of Biomedical Materials Research Part A 2005;74A(3):489-496.

125. Katta P, Alessandro M, Ramsier RD, Chase GG. Continuous Electrospinning of Aligned Polymer Nanofibers onto a Wire Drum Collector. Nano Lett. 2004;4(11):2215-2218.

126. Veli E. Kalayci, Prabir K. Patra, Alexandre Buer, Samuel C. Ugbolue, Yong K. Kim, Steven B. Warner. Fundamental Investigations on Electrospun Fibers. Journal of Advanced Materials 2004;36(4):43.

127. Lannutti J, Reneker D, Ma T, Tomasko D, Farson D. Electrospinning for tissue engineering scaffolds. Materials Science and Engineering: C 2007;27(3):504-509.

128. Annis D, Bornat A, Edwards RO, Higham A, Loveday B, J. W. An elastomeric vascular prosthesis. Trans. Am. Soc. Artif. Intern. Organs 1978;24:209-14.

129. Kim K YM, Zong X. Control of degradation rate and hydriphilicity in electrospun non-woven poly(D,L-lactide) nanofiber scaffolds for biomedical applications. Biomaterials 2003;24:4977-4985.

130. Schmitt. Importance of distinct water environments in hydrolysis of poly(dl-lactide-coglycolide). Macromolecules 1994;27(3).

131. Grizzi. Hydrolytic degradation of devices based on poly(dl-lactide) size-dependence. Biomaterials 1995(16):305-311.

132. Williams D. Biocompatibility of Tissue Analogs 1985.

133. Zeng J, Xu X, Chen X, Liang Q, Bian X, Yang L, Jing X. Biodegradable electrospun fibers for drug delivery. Journal of Controlled Release 2003;92(3):227-231.

134. Peter Atkins, Paula Jd. Physical chemistry; 2002.

135. Lin VSY, Motesharei K, Dancil K-PS, Sailor MJ, Ghadiri MR. A Porous Silicon-Based Optical Interferometric Biosensor. Science 1997;278(5339):840-843.

136. S. Chan, P. M. Fauchet, Y. Li, L. J. Rothberg. Nanoscale Microcavities For Biomedical Sensor Applications. Phys. stat. sol. (a) 2000;182:541-546.

137. Philip G. Collins, Phaedon Avouris. Nanotubes for electronics. Scientific American 2000;283(6):62-69.

138. Taylor. Royal Society of London 1969;A313.

139. Li. Electrospinning of nanofibers: Reinventing the Wheel. Advanced Materials 2004;16(14).

140. W. TEO, Ramakrishna S. A review on electrospinning design and nanofibre assemblies. Nanotechnology 2006;17:R89-R106.

141. Zussman E RD, Yarin A. Failure modes of electrospun nanofibers. Applied Physics Letters 2003;82(22):3958-3960.

142. Dalton AB, Stephan C, Coleman JN, McCarthy B, Ajayan PM, Lefrant S, Bernier P, Blau WJ, Byrne HJ. Selective Interaction of a Semiconjugated Organic Polymer with Single-Wall Nanotubes. J. Phys. Chem. B 2000;104(43):10012-10016.

143. Panhuis MIH, Salvador-Morales C, Franklin E, Chambers G, Fonseca A, Nagy JB , Blau WJ, A M. Characterization of an interaction between functionalized carbon nanotubes and an enzyme. J Nanosci Nanotechnol 2003;3:209-213.

144. Zhao Q, Wagner H. Raman spectroscopy of carbon-nanotube-based composites. Philosophical Transactions of the Royal Society A: Mathematical, Physical and Engineering Sciences 2004;362(1824):2407-2424.

145. Meyyappan M. Carbon nanotubes science and applications: CRC Press; 2004.

146. Souheil Zekri, Dan Hernandez, Douglas Pringle, Thomas J. Koob, Ashok Kumar. Development of NDGA Crosslinked Single Wall Carbon Nanotube-collagen fiber Nanocomposites for Orthopaedic Applications. Journal of Biomedical Materials Research Part A 2007;In review.

147. A. D. Mirzabekov. DNA sequencing by hybridization-a megasequencing method and a diagnostic tool. Trends Biotechnol 1994;12:27-32.

148. J.R. Lakowicz. Principles of Fluorescence Spectroscopy. NewYork: Kluwer Academic/Plenum Press; 1999.

149. P.R. Selvein. The renaissance of fluorescence resonance energy transfer. Nat. Struct. Biol. 2000;7:730-734.

150. Y. Singh, A. Pandey, K.K. Dubey, G. Wattel, K. Mishra. Fluorescence resonance energy transfer: A diagnostic tool in oligonucleotide therapy. Curr. Sci. 2000;78:487-492.

151. C.T. Wittwer, M.G. Herrmann, A.A. Moss, R.P. Rasmussen. Continuous Fluorescence Monitoring of Rapid Cycle DNA Amplification. Biotechniques 1997;22:130-139.

152. M. Schena. Microarray Biochip Technology. Natick, MA: Eaten Publisher; 2000.

153. A.N.Drobyshov, N.Malogina, V.Shick, D.Pobedimskaya, G.Yershov, A.D. Mirzabekov. Sequence analysis by hybridization with oligonucleotide microchip: identification of β-thalassemia mutations. Gene 1997;188:45-52.

154. R. Guckenberger, M. Heim, G. Cevec, H. F. Knapp, W. Wiegrabe, A. Hillebrand. Scanning tunneling microscopy of insulators and biological specimens based on lateral conductivity of ultrathin water films. Science 1994;266:1538-1540.

155. S. Wannmalm, L. Edman, R. Rigler. Conformational fluctuations in single DNA molecules. Proc. Natl. Acad. Sci. 1997;94:10641-10646.

156. S. B. Smith, Y. Curi, C. Bustamante. Overstretching B-DNA: The Elastic Response of Individual Double-Stranded and Single-Stranded DNA Molecules. Science 1996;271:795-799.

157. T.R. Strick , J.F. Allemand, D. Bensimon, A. Bensimon, V. Croquette. The Elasticity of a Single Supercoiled DNA Molecule. Science 1996;271:1835-1837.

158. S.B. Smith, L. Finzi, C. Bustamante. Direct mechanical measurements of the elasticity of single DNA molecules by using magnetic beads. Science 1992;258:1122-1126.

159. P. Cluzel, A. Lebrun, C. Heller, R. Lavery, J. L. Viovy, D. Chatenay, F. Caron. DNA: An Extensible Molecule. Science 1996;271:792-794.

160. M. S. Spector, J. M. Schnur. DNA Ordering on a Lipid Membrane. Science 1997;7(275):791-792.

161. K. Umemura, F. Nagami, T. Okada, R. Kuroda. AFM characterization of single strand-specific endonuclease activity on linear DNA. Nucleic Acids Research 2000;28(9):E39-e39.

162. D. Anselmetti, J. Fritz, B. Smith, X. Fernandez-Busquets. Single Molecule DNA Biophysicswith Atomic Force Microscopy. Single Mol. 2000;1:53-58.

163. L.L. Hench, J.K. West. Molecular Orbital Models of Silica. Annual Review of Materials Science 1995;25:37-68.

164. C. J. Brinker, G.W. Scherer. J. Sol → gel → glass: I. Gelation and gel structure. Non-Crystalline Solids 1985;70:301-322.

165. A. Kumar, R. Malhotra, B. D. Malhotra, S. K. Grover. Co-immobilization of cholesterol oxidase and horseradish peroxidase in a sol-gel film. Analytica Chimica Acta 2000;414:43-50.

166. R.L. Smith, S .D. Collins. Porous silicon formation mechanisms. J. Appl. Phy. 1992;71(8):1-22.

167. N. Isola, D.L. Stokes, T. Vo-Dinh. Surface-enhanced Raman Gene Probes for HIV Detection. Anal. Chem. 1998;70:1352.

168. L.T. Canham. Silicon quantum wire array fabrication by electrochemical and chemical dissolution of wafers. Appl.Phy Lett. 1990;57:1046-1048.

169. J. M. Lauerhaas, M. J. Sailor. Chemical Modification of the Photoluminescence Quenching of Porous Silicon. Science 1993;261:1567-1568.

170. A. Janshoff, K.P.S.Dancil, C. Steinem, D.P. Greiner, V.S.Y. Lin, C. Gurtner, Motesharel, M.J. Sailor, M.R. Ghadiri. Macroporous p-Type Silicon Fabry-Perot Layers Fabrication, Characterization, and Applications in Biosensing. J. Amer. Chem. Soc 1998;120:12108 -12116.

171. R. Jarimaviciute-Zvalioniene, V. Grigaliunas, S. tamulevicius, A. Guobiene. Fabrication of Porous Silicon Microstructures using Electrochemical Etching. J. Materials Science 2003;9:317-320.

172. A. G. Cullis, L. T. Canham, P. D. J. Calcott. The structural and luminescence properties of porous silicon. Applied Physics Reviews 1997;82:909-965.

173. M. F. Garcia-Parajo, J.A. Veerman, R. Bouwhuis, R. Vallee, N. F. Van Hulst. Optical probing of single fluorescent molecules and proteins. CHEM PHYSCHEM 2001;2:347-360.

174. O. Meurman, H. Sarkkinen, O. Ruuskanen, P. Hanninen, P. Halonen. Diagnosis of respiratory syncytial virus infection in children: Comparison of viral antigen detection and serology. Med. Virol. 1984;14:61-65.

175. M. Gale, M. S. Pollanen, P. Markiewicz, M. C. Goh. Sequential assembly of collagen revealed by atomic force microscopy. Biophysical Journal 1995;68:2124-2128.

176. Y. Fang, J. H. Hoh. Early Intermediates in Spermidine-Induced DNA Condensation on the Surface of Mica. J. Ame. Chem. Soc. 1998;120(25):8903-8909.

177. Souheil Zekri, Arun Kumar, Shree R. Singh, Ashok Kumar. Analysis of Mesocavity DNA Biochip for Respiratory Syncytial Virus (RSV) Diagnosis. Journal of Biomedical Nanotechnology 2007;3(2):139-147.

ABOUT THE AUTHOR

Souheil Zekri is a native of Tunisia, North Africa. He has been interested in engineering since middle school when he decided to join an engineering preparatory high school. His engineering training continued through the undergraduate curriculum in mechanical engineering when he joined the University of South Florida to study and play tennis for the school's varsity team. As he became more interested in multidisciplinary research, Souheil joined the robotics group in the mechanical engineering department where he completed a masters degree. After receiving a GK-12 fellowship from the industrial engineering department, Souheil decided to pursue a PhD in mechanical engineering with a concentration in biomechanics. Along the way, Souheil received a second masters in biomedical engineering. His future interests are to continue conducting research in the field of biomechanics and help the K-12 education system by participating in the enrichment of teacher's and student's knowledge in math and science.